Faculty of Science and Engineering
Department of Petroleum Engineering

Enhanced Gas Condensate Recovery by CO_2 Injection

Abdullah S. Al-Abri

This thesis is presented for the Degree of
Doctor of Philosophy
of
Curtin University of Technology

March 2011

DECLARATION

To the best of my knowledge and belief this thesis contains no material previously published by any other person except where due acknowledgment has been made. This thesis contains no material which has been accepted for the award of any other degree or diploma in any university.

Signature……..

Date……

ABSTRACT

Perhaps no other single theme offers such potential for the petroleum industry and yet is never fully embraced as enhanced hydrocarbon recovery. Thomas et al. (2009, p. 1) concluded their review article with *"it appears that gas condensate reservoirs are becoming more important throughout the world. Many international petroleum societies are beginning to have conferences specifically oriented to gas condensate reservoirs and discussing all parameters germane to such systems."* Gas condensate reservoirs however, usually experience retrograde thermodynamic conditions when the pressure falls below the dewpoint pressure. Condensate liquid saturation builds up near the wellbore first and then propagates radially away along with the pressure drop. This liquid saturation throttles the flow of gas and thus reduces the productivity of a well by a factor of two to four (Afidick et al., 1994; Barnum et al., 1995; Smits et al., 2001; Ayyalasomayajulla et al., 2005). The severity of this decline is to a large extent related to fluid phase behaviour, flow regime (Darcy or non-Darcy), interfacial forces between fluids, capillary number, basic rock and fluid properties, wettability, gravitational forces as well as well type (well inclination, fractured or non-fractured).

Thomas et al. (2009, p. 4) added *"... for gas condensate systems which exhibit high interfacial tensions where the pore throats are very small, which may correspond either to low permeability rocks or high permeability rocks but with very large coordination number, the success of flowing the liquid from the rock, once it has condensed, will be limited. In such cases, vaporisation (lean gas cycling) or injection of interfacial tension reducing agents (CO_2) may be the only option to enhance the performance."* In their comparison of several EOR mechanisms, Ollivier and Magot (2005, p. 217) reported *"since large changes in viscous forces are only possible for the recovery of heavy oil, the reduction (or entire elimination) of interfacial forces by solvents such as injection gases seems to be a practical way to achieve large changes in capillary number."* While the majority of the state of the art publications cover sensational aspects of gas condensate reservoirs such as phase couplings and mass transfer between original reservoir components, very little has been reported on fluid dynamics and interfacial interactions of CO_2 injection into such systems. This, along with the conceptual frameworks discussed above, serves as the motive for this research work.

High pressure high temperature experimental laboratories that simulate reservoir static and thermodynamic conditions have been established to evaluate the: (1) effectiveness of CO_2 injection into gas condensate reservoirs through interfacial tension (IFT) and spreading coefficients measurements at various reservoir conditions, (2) efficiency of the process through recovery performance and mobility ratio measurements; with special emphasis on the rate-dependent, IFT-dependent, and injection gas composition-dependant relative permeabilities, and (3) the behaviour of CO_2 injection into gas condensate reservoirs on a field scale through numerical simulations in heterogeneous, anisotropic, fractured and faulted systems. The study also investigates the performance of various reservoir fluid thermodynamic conditions, injection design variables, and economic recovery factors associated with CO_2 injection.

Condensate recovery was found to be a strong function of CO_2 injection pressure (and thus IFT), displacement flow rate, injection gas composition as well as phase behaviour and fluid properties. These parameters control the orientation and continuity of the fluid phases, solubility, gravity segregation, mobility ratio, and the ultimate recovery efficiency. Simulation analysis also suggests that developments of fractured gas condensate reservoirs depend to a large extent on initial reservoir thermodynamic conditions (initial pore pressure and fluid composition) as well as on production operations (natural depletion, waterflooding, continuous CO_2 injection, gas injection after waterflooding GAW, or water alternating gas WAG).

Much like the interrelation between accuracy and precision in science and engineering statistics, this research work draws a link between the effectiveness (quality metric through IFT measurements) and the efficiency (productivity metric through coreflooding experiments) of CO_2 injection into gas condensate reservoirs. The data reported in this research work should help reservoir engineers better characterise gas condensate systems. The results can also aid the engineering design of CO_2-EOR and CO_2 sequestration projects.

To

The memory of my father

for his wish to see me as an educated person

My mother, brothers & sisters

for their prayers and encouragement

My divine wife

for her greatest support and patience

My son

the light of my life

All those who are committed to real peace and serenity in this world

ACKNOWLEDGMENTS

In the Name of Allah, The Most Gracious, The Most Merciful

'My Lord! Grant me the power and ability that I may be grateful for your favours which You have bestowed on me and on my parents, and that I may do righteous good deeds that will please You, and admit me by your mercy among your righteous slaves' (Quran - 19:18)

The first and foremost acknowledgment for this work goes to Allah without whom all inspiration is relative, empty and incoherent. He has endowed me with an erudite supervisor in the person of Professor Robert Amin. This work would not come into light without his technical guidance, professional support and continuous encouragement. Working with him has been stimulating and rewarding in every possible aspect. He has been able to establish a flexible and creative research environment, which has fostered my own academic maturity. To me, he represents exactly what good advising is: a long-term vision accomplished steadily, one step at a time, with determination, patience, and intelligence. I am also indebted to Associate Professors David Pack and Ahmed Barifcani for their reviews and constructive comments that served to elucidate a better scope of refinement and perfection for the research concepts and publications.

This acknowledgment would be incomplete without the invaluable contributions of my friends and family members: notably, father for nurture, mother for nature, brothers and sisters for supportive culture. I am also grateful to Petroleum Development Oman for their financial support.

Thank you all for your custody of faith, guidance and endorsement at the different stages of implementation of the current work.

RESEARCH WORK AT A GLANCE

Gas condensate reservoirs stand as new frontiers as the petroleum industry is currently undergoing unprecedented surge of activities in securing enough hydrocarbon resources to satisfy the market. Operators realise, however, that applying accumulated knowledge about conventional gas/oil systems in gas condensate reservoirs without rigorous scrutiny may lead to completely incorrect conclusions, and hence incorrect practices. The following lists the papers that have been published in support to this research work:

1. Al-Abri, A., Sidiq, H., & Amin, R. (2009). Experimental Investigation of the Velocity-Dependent Relative Permeability and Sweep Efficiency of Supercritical CO_2 Injection into Gas Condensate Reservoirs. *Natural Gas Science and Engineering* 1, 158-164. DOI: 10.1016/j.jngse.2009.10.002.
2. Al-Abri, A., & Amin, R. (2010a). Phase Behaviour, Fluid Properties and Recovery Efficiency of Immiscible and Miscible Condensate Displacements by $SCCO_2$ Injection: Experimental Investigation. *Transport in Porous Media.* DOI 10.1007/s11242-010-9589-5.
3. Al-Abri, A., Sidiq, H., & Amin, R. (2010a). Enhanced Natural Gas and Condensate Recovery by Carbon Dioxide and Methane Flooding. *Petroleum Science and Technology*. In Press.
4. Al-Abri, A., Sidiq, H., & Amin, R. (2010b). Mobility Ratio, Relative Permeability and Sweep Efficiency of Supercritical CO_2 and Methane Injection to Enhance Natural Gas and Condensate Recovery: Coreflooding Experimentation. *Natural Gas Science and Engineering*. In Press.
5. Al-Abri, A., & Amin, R. (2010b). Interfacial Tension Effects of Hydrocarbon and Non-Hydrocarbon Gas Injection into Gas Condensate Reservoirs. *Chemical Engineering and Technology*. In Press.

TABLE OF CONTENTS

LIST OF FIGURES

LIST OF TABLES

CHAPTER I

INTRODUCTION

1.1 Overview

Natural gas has become an important source of global energy and is projected to be the fastest-growing component of primary world energy consumption. Natural gas currently provides approximately a quarter of the world's energy and its share is increasing significantly (BP Statistical Review of World Energy, 2010). Oil still remains as the world's leading energy source but it has lost a significant amount of its market share to gas and coal (**Fig. 1**). Natural gas has also become the most desirable source of energy from the standpoint of global environmental problems as it is the cleanest of all the fossil fuels. The rapid increase in the worldwide demand for natural gas has resulted in significant growth of international gas trade and stimulated long-term contracts for its sales. Hence, it becomes important to accurately predict the production performance of these reservoirs and meet the desired production rates.

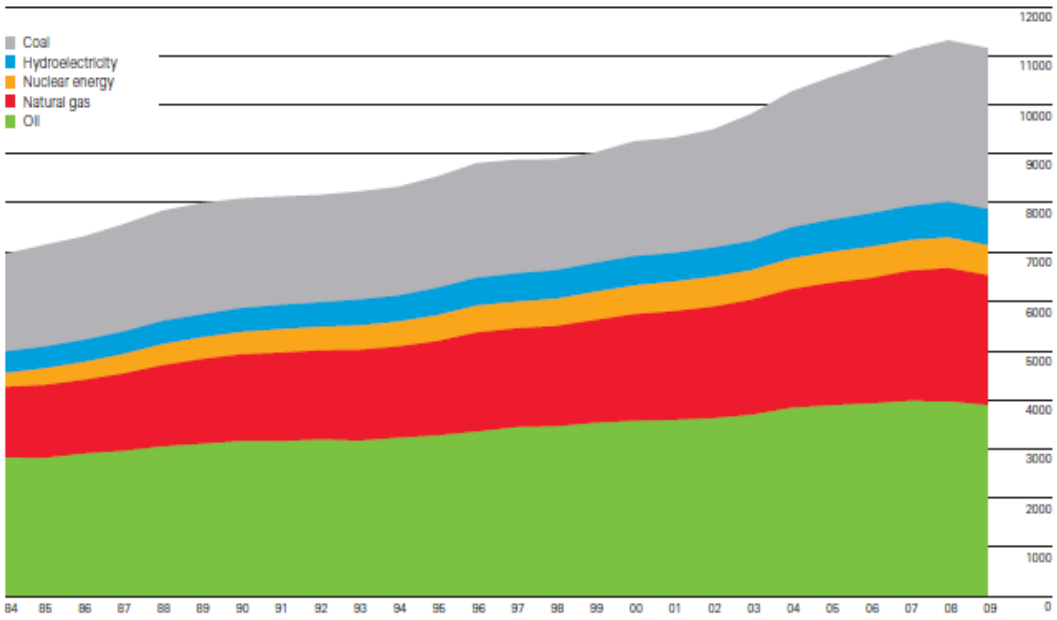

Fig. 1 - World's Energy Consumption for the Last 25 Years Showing a Significant Increase in Natural Gas Demand (BP Statistical Review of World Energy, 2010)

Natural gas reservoirs, however, usually experience retrograde conditions when the pressure falls below the dewpoint pressure. This retrograde condensation occurs first near the wellbore and then propagates radially away along with the pressure drop (**Fig. 2**). Capillary forces often render the condensate immobile and that these microscopic liquid droplets tend to be trapped in small pores or pore throats. The hierarchy of fluid interfacial tensions ensures that water remains in direct contact with the rock, and condensate droplets form a film on the water surface separating the gas from the water (circle inset in Fig. 2). This condensate accumulation around the wellbore not only reduces the effective permeability to gas but will also change the phase composition of the produced fluids. The condensate mobility remains insignificant until a critical liquid saturation is reached at which point both phases will start to flow. The gas and liquid will then start to compete for the available flow paths and this dynamic competition is described by the relative permeability relationships (square inset in Fig. 2).

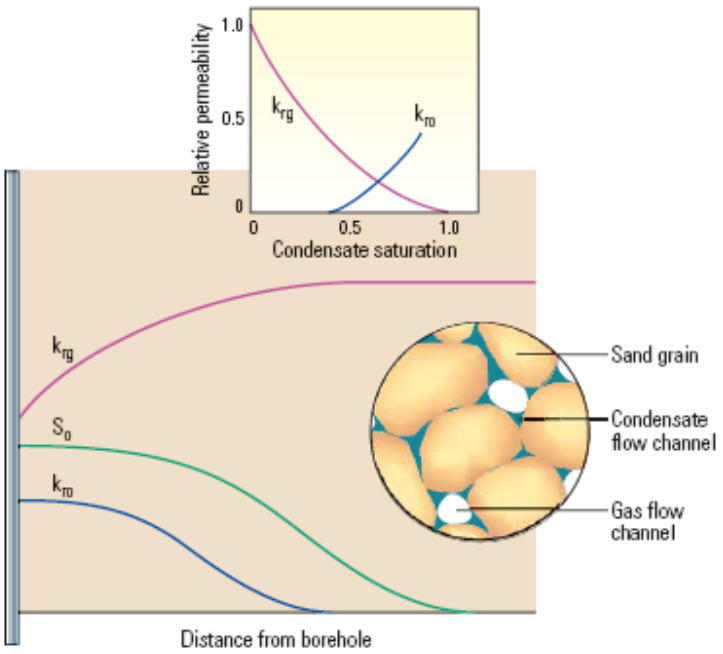

Fig. 2 - Saturation Distribution for a Typical Gas Condensate System (Fan et al., 2005)

The near-well chocking can reduce the productivity of a well by a factor of two to four (Afidick et al., 1994; Barnum et al., 1995; Smits et al., 2001; Ayyalasomayajulla et al.,

2005). The severity of this decline is to a large extent related to fluid phase behaviour, flow regime (Darcy or non-Darcy), interfacial forces between fluids, capillary number, basic rock and fluid properties, wettability, gravitational forces as well as well type (well inclination, fractured or non-fractured). Some of these factors play a more significant role in condensate accumulation than others depending on the reservoir conditions. Predicting and assuring well deliverability is critical to meeting contractual obligations for gas delivery. Several methods have been proposed in the literature to restore gas production rates after condensate dropout. These methods suggest either changing the phase behaviour of reservoir fluids or maintaining reservoir pressure above the dewpoint pressure; including gas cycling, waterflooding, methanol treatments, wettability alteration, or hydraulic fracturing (Henderson et al., 1991; Barnum et al., 1995; Fishlock and Probert, 1996; Settari et al., 1996; Luo et al., 2000; Kumar, 2000; Li and Firoozabadi, 2000; Al-Anzi et al., 2004).

Gas injection is the worldwide second most common technology that is currently embraced for enhanced recovery projects, next only to steam injection (Hinderaker et al. 1996). Gas injection accounts for 29% of the worldwide incremental enhanced production (Moritis, 2004). The injected gas could be natural gas, methane, nitrogen or carbon dioxide. Historically, globally and over the years, operators used to cycle natural gas after it had been produced. The increase in demand, however, makes gas cycling a less attractive option (Hagoort et al., 1998; Manrique et al., 2007). The same argument probably goes for methane injection. Nitrogen is a potential alternative injection gas. It is available everywhere because it can be produced from air at low cost using cryogenic or membrane separation (Evison and Gilchrist, 1992). Economic evaluations show that nitrogen injection is realistic provided that the gas condensate reservoir is sufficiently rich (Donohoe and Buchanan, 1981; Eckles et al., 1981; Huang et al., 1986; Sanger and Hagoort, 1998).

Carbon dioxide (CO_2) injection is another promising technology for managing gas condensate reservoirs while extensively reducing greenhouse gas emissions. Enhancing the recovery of natural gas and condensate resources makes storage of CO_2 in depleted gas condensate reservoirs interesting due to the potential recovery upside. The abundant literature suggests that CO_2 injection offers many advantages over the injection of any of the aforementioned gases as it greatly promotes the swelling of the oil net volume, reduces its viscosity and interfacial tension as well as reducing the density difference between oil

and water and thus provides less room for gravity segregation (Orr et al., 1982; Orr et al., 1984; Martin and Taber, 1992; Blunt et al., 1993).

Generally, the flow of gas and condensate in reservoir pores is governed by three fundamental forces: capillary, gravitational and viscous. Since large changes in viscous forces are only possible for the recovery of heavy oil, the reduction (or entire elimination) of interfacial forces by solvents such as injection gases seems to be a practical way to achieve large changes in capillary number (Ollivier and Magot, 2005), thus obtaining a better recovery. The majority of published scientific work covers some of the sensational aspects of the gas condensate reservoirs but the actual mechanisms by which the residual condensate might be mobilised by CO_2 injection in particular are not often mentioned. This is partly because such accumulations exhibit complex phase behaviour and heterogeneous nature, but also because some background in interfacial science and fluid dynamics is required. This serves as the rationale for this research work.

1.2 Research Objectives and Tasks

The goal of this research work is to understand, by means of experiments and numerical simulation, the interplay among viscous, gravitational, and capillary forces during CO_2 injection and the implications for enhanced gas and condensate recovery coupled with CO_2 sequestration. The primary objectives can be summarised as:

1. Evaluate the effectiveness of CO_2 injection into gas condensate reservoirs through laboratory interfacial tension (IFT) and spreading coefficient measurements at various reservoir conditions,
2. Evaluate the efficiency of CO_2 injection into gas condensate reservoirs through recovery performance and mobility ratio measurements; with special emphasis on the rate-dependent, IFT-dependent, and injection gas composition-dependant relative permeabilities,
3. Evaluate the behaviour of CO_2 injection into gas condensate reservoirs on a field scale through numerical simulations in heterogeneous, anisotropic, fractured and faulted systems. The study also investigates the performance of various reservoir fluid thermodynamic conditions, injection design variables, and economic recovery factors associated with CO_2 injection.

1.3 Significance

Because it investigates the microscale interfacial interactions as well as the macroscale recovery performance of CO_2 injection into gas condensate reservoirs as an enhanced recovery process, this study stands out as the vast majority of past studies have either:

- Concentrated on examining the interactions between the natural gas and the liquid condensate in attempts to understand the phase couplings and mass transfer between original reservoir components, or
- Focused on enhanced recovery mechanisms such as CO_2 injection in conventional oil/gas reservoirs.

The results presented in this study will be of value to operators as they recognise that the use of accumulated knowledge about conventional gas/oil systems in gas condensate reservoirs without rigorous scrutiny may lead to incorrect conclusions, and hence incorrect practices.

The first objective reveals the microscopic nature of interfacial boundary interactions that have long been recognised to govern both the distribution of fluids and their flow behaviour in porous media (Wanger and Leach, 1966; Taber, 1969; Harbert, 1983). The interfacial tension between the gas and oil (or condensate) phases may vary by several orders of magnitude in the primary production of near-critical gas condensates or volatile oils and in near-miscible gas-injection processes. Upon such variations, the flow regime changes from an emulsion-like flow at very low IFTs to a capillary-dominated flow at high IFTs (Bardon and Longeron, 1980; Batycky and McCaffery, 1978). These changes are reflected in the parameters characterising multiphase flow through porous media such as the capillary pressure, the phase permeabilities, and residual saturations after drainage with gas. In addition, the first objective investigates the spreading coefficient that controls the orientation and continuity of the fluid phase in the reservoir pores. The spreading coefficient also affects the gas-oil-water distributions, and consequently the recoveries during a gas injection program (Hartman and Cullick, 1993; Vizika and Lombard, 1996; Melean et al., 2003; Mani and Mohanty, 1996).

The second objective demonstrates the relative permeability, mobility ratio and recovery efficiency of liquid condensate following CO_2 injection at various pressure, temperature, and flow rate conditions. The multiphase flow behaviour in gas condensate reservoirs and, in particular, the effects of critical condensate saturation, shapes of relative permeability curves and the effect of capillary forces have long remained as the crux of the reservoir engineering difficulties when managing gas condensate reservoirs (Bourbaiux et al., 1994; Kalaydjian et al., 1996; Henderson et al., 1998; Mott et al., 2000). These parameters serve as inputs to numerical simulators for reservoir performance evaluations. The measured relative permeability as well as the interfacial tension data should facilitate the design of an integrated CO_2-EOR and CO_2 sequestration.

The third objective investigates the bulk interactions of multiphase flow associated with CO_2 injection into heterogeneous, anisotropic, and fractured gas condensate reservoirs through compositional simulations. The simulator captures the microscale physics and fluid dynamics that are primarily influenced by the relative magnitude of the dominant reservoir forces (namely, gravity, capillary, and viscosity). The magnitude of these forces is accounted for through effects of interfacial tension, spreading coefficient, relative permeability, and injection patterns. The simulations throughput have the potential to provide valuable insights for reservoir engineers in regards to the choice of the best injection design and its optimisation.

1.4 Review of Chapters

This thesis is organised into 6 chapters. Chapter II critically reviews the literature associated with the distinctive nature of gas condensate reservoirs, conventional production mechanisms, condensate dropout phenomenon and subsequent productivity decline. It also shows the major microscale transport processes and fluid dynamics that strongly affect the performance of gas injection processes. The chapter demonstrates the available studies on interfacial tensions, relative permeabilities and spreading coefficients as well as on the displacement and remedial practices proposed to mitigate the condensate blockage. This chapter will open the horizon for the need to better understand, forecast, and manage gas condensate reservoirs.

Chapters III and IV present the experimental design and procedure utilised during the interfacial tension and relative permeability measurements at various pressure and temperature conditions. The experimental program is systematically shown in terms of setup, fluids, data acquisition and analysis procedures. These chapters form the backbone of the laboratory investigations conducted during the course of this research work. The chapters include all the breakthroughs, results, and discussions on the effects of CO_2 injection at reservoir conditions on condensate recovery.

Chapter V presents the results of the compositional simulation of CO_2 injection into a heterogeneous and fractured gas condensate reservoir. The chapter investigates the recovery performance of various reservoir fluid thermodynamic conditions (reservoir fluid composition and pore pressure) as well as several development strategies (natural depletion, CO_2 injection, injection flow rate, waterflooding, gas injection after waterflooding, and WAG). Chapter VI summarises the conclusions in accordance with the research objectives and provides recommendations for further research into the subject.

CHAPTER II

LITERATURE REVIEW

This chapter presents a critical review of the literature in support of the conceptual framework for the study. It highlights the subject of gas condensate reservoirs with special emphasis on the phase and flow behaviour, condensate banking phenomena, transport mechanisms, and fluid dynamics. These factors lie at the heart of reservoir engineering activities as they affect the performance of a gas condensate reservoir during the exploitation process.

2.1 Gas Condensate Reservoirs

Gas condensate reservoirs have more recently stimulated an immense popular interest in hydrocarbon exploration and production. Gas from gas condensate reservoirs is now a significant percentage of the world's gas supply. The condensate has a high value in the market place so the economical recovery of the maximum amount of condensate must be a prime consideration to the reservoir engineer. Gas and condensate liquids are more benign to the environment compared to black oil; there is therefore, an increase in usage of such fluids worldwide.

Gas condensate reservoirs may exist at pressures less than 2,000 psi and at temperatures below 100 ^{o}F but most commonly they occur in the range of 3,000 to 10,000 psi and 200 to 400 ^{o}F (Roussennc, 2001). Wall (1982) presents the following argument for the fact that gas and gas condensate reservoirs are usually found at great depths. He submits that the greater the temperature and pressure to which organic matter has been subjected the greater is the degree of degradation of complex organic molecules. Consequently the deeper the burial of source rock the greater is the likelihood of a relatively high proportion of lighter hydrocarbon. Gas condensate reservoirs consist predominantly of methane and other short-chain hydrocarbons, but also contain some heavy-ends.

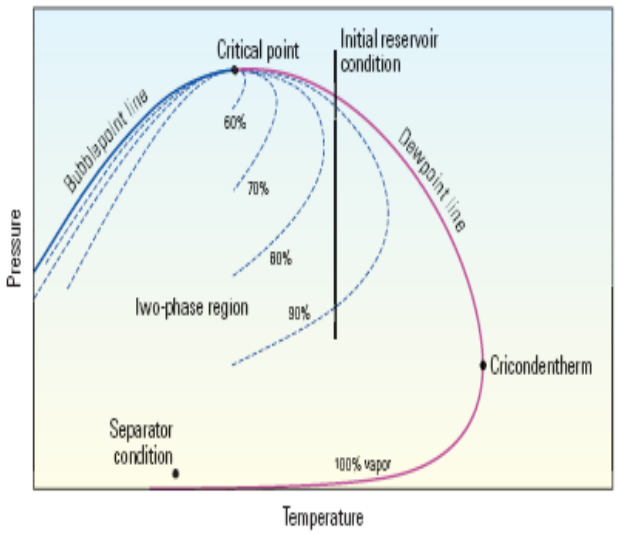

Fig. 3 - Phase Diagram of a Typical Gas Condensate System (Fan et al., 2005)

Gas condensate reservoirs are typically single-phase gas at discovery as the initial reservoir pressure might be above or close to the critical pressure (black vertical line in **Fig. 3** above). Once production wells are put on stream, there exists an isothermal pressure decline and, at the saturation pressure, a liquid hydrocarbon phase is formed. The amount of this liquid condensation depends on the reservoir dewpoint, drawdown pressure, and the thermodynamic properties of the initial gas. The liquid dropout occurs first near the wellbore and then propagates radially away along with the pressure drop (**Fig. 4**).

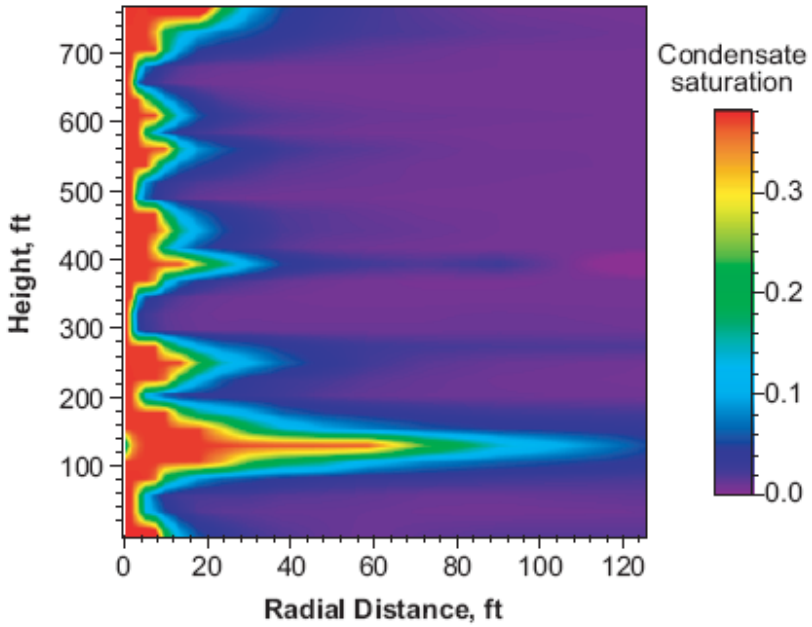

Fig. 4 - Buildup of Liquid Condensate in the Vicinity of a Wellbore (Kamath, 2007)

Generally, the flow of natural gas and condensate in reservoir pores is governed by three fundamental forces: capillary, gravitational and viscous. The flow within the bulk of the reservoir is mainly controlled by gravity and capillary forces due to the low fluid velocity, whereas the flow near the wellbore is dominated by the balance of the shear (viscous) and capillary forces (Ursin, 2004). The productive capacity of a gas condensate reservoir depends on its thermodynamic state. This capacity is controlled by reservoir permeability and thickness, and by the viscosity of gas when the reservoir is above the dewpoint pressure. The degree of productivity below the dewpoint, however, is a function of the critical condensate saturation (S_{cc}), and the shape of the gas and condensate relative permeability curves (Lal, 2003).

The production of hydrocarbons from gas condensate reservoirs presents more challenges to reservoir engineers when compared to production from more conventional gas or black (non-volatile) oil systems (Thomas et al., 2009). These challenges are mainly due to the complex nature of phase behaviour and fluid flow in porous media exhibited by gas condensate mixtures. The non-conventional flow behaviour of gas condensates is attributed to the distribution of the condensate in pores, and the relatively low interfacial tension between the hydrocarbon phases compared to that of gas/oil systems. Applying

accumulated knowledge about conventional gas/oil systems to gas condensate reservoirs without rigorous scrutiny may lead to incorrect conclusions, and hence incorrect practices.

Several production mechanisms for the recovery of gas condensate fluids have been suggested in the literature. These range from simple pressure depletion (blowdown) to pressure maintenance schemes to the more sophisticated enhanced recovery techniques. Waterflooding has been practiced as an art in the petroleum industry to displace hydrocarbons when attempting to maximise recovery from oil reservoirs. Other production mechanisms such as gas injection and WAG are possibly more a subject of research than field application. The author is not aware of a gas condensate field being produced by such production methods.

Pollard and Bradley (1962) suggest that the following factors should be considered when selecting an optimum production method for a gas condensate reservoir:

1. Reservoir formation and fluid characteristics:
    - Occurrence or absence of black oil.
    - Size of reserves.
    - Properties and composition of reservoir hydrocarbon.
    - Productivities and injectivities of wells.
    - Permeability variation that controls the degree of bypassing of injected gas.
    - Degree of natural water drive if existing.
2. Reservoir development and operating costs.
3. Plant installation and operating costs.
4. Market demand for gas and liquid petroleum products.
5. Future relative value of the products.
6. Existence or absence of competitive producing conditions between operators (in the same reservoir).
7. Taxes and royalties.
8. Special hazards or risks to the investment (e.g. political instability).
9. Overall economic analysis.

The need to accurately predict the production performance of gas condensate reservoirs stems from the fact that sale contracts of gas and liquefied natural gas are signed

in the early stages of exploitation of such hydrocarbon accumulations. To be able to meet sale demands over usually long contract periods of 20 to 30 years, engineers need to be able to predict the production performance of gas condensate wells fairly accurately. Condensate banking phenomenon is considered to be the most important factor leading to a significant reduction in the productivity index of a gas condensate well. Better understanding of the fluid dynamics and interfacial interactions around the wellbore region in particular, on the other hand, holds the key for an increased flow of natural gas and condensate into the well. The role of these two factors is not yet fully realised in the industry and it is still a rich subject of research.

2.2 Condensate Banking

Gas condensate reservoirs often experience rapid decline as soon as the condensate starts to build up and form a ring around the production wells. The amount of liquid phase present depends not only on the pressure, temperature and composition, but also on the properties of the fluids and relative permeability (Hinchman and Barree, 1985; Sognesand, 1991). This region ranges in size from tens of feet for lean condensates to hundreds of feet for rich condensates. Its size is proportional to the volume of gas drained and the percentage of liquid dropout. It extends farther from the well for layers with higher permeability than average since a layer volume of gas has flowed through these layers. A dry gas, by definition, has insufficient heavy components to generate liquids in the reservoir, even with near-well drawdown. A lean gas condensate generates a small volume of the liquid phase, less than 100 bbl/million ft^3, and a rich gas condensate generates a larger volume of liquid, generally more than 150 bbl/million ft^3 (**Fig. 5**).

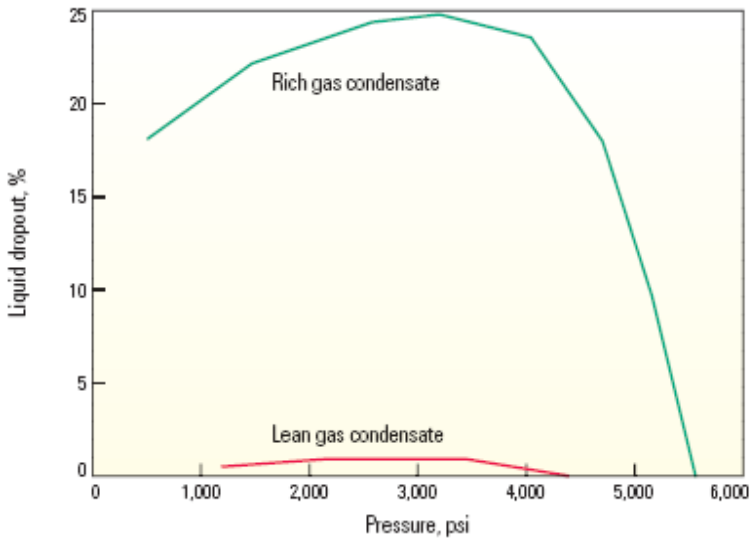

Fig. 5 - Magnitude of Liquid Dropout in a Gas Condensate Reservoir (Fan et al., 2005)

Conceptually, once the bottomhole pressure drops below the dewpoint pressure there exist three regions with different liquid saturations (Fevang and Whitson, 1995; Ali et al. 1997; Gringarten and Al-Lamki, 2000). These regions are shown in **Fig. 6** as follows:

- Region A which includes most of the reservoir away from production wells. Since this region could still be above the dewpoint pressure, there is only one hydrocarbon gas phase present. The interior boundary of this region occurs where the pressure equals the dewpoint pressure of the original reservoir gas. This boundary is not stationary, but moves outward as hydrocarbons are produced from the well and the formation pressure drops, eventually disappearing as the outer-boundary pressure drops below the dewpoint.
- Region B which features a rapid increase in liquid saturation and a corresponding decrease in gas relative permeability. This condensate liquid is usually trapped in the small pore throats as a result of the capillary forces acting on it and thus, it is immobile. Even for rich gas condensates with substantial liquid dropout, condensate mobility, which is the ratio of relative permeability to viscosity, remains insignificant away from wellbores. This is to say that the condensate that forms in most of the reservoir is lost to production unless the

depletion plan includes an enhanced recovery scheme such as gas cycling, CO_2 injection, WAG, etc.

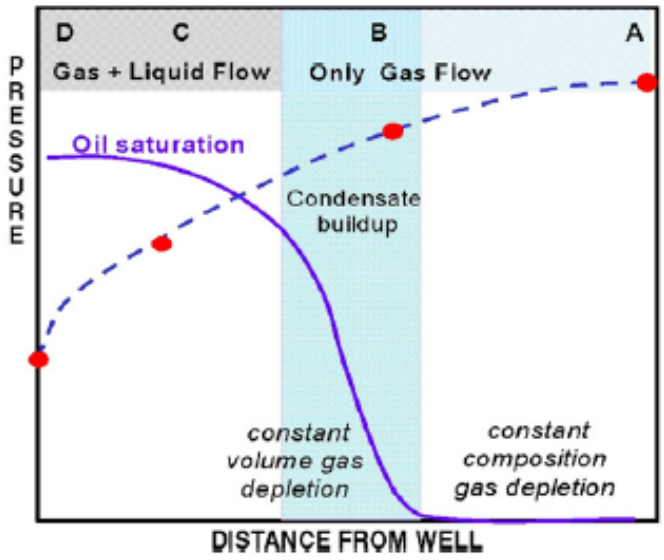

Fig. 6 - Pressure-Flow Regime as a Function of Distance from the Wellbore (Dawe and Grattoni, 2007)

- Region C which forms closer to the well where the liquid saturation reaches a critical value, and the effluent travels as two-phase flow with constant composition, that is constant vapour/liquid ratio if the liquid saturation is high enough (Whitson and Brule, 2000). Studies show that a minimum liquid saturation, that is critical saturation, of 30 to 50% is required for the liquid to become mobile (Gravier et al., 1986; Danesh et al., 1989). These figures may go lower in the presence of interstitial water (Danesh et al., 1991). This liquid condensate may be pushed into the wellbore by the gas due to its high velocity, but the gas can also strip some of the lighter components from the liquid, so called “velocity stripping’.

Some researchers argue that there may also exist a fourth region (Region D in Fig. 6) in the immediate vicinity of the well where low IFTs at high rates yield a decrease in the liquid saturation and an increase in the gas relative permeability (Economides et al., 1987; Fussel, 1973).

The productivity loss associated with condensate buildup can be substantial. Barnum et al. (1995) presented a study assessing the historical frequency and severity of productivity impairment due to near wellbore condensate buildup. Their study looked at published industry data, published laboratory data and a simulation study. Their main conclusion was that the recovery factor of gas condensate radial wells is only affected by condensate blocking if the well's permeability-thickness (kh) is less than 1,000 md-ft. For higher quality reservoirs, productivity loss is not very severe. El-Banbi et al. (2000) showed that the well productivity of vertical wells in a moderately rich gas condensate reservoir initially decreased rapidly and then increased as the reservoir was depleted. This phenomenon was explained by subsequent compositional simulations (Hinchman and Barree, 1985; Fussel, 1973; Ahmed et al., 1998). The condensate buildup not only impedes the flow of gas and thus reduces its effective permeability but also changes the phase composition of the produced fluids.

Engineer (1985) studied the Cal Canal Field in California, which produced a very rich gas condensate fluid and had a very high water saturation of 59%. The total gas recovery expected from the field was as low as 10% owing to the high condensate and water saturation in the near wellbore region. Afidick et al. (1994) studied the decline in productivity of the Arun gas condensate reservoir due to the condensate accumulation. Experimental PVT analysis of the reservoir fluid showed that the reservoir fluid was a lean gas condensate with maximum liquid dropout of 1.1%. The decline in the productivity of the wells by a factor of around two as the reservoir pressure fell below the dewpoint pressure was attributed to accumulation of condensate around the wellbore. The accumulation of condensate around the wellbore was confirmed by well tests and the analysis done on the reservoir cores.

Shell and Petroleum Development Oman reported a 67% productivity loss for wells in two fields (Smits et al., 2001). Other large gas condensate resources which have reported significant reductions in productivity due to condensate blockage include the Shtokmanovskoye field in the Russian Barents Sea, the Karachaganak field in Kazakhstan, the North field in Qatar, and the Cupiagua field in Colombia (Elliot et al., 1998). Boom et al. (1996) showed that even for lean fluids with low condensate dropout, high condensate

saturations could build up as many pore volumes of gas pass through the near wellbore region.

2.3 Methods to Treat Condensate Blockage

Several methods have been proposed and investigated to treat damage caused by condensate accumulation. The most common approaches to treat damage caused by condensate blocking suggest either changing the phase behaviour of reservoir fluids, or reducing the pressure drawdown and thus maintaining reservoir pressure above the dewpoint. This section highlights research findings of the impact of a variety of treatment techniques on the thermodynamic interactions taking place in-situ as well as on the production performance.

Kossack and Opdal (1986) did simulations to study the performance of slug injection of methane followed by nitrogen. They studied the effect of slug injection in a homogenous and heterogeneous layered reservoir with both isotropy and anisotropy. Their results show that the heterogeneities allow the nitrogen to mix with the condensate when the methane slug is small but the incremental recovery with a methane slug over nitrogen injection is large enough to pay off the cost of methane. Cullick et al. (1989) performed simulation and experimental studies to investigate the efficiency of Water Alternating Gas (WAG) to improve recovery from gas condensate reservoirs. They proposed the use of WAG instead of dry gas injection in the full pressure maintenance process and also as an alternative to early blowdown. Their results show an improvement of about 28% to 54% in total recovery over that with continuous gas injection for full pressure maintenance.

Henderson et al. (1991) performed coreflood experiments to study the effect of water injection on gas condensate recovery, above and below the dewpoint. They found that residual hydrocarbon saturation after waterflooding depends on the prevailing IFT between the gas and condensate. The authors also showed that gas and condensate displacement by water is complex and cannot be represented by data from water-oil and water-gas displacements and requires special three-phase relative permeability measurements to describe waterflooding and subsequent depressurisation. Sanger and Hagoort (1998) investigated the efficiency of nitrogen to evaporate gas condensate compared to methane. They found that methane can evaporate more condensate than nitrogen. The authors

reported that the evaporation capacity of methane is more than 20 times higher than that of nitrogen. The disadvantages of injecting nitrogen is that the dewpoint of the mixture is higher than the reservoir gas and thus leads to in-situ condensate drop out due to mixing with gas condensate reservoir.

Fishlock and Probert (1996) studied the performance of water injection for lean and rich gas condensate fluid systems. They found that hydrocarbon recoveries are higher for leaner fluids than richer fluids because less condensate blockage is formed in the production of lean gases. Ahmed et al. (1998) studied the effectiveness of lean gas, N_2, and CO_2 huff 'n' puff injection technique in removing the liquid accumulated in and around the wellbore. The huff 'n' puff injection technique uses the same well alternatively as producer and injector. The authors concluded that pure CO_2 is the most effective gas in reducing the liquid dropout compared to others when injected at the same pressure. The authors also showed that the huff 'n' puff injection of gases is most effective when initiated before the maximum liquid dropout is reached. An insufficient amount of gas injection could increase the liquid dropout.

Luo et al. (2000) conducted experiments on an actual rich gas condensate fluid to investigate condensate recovery and to quantitatively determine the revaporisation efficiency of retrograde condensate by lean gas injection. Their analysis of the produced condensate phase shows that a greater percentage of the heavier components are vaporised and recovered when gas is injected below the saturation pressure. Their results also show that cumulative condensate recovery is higher when injection is done above the saturation pressure. The authors also observed that during gas injection at the reservoir pressure, the mass transfer between the dry-gas injected and the original gas condensate leads to a rise in dewpoint pressure and earlier retrograde condensation, which may reduce the condensate recovery to some extent. Ahmed et al. (2000) analysed the effect of waterflooding in gas condensate reservoirs and compared it with gas injection. Their results showed improvement in gas and condensate production rates for both gas and water injection. Although gas injection showed higher condensate recovery factors, the authors suggest that gas injection may not be economical due to large initial investment required, higher operating costs, and delay of gas sales. They further showed that, if water injection is planned to be used in gas condensate reservoirs, the reservoir should be blown-down

before water invades the majority of the producing wells and increases the water cut. Blow-down also helps re-mobilise some of the gas trapped by the injected water.

Jamaluddin et al. (2001) did PVT experiments to study the effect of CO_2 and propane on the phase behaviour of the reservoir gas condensate fluid. They found that CO_2 increases the dewpoint of the mixture but reduces the total liquid dropout below the dewpoint whereas propane reduces the dewpoint as well as the total liquid dropout. The authors suggest huff 'n' puff injection of propane would efficiently reduce the damage due to condensate blocking. Marokane et al. (2002) studied the injection of produced gas to remove the condensate bank for lean and rich gas condensate fluids. The authors found that to achieve maximum recovery for a lean gas condensate, produced gas should be injected after the average reservoir pressure around a producing well falls below the maximum liquid dropout pressure. For rich gas condensate, gas injection is more efficient when the produced gas is injected at a pressure greater than the maximum liquid dropout pressure.

Al-Anzi et al. (2004) experimentally studied the revaporisation of condensate in cores by methane. They showed that methane flooding revaporised condensate and restored the gas permeability to single-phase flow values. Revaporisation of condensate was controlled by the partitioning of the hydrocarbon components into the flowing gas phase when the injection was done below the minimum miscibility pressure (MMP). Increase in injection pressure and rate expedited the revaporisation of condensate. Hoier et al. (2004) studied miscible gas injection for partial pressure maintenance in an under-saturated oil (Smorbukk South Field) exhibiting compositional variation. The authors' generated a MMP gradient for a given injected gas, from the compositional, reservoir pressure and saturation pressure gradients. The authors concluded that once the injected gas develops miscibility at the injection point, the developed miscible front will first-contact miscibly displace the downstream fluid, independent of whether the downstream fluid is miscible or immiscible with the injected gas.

Du et al. (2000), Walker et al. (2000) and Al-Anzi (2002 and 2003) investigated the use of methanol to treat damage due to condensate and water blocking. The authors show that an enhanced flow period is observed in both low and high permeability cores after methanol treatment, during which condensate accumulation is delayed. Their experiments showed:

- Significant improvement in oil and gas relative permeability is observed during the enhanced flow period after methanol treatment. Also, the treatment is more effective in the presence of high water saturation as methanol effectively removes the damage due to water blocking in addition to treating the damage due to condensate dropout.
- Significant improvement due to methanol treatment is achieved only after a certain volume of methanol injection, after which the relative improvement is negligible or reduces significantly.

Methanol treatments remove both water and condensate by a multi-contact miscible displacement if sufficient methanol is injected. Methanol treatments resulted in a significant but temporary enhancement in productivity for both low and high permeability cores. However, removal of water-blocks would be expected to have a long lasting impact on a well's productivity index (PI).

Hydraulic fracturing has been used to enhance gas productivity (Kumar, 2000; Barnum et al., 1995). In many wells it is possible to reduce the drawdown, i.e. increase the flowing bottomhole pressure by inducing a hydraulic fracture that significantly increases the area available to flow. This allows the well to be produced at a higher bottomhole pressure for longer periods of time thereby delaying the onset of condensate formation around the wellbore. The success of hydraulic fracture stimulation depends on the placement of sufficient quantity of proppant without changing the integrity of the formation, the rate at which fracture fluids are produced from the fracture, and the degree to which the fracture "cleans up" after the treatment. Settari et al. (1996) conducted a simulation study to investigate the improvement of PI due to hydraulic fracturing in the Smorbukk field. Their results show that fracturing can restore 50 to 70% of the PI loss due to condensate blocking compared to a non-fractured well in a low permeability zone. In higher permeability zones, fracturing can increase the PI more than the single phase PI. They found that PI improvement is more sensitive to the fracture length in low permeability zones, whereas PI is more sensitive to the fracture conductivity in high permeability zones.

Kumar (2000) studied the effect of an idealised vertical fracture in a gas condensate well. The author predicted that for two-phase flow of gas and condensate, the productivity of a fractured well can be as high as eight times the productivity of an unfractured well. Lolon et al. (2003) showed that the fracturing fluid that remains in the fracture and formation after a hydraulic fracture treatment blocks the gas flow into the fracture and thus reduces the effective fracture length. Pressure transient tests performed on hydraulically fractured wells also support this and reveal that the effective fracture half-lengths are substantially less than the designed length from fracture stimulation. Thus the predictions from simulating idealised fractures are too optimistic.

Li and Firoozabadi (2000) proposed enhancing the gas condensate well deliverability by altering the wettability of the near wellbore region from strong liquid wetting to preferential gas wetting. They used chemicals FC 754 and FC 722 (from 3M Chemical) to alter wettability and showed that permanent gas wetting can be established in Berea and chalk through chemical treatment. Tang and Firoozabadi (2000 and 2002) used FC 759 and FC 722 to alter the wettability from strong liquid wetting and intermediate gas wetting. These chemicals have a fluorochemical group that provides water and oil repellency, a silanol group that chemically bonds to the rock surface providing a durable treatment. The authors concluded from their experiments that treatment with the chemical FC759 can yield:

- Wettability alteration from strong liquid wetting to stable intermediate gas wetting at room temperature as well as at high temperatures,
- Neutral wetting for gas, oil, and water phases in two-phase flow,
- A significant increase in oil mobility for a gas/oil system,
- Improved recovery behaviour for both gas/oil and oil/water systems.

Austad and Standnes (2003) studied wettability alteration in carbonate formations from oil wet to water wet by using cationic surfactants. They showed that surfactants of the type tera-alkyl ammonium dissolved in water are able to change the wettability from oil wet to water wet in an irreversible way by desorbing organic carboxylates. The efficiency of the surfactant increases as the number of the Ethoxy (EO) group increases. Mohanty and Adibhatla (2004) studied the possibility of changing carbonates and sandstones wettability

to neutral wet by using surfactants. They showed that as the number of fluoro group increases, rock become less water-wet. One day of ageing period and 1 wt% concentration appear to be sufficient for altering the wettability. They further stated that wettability alteration may reduce the brine saturation near the hydraulic fracture faces and increase gas productivity.

2.4 Mass Transport Mechanisms and Fluid Dynamics

Multiphase flow behaviour strongly influences the microscopic and macroscopic displacement efficiencies and ultimately affects the performance of gas injection processes. The relative magnitude of the dominant reservoir forces (namely, gravity, capillary, and viscosity) primarily controls mass transport and fluid dynamics in the porous media. The relative influence of such forces is conventionally reported through the effects of interfacial tension, spreading coefficient, relative permeability, and injection patterns. This section highlights the various multiphase fluid dynamics operational during any gas injection process.

2.4.1 Mass Transport in Porous Media

Gas condensate reservoirs are usually initially developed through simple pressure depletion or a simple pressure maintenance scheme in the form of waterflooding. Either way, liquid condensate is expected to build up around the wellbores as a natural product of the drawdown pressure required to produce hydrocarbons. The main disadvantage of waterflooding gas condensate reservoirs is the bypassing and trapping of gas and liquid condensate, which can result in up to 50% of the gas being unrecovered (Dake, 1983; Fisherman and Prior, 1983). Once bypassing has occurred, the objective of enhanced recovery schemes becomes to maximise the mass transfer between the bypassed and the flowing injected fluid. Gravity-driven, pressure-driven, and capillary-driven crossflows along with molecular diffusion and transverse dispersion have been identified as the significant mass-transfer mechanisms.

2.4.1.1 Gravity-Driven Crossflow

Gravity can create crossflows in the vertical direction owing to possible density contrasts between the injection and reservoir fluids. Gravity drainage from bypassed regions can be significant if capillary retention forces are small. Slow rate displacements in long, thin reservoirs lie closer to gravity dominated regime. Mixing and phase interactions between the bypassed and injected fluids may lower the interfacial tension, decreasing the capillary pressure and allowing gravity forces to mobilise bypassed hydrocarbons. Zhou et al. (1993) reported that for a system with a capillary to gravity ratio ($N_{c/g}$) of less than 0.2, the flow is gravity dominated. For a system with $N_{c/g}$ between 0.2 and 5.0, the flow is in capillary-gravity equilibrium. For a system with $N_{c/g}$ greater than 5, the flow is capillary dominated.

Gravity-driven crossflow, when present, may be the most significant form of mass transfer (Dindoruk and Firoozabadi, 1996a; Dindoruk and Firoozabadi, 1996b). Schechter and Guo (1996) have developed a model based on Darcy flow and film flow for gravity drainage in naturally fractured reservoirs. The model was used to simulate experimental data obtained under thermodynamic equilibrium conditions. The model identified two regions: the first is full pore flow and film flow and the second is only film flow. Schechter and Guo (1996) conducted non-equilibrium gravity drainage experiments in a CO_2-spraberry oil system under slightly immiscible flooding conditions. Rapid drainage was observed in the high permeability Berea sandstone (low capillary forces). However, in a low permeability reservoir core, the drainage was much slower and as a result, light ends were preferentially recovered. In order to account for the non-equilibrium conditions of gravity drainage observed experimentally, Schechter and Guo (1996) coupled a Fickian diffusion model to their gravity drainage model. The model suggested that molecular diffusion may be the dominating recovery mechanism in low permeability reservoirs.

2.4.1.2 Pressure-Driven Crossflow

Pressure gradients are established between the flowing injected fluid and the bypassed reservoir hydrocarbons as the injected fluid flows through the reservoir. The resulting transverse flow is called viscosity-driven or pressure-driven crossflow. The viscous to capillary force ratio can be used to determine the influence of such crossflows:

$$Ca = \frac{u\mu_f}{\gamma}, \quad \text{.....1}$$

where u is the superficial velocity, μ_f is the viscosity of the injected fluid, and γ is the IFT.

When the superficial velocity increases, the viscous forces increase and overcome both capillary retention and gravity. These pressure gradients are particularly important in viscous fingering and gravity override floods. Viscous fingering can be expected to occur in displacements with adverse mobility ratios, M > 1, that is when a more mobile phase displaces a less mobile phase. Displacement is stable during miscible floods with favorable mobility ratios (M < 1) in relatively homogenous media. As the mobility ratio increases, the injected fluid front becomes less stable and small perturbations within the permeability field of the medium can lead to fingering. Fingering may cause early injected fluid breakthrough at the production well and poor recovery.

Oldenburg et al. (2001) studied the effect of pressure, temperature and composition on the physical properties of CO_2 and methane. Their results demonstrate that the density and viscosity of pure CO_2 increases with both pressure and temperature. However, these density and viscosity values tended to decrease when methane mixed with the CO_2. The authors also observed that the greater increase in CO_2 density with pressure and temperature, relative to methane, makes CO_2 migrate downward, whilst the greater viscosity of CO_2 tends to create a favourable mobility ratio when CO_2 is used to displace methane in the porous strata, thus providing a more stable displacement front. Experimental work indicated that viscous crossflow between the fluids occurs only near the ends of the fingers (Perkins et al., 1965). Initiation of a finger is the result of the small, but ubiquitous permeability heterogeneity of the medium. Initial growth of fingers can occur only if the rate of growth is greater than the longitudinal dispersion zone. Finger growth increases with increasing mobility ratio or decreasing frontal stability.

2.4.1.3 Capillary-Driven Crossflow

Capillary-driven crossflow was first observed in water-wet reservoirs during secondary waterflooding. While viscous crossflow results from transverse pressure

gradients arising from mobility changes across a front, capillary crossflow is due to saturation changes across a front. In layered or stratified reservoirs, where gravity and viscous forces will be less important than capillary forces, fluids will tend toward capillary equilibrium. In the process, water imbibition due to capillary pressure gradients can occur behind the advancing water front and lead to an incremental increase in oil recovery (Goddin et al., 1966). Stearn (1991) has investigated the effects of waterblocking or capillary induced bypassing during tertiary displacements. He conducted tertiary miscible CO_2/crude oil displacements in water-wet and mixed-wet rocks. The solvent always displaced the water to mobilise and recover the oil. He found that in water-wet cores, the solvent displaced the water from the largest pores because the entry pressure was lowest. This leads to pore level bypassing, or waterblocking. Yokoymam and Lake (1981) demonstrated that heterogeneity distribution in the reservoir will control the degree of capillary crossflow in the transverse and longitudinal directions.

Morel et al. (1990) were the first to document capillary crossflow for nitrogen gas injection at laboratory-scale, single-fracture/matrix combination. Nitrogen, while being less mobile with an idealised oil (methane-pentene), gave excellent recovery compared to a more miscible methane flood, thereby demonstrating the significant influence that capillary pumping has on the mass transfer of pentene from a matrix block. Capillary pumping phenomenon takes place when the solvent-oil phase behavior is such that the solvent-oil IFT decreases with distance into the bypassed region, then a gradient, favorable for capillary crossflow, is established. The injected solvent will flow into the bypassed region as a result of a difference in capillary pressure at the fluid interface. Nitrogen develops a favorable IFT gradient whereas methane, and most other hydrocarbon gases, exhibit unfavorable IFT gradients. Subsequent simulations by Hu et al. (1990) and Fayers and Lee (1992) validated the capillary pumping process.

2.4.1.4 Dispersion and Molecular Diffusion

During the flow through porous media, the additional mixing caused by uneven flow or concentration gradient is called dispersion. It results from the different paths and speeds and the consequent range of transit times available to tracer particles convicted across a permeable medium. Dispersive mixing is a result of molecular diffusion and mechanical

dispersion. Perkins et al. (1965) provided an analysis of the dispersion phenomena and correlations for two types of dispersion; (1) longitudinal direction, and (2) transverse to the direction of gross fluid movement. An idealised two-dimensional flow scenario like that shown in **Fig. 7** helps to illustrate transverse and longitudinal dispersion (Stalkup, 1983). Both, having different magnitudes, have to be considered separately. Dispersive mixing plays an important role in determining how much solvent will dissolve/mix with solute to promote miscibility. Molecular diffusion will cause mixing along the interface. The net result will be a mixed zone growing at a more rapid rate than would be obtained from diffusion alone. Diffusion is a special case of dispersion and a result of concentration gradient, with or without the presence of the velocity field (Bear, 1972).

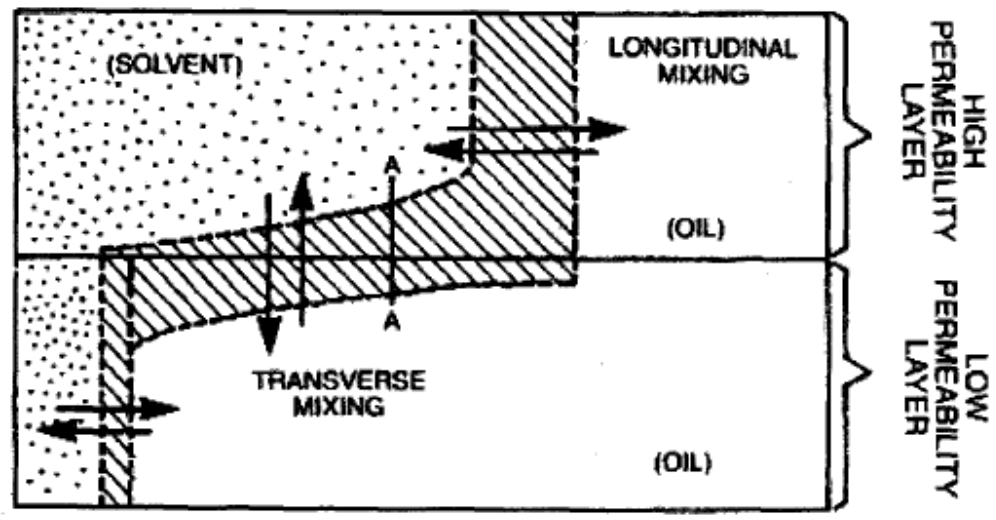

Fig. 7 - Transverse and Longitudinal Mixing (Stalkup, 1983)

The Peclet number (P_e) is commonly used to assess the magnitude of dispersion in a system. This is a ratio of characteristic times for dispersion to characteristic times for convection:

$$P_e = \frac{vL}{\phi K} \quad \text{.....2}$$

For large P_e, dispersion effects are small, and displacement is convection dominated. In field scale displacements, P_e is usually very large. For reservoir displacements,

convection dominates. Stalkup (1983) reported that transverse dispersion is one mechanism that may tend to decrease the amount of bypassed hydrocarbons particularly for viscous fingering or gravity-dominated gasfloods. His research concluded that dispersion affects mixing or concentration within the front, but not the speed of the front. Other studies show that macroscopic transverse dispersion is an important mechanism in helping damp frontal instabilities (Mahadevan et al., 2002).

2.4.2 Interfacial Tension

Interfacial tension (IFT) is the most important factor that may cause one-third of the total oil in place to be unrecoverable by gas drive or water flooding alone (Jennings and Newman, 1971). The interactions of rock pore geometry and interface boundary conditions determine the microscopic displacement efficiency. The major interfacial interactions include interfacial tension, capillarity, wettability, and interface mass transfer. It has long been recognised that these interactions govern both the distribution of fluids and their flow behaviour in porous media (Wanger and Leach, 1966; Taber, 1969; Harbert, 1983). These interfacial properties are strongly dependent on thermodynamic conditions such as pressure, temperature, and phase composition. The IFT between the gas and oil (or condensate) phases may vary by several orders of magnitude in the primary production of near-critical gas condensates or volatile oils and in near-miscible gas-injection processes. Upon such variations, the flow regime changes from an emulsion-like flow at very low IFT to a capillary-dominated flow at high IFT (Bardon and Longeron, 1980; Batycky and McCaffery, 1978). These changes are reflected in the parameters characterising two-phase flow through porous media such as the capillary pressure, the phase permeabilities, and residual saturations after drainage with gas. Residual saturations are higher, and permeabilities are lower for capillary-dominated flows (high IFTs), while for very low IFTs, residual saturations tend to zero and the oil and gas relative permeabilities tend to the corresponding phase saturations (Harbert, 1983).

Capillary (and to a lesser extent gravitational) forces render certain amounts of condensate immobile and thus lost to production. These forces resist the externally applied viscous forces and hence, to a large extent govern the mobility of the reservoir fluids. The condensate trapping is best expressed as a competition between viscous forces, which tend

to mobilise the condensate; capillary forces which tend to trap it; and gravitational forces which tend to pull the freely-floating liquid condensate drop downwards towards the lower edge of the pore channel. The capillary number and the bond number are dimensionless groups that gauge the IFT forces relative to the buoyancy and viscous forces (Blom and Hagoort, 1998). The capillary number or "critical displacement ratio", N_{ca}, illustrates the ratio between the viscous to capillary forces (Moore and Slobod, 1951; Wanger and Leach, 1966; Foster, 1973; Melrose and Brandar, 1974; Morrow, 1991), while the bond number, N_B, describes the ratio between the gravitational force and the capillary force (Melean et al., 2003) as follows:

$$N_{ca} = \frac{v\mu}{\gamma \cos\theta} \quad \text{.....3}$$

$$N_B = \frac{k\Delta\rho_{go}}{\gamma_{go} \cos\theta} \quad \text{.....4}$$

where μ is the injection gas viscosity; v is the injection gas velocity; k is the absolute permeability; $\Delta\rho_{go}$ is the oil and gas phases density difference; γ is the interfacial tension between the crude oil and the injected solvent; such as CO_2; and θ is the contact angle. The externally applied pressure must at least counteract the capillary pressure in order to displace the residual condensate from a pore channel. Upon the increase of the miscibility between the gas and oil phases, the fluid-dependent quantities $\Delta\rho_{go}/\gamma_{go}$ and μ/γ_{go} increase towards infinity, meaning that a transition from capillary-to-gravity and viscous-dominated flow takes place.

A landmark paper by Arps (1964) demonstrated the value of engineering concepts in the hunt for oil, and the understanding in particular of the effects of capillarity on effective column heights, and the function of relative permeability as a factor in fluid production. Wagner and Leach (1966) performed immiscible displacement tests over a range of interfacial tensions and velocities to determine the displacement efficiency and the effect on the residual saturation. Their experiments showed a rapid decrease in residual saturation when the IFT falls below a threshold value. Earlier authors who observed the dependence of relative permeability and residual saturation on IFT in their laboratory experiments were

Moore and Slobod (1951), and Mungan (1966). Melrose and Brandner (1974) presented mechanisms for understanding the role of capillary forces in the entrapment of residual oil in an oil-water system.

Bardon and Longeron (1980) had experimentally validated the strong effect of IFT on the relative permeability in gas-oil systems. They conducted unsteady-state measurements at interfacial tensions down to 0.001 dyne/cm. Their study showed that residual oil saturations and relative permeabilities are affected strongly by interfacial tension. Fulcher et al. (1985), based on their experimental and modelling studies, concluded that relative permeability was better modelled when based on the individual IFT and viscosity variables rather than the capillary number. They reported that residual oil saturation decreased to approximately zero when the capillary number increased to 0.01. In their study they observed no rate effect as the test velocity did not exceed 24 m/day.

Asar and Handy (1988) investigated the influence of interfacial tension on the relative permeability of gas/oil in a gas condensate system. They postulated that the irreducible gas and liquid saturations approach zero as interfacial tension approaches zero. In addition, they observed that condensate could flow at a low condensate saturation (S_{cc} = 10%). Finally, it was concluded that liquid could flow at a very low liquid saturation at low interfacial tensions in a condensate reservoir. This is significant as regions with two-phase (gas and liquid) conditions have low interfacial tension. Munkerud (1989) developed and tested techniques for measurement of gas condensate fluid system by pressure depletion and dynamic displacement of retrograde liquid at different interfacial tensions. His measurements showed that the relative permeability curves to the gas condensate model system in a depletion process are similar to curves of ordinary gas-oil systems. He also pointed out the strong dependence of relative permeability to gas and liquid on IFT between the two phases.

2.4.3 Miscibility Development

Oil and Gas Journal's biannual EOR survey (2002) clearly demonstrates the industry inclination towards miscible gas floods and that commercial immiscible projects have decreased significantly over the past few decades with no immiscible floods planned for the immediate future. The fundamental definition of miscibility (Stalkup, 1983) implies

that the necessary and sufficient condition for miscibility development is the absence of an interface between the injected and the reservoir fluids (in other words, a condition of zero IFT). Interestingly this results in a capillary number of infinity, and theoretically all the oil in the reservoir can be produced. Furthermore, as the capillary number controls the microscopic displacement efficiency of the flood, miscible floods have the potential to demonstrate nearly 100% microscopic displacement efficiencies in the gas swept zones.

Adamson and Flock (1962) studied the effects of viscous fingering and viscosity ratio on oil recovery in a liquid-liquid miscible drive. Their study indicated that displacement of crude oil by propane in a consolidated Berea sandstone core yields an ultimate recovery of 64% of the original oil in place (OOIP) after the injection of 1.5 pore volumes (PV). This low recovery was due mainly to the adverse viscosity ratio (70.5) encountered during the displacement. It was observed that the propane travelled through the core quite rapidly, developing a wide transition zone with many fingers. Subsequent displacements carried out on the same core with a mixture of propane and varsol at a viscosity ratio of 8.5 resulted in a narrow transition front, with recoveries close to 100% of OOIP. Hence they concluded that the efficiency of enriched gas drive displacement is influenced primarily by the sweep efficiency within the core, which in turn is controlled by the mobility ratio, reservoir heterogeneity, and gravitational segregation effects. They suggested that in order to determine the miscibility pressure and temperature of a system in the laboratory, it would be necessary to suppress or eliminate all causes of poor efficiency. Their observation indicated that low oil recovery in a gas injection system is not by itself a conclusive evidence of lack of miscibility.

Giraud et al. (1971) conducted one and two-dimensional (experimental and simulation) gas displacement of ternary mixtures and actual reservoir oils in the laboratory to analyse the behaviour of mixing zones under dynamic miscibility conditions. Their study was aimed at identifying the differences between dynamic miscibility, vaporising gas drive miscibility, and true miscibility, as well as to determine the impact of those differences on sweep efficiency. The authors illustrated the following differences between dynamic miscibility and vaporising gas drive, as well as between dynamic miscibility and true miscibility. Vaporising gas drive is characterised by a sharp saturation front, which moves like a piston. Its advantages over conventional gas drive include lower residual

liquid behind the front, and the residual liquid is slowly re-vaporised in the gas phase as the front moves on. True miscible displacement on the other hand has no sharp front. A smooth transition zone is created between the displaced oil and the displacing gas and no liquid saturation is left behind the transition zone. Under dynamic miscibility, the sizeable liquid saturation behind the front is quickly and completely re-vaporised, resulting in almost total recovery like in true miscible displacement.

Giraud et al. (1971) suggested that any displacement in which almost total recovery is obtained by mass transfer between phases (vaporising and condensing gas drives) should be carefully analysed by laboratory experiments under reservoir conditions. Experiments conducted in a one-dimensional coreflood showed a mixing zone of nearly constant composition. The mixing zone was indicated by the concentration profiles of the ternary mixture in the core. It was shown that the mixing zone is not a straightforward mixture of the oil in place and injected gas. Hence, a liquid phase, in thermodynamic equilibrium with the gas must remain in the mixing zone, and behind as a residual saturation. A constant residual liquid saturation was indicated during simulation runs, as indication of two phase flow occurring in the mixing zone. The mobility profile computed by the numerical model differs drastically from the classical S-shaped profile of a true miscible displacement, an indication of a low mobility buffer present between the oil in place and the more mobile injected gas. This was attributed to the discontinuity of the effective permeability to the mobile phase at the saturation front, suggesting a partial front stabilisation. It was found that real sweep efficiency is much better under dynamic miscibility conditions than true miscibility conditions.

Stalkup (1983) presented a review of miscible displacement and field behaviour for major miscible flood processes, including first contact miscible, rich gas drive, vaporising gas drive, and carbon dioxide flooding. The review focused on phase behaviour and miscibility, sweepout, displacement efficiency, and process design. In addition, rules of thumb and ranges of conditions for applicability of each process were discussed and a comparison of the incremental recovery observed from field trials of the different processes was made. First contact miscible solvents mix with reservoir oils in all proportions and the mixtures always remain single phase. Other solvents not directly miscible could achieve miscibility under appropriate conditions of pressure and

composition. Miscibility in these solvents is achieved by in-situ mass transfer of oil and solvent components through repeated contact with the reservoir oil. This type of miscibility is termed multiple-contact or dynamic miscibility. The vaporising gas drive process achieves miscibility by in-situ vaporisation of intermediate molecular weight hydrocarbons from the reservoir oil into the injected gas, while the rich gas (condensing gas) drive involves mass transfer of the same components in the opposite direction. Flue gas and nitrogen achieves miscibility at high pressures by the vaporising gas drive mechanism. Vaporising gas drive (VGD) miscibility depends on oil composition, temperature, pressure and density of the oil. High gravity oils are generally required (> 40 ^{o}API, i.e. s.g < 0.83) and 3,500 psi (24.132 MPa) is about the lower pressure limit for miscibility to occur.

Holm (1986, 1987) provided an explanation and definition of the terms miscibility and miscible displacement, and how to determine the conditions at which multi-contact miscible displacements occur. He defined solubility as the ability of a limited amount of one substance to mix with another substance to form a single homogenous phase, and miscibility as the ability of two or more substances to form a single homogenous phase when mixed in all proportions. For petroleum reservoirs, miscibility was defined as the physical condition between two or more fluids that will permit them to mix in all proportions without the existence of an interface. If two fluid phases form after some amount of one fluid is added to others, the fluids are considered immiscible, and an IFT exists between the phases. When a substantial IFT exists between phases in a porous medium, capillary forces prevent the complete displacement of one of those phases by the other. Miscible displacement implies that the IFT between the displaced and displacing fluid is zero. There are two types of miscible displacement, first-contact and multi-contact (dynamic). The most common method used for determining the conditions at which multi-contact miscibility occurs is known as “slim-tube” displacement. The slim-tube described by Holm is a 12 to 24 m long; 0.6 cm internal diameter high pressure tube packed with clean sand or glass beads, to a permeability of about 3 to 5 darcies. This sand pack is saturated with the reservoir oil of interest, and a series of displacements is carried out by the injection of the fluid of interest at different pressures. Miscible displacement is achieved at the displacement pressure where about 95% of the oil in the tube is recovered after about 1.3 PV’s of fluid has been injected. Visual observation of the fluids produced

from the tube near the completion of the flood is helpful in determining the conditions of miscibility.

Morel (1991) treated the subject of miscible gas flooding. This summary will however, focus on the explanation of multi-contact miscible (MCM) VGD floods on the ternary diagram. VGD form of MCM is based on the vaporising of intermediate (preferentially C_2-C_5) components from the reservoir oil into the injected gas, at high pressure, thereby creating a miscible transition zone. A ternary diagram is a practical way of visualising the development of VGD miscibility. A ternary diagram representation of the equilibria involved in the flue gas and nitrogen miscibility processes is possible, but the choice of poles is difficult. The best solution is to choose flue gas (or nitrogen) as a pole, with the two other poles being C_1-C_6 and C_{7+}; hence, a pseudo-binary mixture represents the reservoir oil. Under specific conditions of temperature and pressure, and the dew and bubble point curves are plotted inside the triangle (**Fig. 8**), thus defining the two-phase zone. Point C is representative of the mixture of the three pseudo-components, which has T and P as critical temperature and pressure. The injected high pressure gas is represented by point G and the virgin reservoir oil by point O. It is necessary that point O should be on the right side of the critical tie line (tangent to the phase envelope at point C) for miscibility to develop. This implies that the oil is relatively rich in intermediate components. The various exchanges involved are presented schematically in **Fig. 8** and **Fig. 9**.

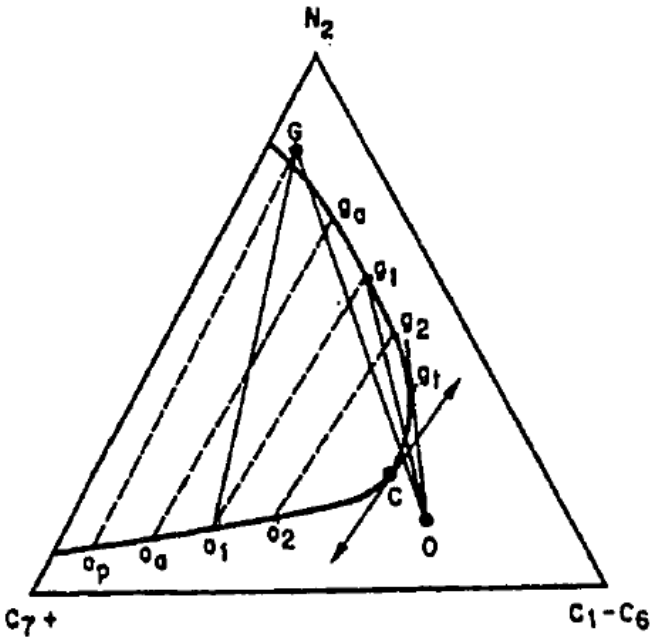

Fig. 8 - Ternary Diagram of a Vaporising Gas Drive Process (Morel, 1991)

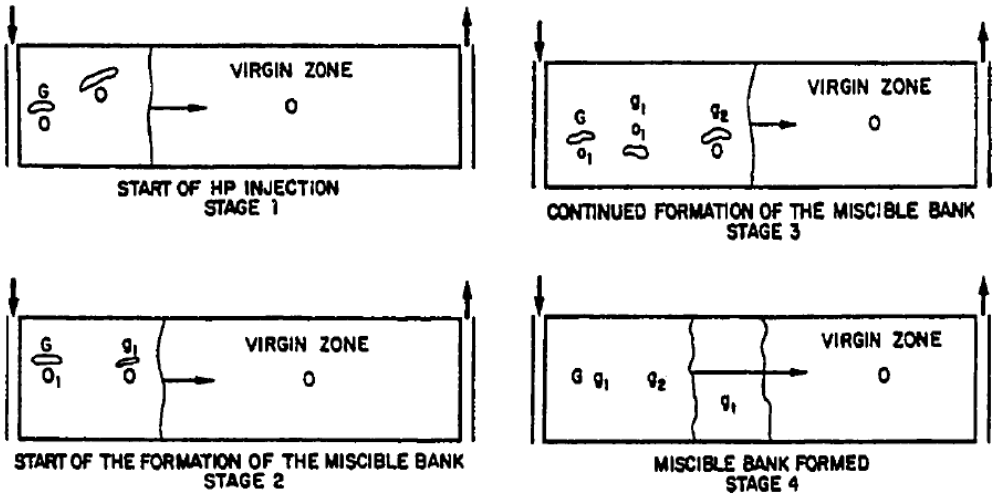

Fig. 9 - Formation of Miscible Bank in Vaporising Gas Drive (Morel, 1991)

Initially, virgin oil and injected gas are immiscible and line GO, which represents this, passes through the two-phase zone. This implies that near the wellbore, some residual oil with original composition O remains unchanged (Fig. 9, Stage 1). As oil and gas are not in equilibrium, thermodynamic exchanges occur, leading to equilibria g_1 and o_1. The gas is now enriched with intermediate and heavy components compared to G. Oil o_1 generally

occupy a smaller volume than O, so the oil saturation remains below the critical mobility value behind the front. Gas g_1 moves ahead, chased by the fresh injected gas G while the oil remains in place (Stage 2). At this stage of the process, g_1 contacts virgin oil O. Since they are not in equilibrium, they divide into two phases, g_2 and o_2, with g_2 being in contact with the displacement front. On the other hand, oil o_1 in contact with gas G gives o_a, which is poorer in intermediate components (Stage 3). The process will continue until the gas in contact with the virgin oil reaches point g_t, defined as the intercept of the tangent to the two-phase envelope from the oil representative point O. There, full miscibility is achieved and no residual oil remains. Behind the miscible bank (Stage 4), residual oils o_1 and o_2 previously formed, continue becoming poorer in light fractions while in contact with fresh gas G. The extreme composition of these residual oils is o_p, located on the tie line that passes through G gas composition. This o_p does not exchange any intermediate components with G, and will remain trapped in the reservoir.

Mohanty et al. (1994) identified pore scale mechanisms that lead to the formation of a residual oil saturation in high pressure miscible floods in the absence of water shielding. They conducted high pressure displacement experiments with reservoir oil in a two-dimensional, transparent micromodel. A slim-tube was attached upstream of the micromodel to create a gradual transition from the oil to solvent, similar to what a pore in the swept zone in the middle of a reservoir would experience. Corefloods were also conducted at reservoir pressure to evaluate the miscible flood residual oil saturation, S_{orm}. First-contact miscible equimolar mixture of ethane, propane, and n-butane ($C_2C_3C_4$) was used to displace the reservoir oil in a non water-wet core at connate water saturation. The solvent was fond to leave a residual of approximately 10% after 10 PV throughputs. Based on the results of their study, it was concluded that water blockage, structure of the core, and PVT behaviour could not be blamed for the residual oil. It was, however, suspected that the interaction between the phase behaviour and bypassing is the cause of this residual in dead-end pores.

Thomas et al. (1994) pondered on the question of whether it is necessary to achieve miscibility in order to optimise the recovery, or whether a degree if immiscibility (near-miscibility) is adequate for field implementation of enhanced oil recovery. It was suggested that laboratory optimisation tests should concentrate on the interaction between viscosity,

IFT, and pore size distribution. This implies the quantification of IFT reduction and how it interacts with mobility in the pore size distribution, rather than on the assessment of what is miscible. They speculated that zero IFT is unnecessary in many cases, unless the pore throat size distribution is extremely tight and the rock is oil-wet.

Also in 1995, Thomas et al. provided evidence suggesting that many of the laboratory techniques used to design a gas injection project, as well as the interpretation of the tests were not really giving the information they were intended to provide. They said that specific testing can be made to gain insight into the most important features of a gas injection project, the interaction between the level of IFT or mobility, will enable the operator to concentrate on designing a gas to optimise the dominant factor. The authors suggested that most gas injection projects should involve a gas, which exhibits properties in the near-miscible range. This was supported by the fact that gas injection provides greater benefit than waterflooding, because as the IFT is reduced, smaller pore throat radii will be accessed by the injected gas and as long as the gas-oil IFT is lower than the water-oil IFT, gas injection, no matter how immiscible, would be of benefit. The major limitation of gas injection, however, is that it has a more adverse mobility ratio than water. Hence the most important question is, how the benefit of reduced IFT interacts with the adverse oil to gas viscosity ratio. This question, they said, should be the focus of laboratory tests aimed at designing gases for injection in enhanced oil recovery projects.

2.4.4 Spreading Coefficient

The spreading coefficient, along with wettability, affects the gas-oil-water distributions, and consequently the recoveries during a gas injection program (Blunt et al., 1994; Oyno et al., 1995; Vizika and Lombard, 1996). The spreading coefficient is a parameter that reflects the ‘balance’ between the three interfacial tensions in condensate/water/gas systems (Rowlinson and Widom, 1982). Mathematically, it can be expressed as:

$$S = \gamma_{wg} - (\gamma_{wo} + \gamma_{og}) \quad \text{.....5}$$

where γ_{ij} is the IFT corresponding to each pair of the various phases normally present in the system.

Although the above definition dates back to 1871, the importance of the spreading coefficient in determining the mechanisms involved in three-phase flow behaviour has only been recently appreciated. Experiments with three-phase systems are usually labour intensive, time consuming, and expensive. Therefore, empirical models such as Stone's model and Parker's model are often used to estimate three-phase properties from two-phase gas-oil and water-oil experimental data. These correlations do not include the spreading coefficient as one of the parameters explicitly and often lead to inaccurate predictions. Mani and Mohanty (1996) published an interesting paper that proposes a mechanistic model that includes the effects of the spreading coefficient on capillarity-controlled three-phase flow in porous media.

The equilibrium value of the spreading coefficient also determines the orientation and continuity of the fluid phase in the reservoir pores. Rao (2002) conceptually summarised the phase orientation dependence on the spreading coefficient and wettability. He reported that positive spreading coefficient conditions appear to be favourable from an oil recovery point of view. More recent experiments confirm that oil recovery by gas injection decreases with the magnitude of the spreading coefficient for systems with negative spreading coefficients and is independent of the spreading coefficient for positive spreading systems.

There are three primary displacement mechanisms involved in systems with negative spreading coefficients; namely, direct water drainage, direct oil drainage, and double drainage. Direct oil drainage and double drainage involve oil mobilisation and consequently lead to oil recovery. Direct water drainage process is preferred over double drainage if the spreading coefficient is highly negative. The residual oil saturation to gasflood starting after a waterflood is higher for nonspreading oils than for spreading oils. These displacement mechanisms remain the same for positive spreading coefficients, but with an important difference, which arises because oil spreads as a film between the gas and water phases in these systems. Oil gets trapped in three-phase systems if surrounded by gas-oil menisci on all sides. Such trapped oils may still be drained in spreading oil systems, but at very large gas-oil capillary pressures if connected by thick oil films.

The capillary pressure is a function of the pore radius, IFT, and the contact angle. According to Kalaydjian (1992), the contact angle in three-phase flow is strongly associated with the spreading coefficient of the system. If the spreading coefficient is positive, the oil spreads upon the water in the presence of gas and the resulting contact angle is zero degrees. Based on the results of his experimental work, Kalaydjian (1992) proposed the following expression for the drainage pressure curve in a three-phase system at irreducible water saturation:

$$P_c = P_{c0}(S_p) + S_g^{'}\alpha \qquad \text{where} \qquad S_g^{'} = \frac{S_g}{1 - S_{wir} - S_{org}} \quad \text{.....6}$$

where S_p denotes the spreading coefficient and P_{c0} denotes the threshold capillary pressure above which the drainage beings. Notice that the threshold pressure is a function of the spreading coefficient. As the spreading coefficient becomes more negative, the capillary pressure threshold decreases. This trend is consistent with the Leverett Function.

Kalaydjian (1992) observed that the spreading coefficient not only influences the threshold capillary pressure, but it also affects the residual oil saturation and the contact angle for both drainage and imbibitions processes. For example, consider the drainage experiments which are more prevalent to the tertiary gas injection process. The residual oil saturation to gas increased by less than 1 percentage from 1.0% to 1.3% as the spreading coefficient decreased from 15.7 to -1.1. However, the residual saturation increased sharply to 10% when the spreading coefficient was decreased to -4.8. The trend slowed again as only a 1.5% increase was observed between a spreading coefficient of -4.8 and -90.0. Kalaydjian (1992) also observed that the pressure required to drain an oil pocket in a negative system is nearly doubled compared to a positive system. Kalaydjian (1992) suggests that this increased drainage pressure is the reason why the residual oil saturation increases so dramatically once the spreading coefficient becomes negative.

The drainage experiments also directly verified the expression given previously relating the contact angle to the spreading coefficient and the IFT. A comparison of the contact angle estimated from the measured capillary pressure using the Laplace Equation and the contact angle estimated using Eq. 6 for negative spreading systems showed excellent agreement.

Also, the contact angle proved to be independent of the spreading coefficient and nearly equal to zero for the positive spreading systems.

Micromodel experiments (Oren and Pinczewski, 1994) to visualise and characterise the effects of wettability and fluid-fluid spreading on gas flood oil recovery prove that the positive value of the spreading coefficient helps ensure development and maintenance of continuous oil films between injected gas and reservoir water, thereby resulting in minimal losses of the injected gas to the reservoir water. On the other hand a negative value signifies a lens-type discontinuous distribution of oil between water and gas, thereby enabling gas-water contact and consequently lowers the oil recoveries. Although horizontal mode gas injection literature agrees with the inferences of Oren and Pinczewski (1994), the gravity drainage literature does not appear to be in unison about the effects of the spreading coefficient on oil recoveries. Most of the gravity drainage literature (Blunt et al., 1994; Oyno et al., 1995; Vizika and Lombard, 1996) suggests that the presence of oil films is instrumental in increasing oil recoveries in water-wet and mixed-wet porous media. Conversely, the absence of these oil films is responsible for the observed lower recoveries in oil-wet media. However, no agreement on the effects of the spreading coefficient value (positive, zero, negative) on oil recovery appears in the gravity drainage literature.

2.4.5 Relative Permeability

Relative permeability data act as a '*sword of two sides*' as on one hand it characterises the flow behaviour of multiphase fluids in reservoir strata and thus it is a critical parameter for evaluation of reservoir performance. On the other hand, the reliability of these curves is sometimes questionable even for simple fluids under stable conditions. Relative permeability curves are usually the first parameters to be adjusted when history matching reservoir performance. This complexity is magnified when dealing with gas condensate systems as all properties (including liquid dropout and wettability) would be expected to change rapidly (partly due to the large mass transfer between the phases) especially close to the thermodynamic critical points of the reservoir fluids. Accurate and reliable measurements of these data form the crux of the reservoir engineer's responsibilities and thus hold the key for better management of gas condensate reservoirs.

The literature recognises that relative permeability does impact the degree of productivity loss below the dewpoint (Afidick et al., 1994, Barnum et al., 1995). Whitson et al. (1999) showed that relative permeability effects in gas condensate reservoirs can be classified into three categories: (1) near-well steady-state gas/oil flow where saturation hysteresis is severe throughout the life of a well; (2) in the bulk of the reservoir far-removed from the wells, an imbibition process occurs throughout the life of the reservoir, where liquid mobility is (practically) zero and gas flows at a somewhat reduced permeability; and (3) water encroachment, where gas and/or retrograde condensate are trapped in quantities from 15 to 40 saturation percent, and water permeability can be significantly reduced. In terms of reservoir well performance, the near-well relative permeability behaviour is the dominant factor. The far-removed region of condensate accumulation has somewhat reduced gas relative permeability, but this effect is generally a second-order or negligible effect. Trapped saturations and reduced water relative permeability can be important for reservoir performance, but has no direct effect on well performance prior to water breakthrough.

Bourbaiux et al. (1994) and Kalaydjian et al. (1996) designed an experimental procedure to measure the critical condensate saturation (S_{cc}) and the relative permeabilities of natural gas and condensate. The authors also measured on-stream condensate dropout and local condensate saturation using a gamma ray attenuation technique with a specific method of calibration. The authors found that S_{cc} is related to initial water saturation (S_{wi}), with the total critical liquid saturation remaining constant around 26% of the pore volume for the cases they studied. Henderson et al. (1998) measured steady-state relative permeabilities for gas condensate fluids over a wide range of CGR (condensate to gas ratio), IFT and velocities. The authors found that relative permeabilities of both gas and condensate phases are rate sensitive and increase with velocity. The relative permeabilities were also sensitive to the IFT and increased with lowering of IFT.

Fischlock and Smith (1993) conducted experiments to investigate the effect of condensate formation on gas and oil relative permeability in the presence of connate water and three-phase flow in gas condensate systems under combined effect of waterflooding and pressure depletion. The authors observed a reduction in gas relative permeability by almost 60% for condensate saturation of about 23% in the presence of 19% water

saturation. They also observed that the presence of a condensate phase reduced both residual gas saturation to waterflood and critical gas saturation depressurisation. Hinchman and Barree (1985) showed how the choice between imbibition and drainage relative permeability curves could dramatically alter the productivity forecast below the saturation pressure for gas condensate reservoirs.

Chen et al. (1999) performed relative permeability measurements for two North Sea gas condensate fluids to investigate the effects of rock and fluid characteristics on critical condensate saturation and gas and condensate relative permeability. The authors used recombined fluids from two North Sea gas condensate reservoirs and 29 ft composite cores for their study. Their results showed that critical condensate saturation and relative permeability are sensitive to flow rate and interfacial tension. Chen et al. (1999) also showed the condensate relative permeability curve exhibits an unusual convex curvature when potted against condensate saturation. They suggest that high interfacial tension caused the decrease in condensate relative permeability with increasing condensate saturations. Saevareid et al. (1999) conducted steady state coreflood experiments for gas condensate fluids and measured gas and condensate relative permeability as a function of gas-oil interfacial tension and velocity. The authors showed significant improvement in gas and condensate relative permeability with capillary number.

Du et al. (2000), Walker et al. (2000) and Al-Anzi et al. (2003) showed from their coreflood experiments that condensate dropout reduced the gas relative permeability by an order of magnitude and the reduction is even more severe in the presence of high water saturation. The authors also showed that the decline in normalised PI (ratio of PI during two phase flow to PI during single phase flow i.e. ratio of damaged PI to original PI) is almost the same for both high and low permeability rocks. Al-Anzi (2003) also showed that non-equilibrium mass transfer phenomenon occurred in the cores at high flow rates and required more pore volumes of injected fluid to reach steady-state than if local equilibrium existed in the cores. Ayyalasomayajula et al. (2003) conducted steady state coreflood experiments for gas condensate fluids and measured gas and oil relative permeability as a function of capillary number for several different reservoir rocks and for a wide range of K_{rg}/K_{ro} values. The authors showed significant improvement in gas relative permeability with capillary number for all the rock types. The relative permeability

measurements for gas condensate fluids done by various authors have been analysed by expressing gas and condensate relative permeability as a function of K_{rg}/K_{ro} and capillary number.

Gravier et al. (1986) studied rock samples (0.4 to 50 md) from a carbonate gas field to determine gas and condensate relative permeabilites using a ternary pseudo-reservoir fluid of methane/pentane/nonane. They measured the critical condensate saturation and the extent of the reduction of permeability to gas in the presence of immobile condensate saturation. Their results showed that the gas relative permeability decreased from an average value of 0.68 to about 0.10 when the condensate saturation increased from 0 to 30%. The gas relative permeability decreased when the initial water saturation increased. The measured critical condensate saturation was found to be high, ranging from 24.5% to 50.5%.

Danesh et al. (1989) studied the phenomenon of retrograde condensation and flow of gas condensate fluids in porous media using glass micromodels and sandstone cores. The authors observed that the initial formation of condensate in pores is a film-wise process with a hydraulic conductivity throughout the pores. The authors show that at low IFT values the effect of capillary forces become negligible compared to viscous and gravitational forces. The authors also suggest that as condensate forms as a film over the interstitial water, the flow of gas condensate fluid is expected to be different than that of low IFT gas-oil displacements. Munkerud (1989) showed that the relative permeability curves for the gas condensate model system in a depletion process are similar to curves of ordinary gas/oil systems and that gravitational segregation of condensate is pronounced even at liquid saturation below the critical saturation. The author also observed that relative permeability to both gas and oil show strong dependence on IFT.

Nagarajan et al. (2004) compared gas condensate relative permeability measurements for rich and lean reservoir fluids with synthetic fluids. They concluded that relative permeability for reservoir fluids is lower than those measured with model fluids at any given liquid saturation or for the same K_{rg}/K_{ro} ratio. The comparison presented by the authors may not be totally conclusive as there is a lot of inconsistency in these measurements. The measurements done using rich reservoir fluid are compared with synthetic fluids made of either n-heptane and water which does not represent a gas-oil

system or a methane and n-butane binary mixture, which does not have any heavier hydrocarbons to closely imitate heavier components of the rich gas mixture. Also the results are in contradiction with those presented by Mott et al (2000) using reservoir fluids and Kumar et al. (2006) using synthetic gas mixtures which agree with each other over a wide range of capillary numbers.

Kumar et al. (2006) measured gas and condensate relative permeabilities on both sandstone and limestone rocks over a wide range of conditions and fluid type. Measurements were made over a wide range of capillary number (10^{-6} to 10^{-4}). The authors expressed the relative permeability as a function of the capillary number and K_{rg}/K_{ro} ratio and show a significant improvement in relative permeability for capillary numbers greater than 10^{-4}. The authors however neglected the effects of non-Darcy flow, which can be significant at the high flow rates that were used to achieve high capillary numbers. Some researchers including Henderson et al. (1993, 1995) and Bourbiaux and Limborg (1994) have placed a lot of emphasis on the importance of saturation measurements to get the relative permeability curves. Whereas, others including Fevang and Whitson (1995), Fevang (1996), Fevang and Whitson (2000), Ayyalasomayajula et al. (2003), Mott et al. (2000 and 2002), Al-Anzi et al. (2003), Du et al. (2000), and Kumar et al. (2006) showed in their work that condensate saturation near the well does not play a significant role as long as the functional relationship between K_{rg} and K_{rg}/K_{ro} remains the same. They also show that $K_{rg}= f(K_{rg}/K_{ro})$ is the underlying relative permeability relationship determining well deliverability in gas condensate reservoirs. The ratio of K_{rg} to K_{ro} is a function of fluid properties at steady-state (Chopra and Carter, 1986). The fluid properties can be measured by standard PVT experiments.

2.5 Conclusion

This chapter has presented a critical appraisal of the relevant, up-to-date, state-of-the-art literature. It demonstrates the theme of gas condensate reservoirs with emphasis on their distinctive thermodynamics. The chapter covers relevant research findings on mass transport, dispersion and diffusion, interfacial tensions, the need for miscibility development, and relative permeabilities. These concepts are argued and compared with the findings of this research work in the next three chapters.

CHAPTER III

EXPERIMENTAL INTERFACIAL TENSION MEASUREMENTS

This chapter provides a general overview of interfacial phenomena with emphasis on experimental measurement procedures, data analyses, and actual contributions to the petroleum industry. It intends to analyse how the condensate-CO_2 interfacial tension (IFT) and the condensate-wetting behaviour depend on the reservoir thermodynamic conditions.

3.1 Overview

Surface science, historically described as the *world of neglected dimensions*, has more recently been recognised as a vital, if not the vital, component of multiphase fluid flows and recovery processes (Myers, 1999; Hartland, 2004). Surface and interfacial tension is a Newtonian measure of the cohesive (excess) energy present at an interface arising from the imbalance of forces between molecules (gas/gas, gas/liquid, liquid/liquid, gas/solid, and liquid/solid) (Stegemeier, 1959). The common units for this tension are dyne/cm or mN/m.

Petroleum sedimentary rocks are generally permeated by water, oil (or condensate), gas or more often a combination of these fluids. The recovery of such fluids depends on two factors; namely, the microscopic (local) displacement efficiency and the macroscopic (global) sweep efficiency (Pande and Orr, 1989). The latter parameter is characterised by the combined effect of injection patterns, mobility ratio, reservoir heterogeneity, and gravity segregation (Green and Willhite, 1998). The microscopic displacement efficiency is determined by the phase behaviour, interactions of rock pore geometry, and interface boundary conditions (Green and Willhite, 1998). These interactions affect what is known as the spreading coefficient and thus reservoir wettability. Interfacial phenomenon in porous rocks lies at the heart of hydrocarbons recovery as it determines the fraction of hydrocarbons that moves from the swept region toward a producing well. Over the past 15 years or so, there has been a resurgence of interest in developing a more quantitative understanding of displacement mechanisms.

This chapter takes up this challenge with objectives to:

1. Provide a rich summary of the most popular techniques utilised to predict the interfacial tension of various systems in the petroleum industry. This summary includes also the tuning procedures that are normally employed to ensure reliable interfacial tension prediction for real reservoir fluids for reservoir simulation purposes,
2. Investigate the behaviour of interfacial tension of methane (CH_4), nitrogen (N_2) and carbon dioxide (CO_2) with both condensate and brine at various pressure and temperature conditions,
3. Investigate the behaviour of the spreading coefficient with pressure.

The experimental findings presented in this chapter are unique in the sense that the vast majority of previous research has focused on studying the interactions between the co-existing natural gas and the liquid condensate in attempts to understand the phase couplings and mass transfer between original reservoir components. This study, however, investigates the interfacial tension and fluid properties of various injection gases with both reservoir condensate and brine. This provides a narrow footbridge between injection gases (that are normally used as solvents in conventional oil reservoirs) and enhanced condensate recovery in gas condensate reservoirs.

3.2 Prediction Techniques

As is usually the case with many fluid properties, the time and cost involved in obtaining sufficient experimental data for wide ranges of conditions are sometimes prohibitive. Hence, predictive, often empirical or semi-empirical, techniques are employed to estimate such properties. Numerous studies have proposed a wide spectrum of techniques that can be used to predict IFT between reservoir fluids and between reservoir/solvent systems. Various researchers have related the vapour-liquid IFT of pure compounds to a number of fluid properties, such as the density, compressibility and latent heat of vaporisation.

The parachor method (Weinaug and Katz, 1943) and the scaling law (Lee and Chien, 1984) are, by far, the two most commonly used techniques in the petroleum industry for predicting the IFT. MacLeod (1923) recognised based on experimental observations the following relation between surface tension and densities:

$$\frac{\sigma}{(\rho_l - \rho_v)^4} = C \quad \text{.....7}$$

Sugden (1924) related the constant C to the chemical composition of the substance. This parameter, often called parachor, P_σ, represents the molecular volume and chemical composition of a compound under conditions where the effect of temperature is neutralised:

$$P_\sigma = \frac{MW}{\rho_l - \rho_v}\sigma^{\frac{1}{4}} \quad \text{.....8}$$

where σ is the interfacial tension, *MW* is the molecular weight, P_σ is the parachor and, ρ_l and ρ_v are the densities of the liquid and vapour phases respectively.

The parachor is a unique dimensionless constant characteristic of a pure compound that is independent of temperature and pressure. Different correlations have been reported in the literature for estimating the parachor constant. Weinaug and Katz (1943) extended the Macleod-Sugden equation for multi-component systems, treating a mixture as a one-component fluid by using the molar average rule for calculating its parachor value:

$$\sigma^{1/4} = \left[\sum_{i=1}^{i=n} P_{\sigma i} x_i\right](\rho_l)_m - \left[\sum_{i=1}^{i=n} P_{\sigma i} y_i\right](\rho_v)_m \quad \text{.....9}$$

where $(\rho_l)_m$ and $(\rho_v)_m$ are the liquid and vapour phase molar densities respectively, $P_{\sigma i}$ is the parachor value of component *i* in the mixture, x_i is the molar composition of component *i* in the liquid phase, and y_i is the molar composition of component *i* in the vapour phase.

Firoozabadi and Ramey (2007) reported that the IFT between water and pure hydrocarbons can be attributed to the phase density difference using the following function:

$$\text{IFT Function} \equiv \frac{(\sigma_{hw})^{0.25}(T/T_c^h)^{0.3125}}{\rho_w - \rho_h} \quad \text{.....10}$$

where σ_{hw} is the hydrocarbon water IFT and T_c^h is the hydrocarbon phase critical temperature.

The reliability of this relationship was established for various compounds ranging from methane to dodecane. The function can be represented by the following single curve:

$$\sigma_{hw} = 111(\rho_w - \rho_h)^{1.024}(\frac{T}{T_c^h})^{-1.25} \quad \text{.....11}$$

where IFT is in dyne/cm, ρ_w and ρ_h correspond to the respective water and hydrocarbon phase density in g/cm^3.

Ramey (1973) suggested a graphical correlation for water/hydrocarbon interfacial tension estimation (Ahmed, 2007). This correlation was curve-fit by Whitson and Brule (2000) through the following expression:

$$\sigma_{hw} = 20 + 0.57692(\rho_w - \rho_h) \quad \text{.....12}$$

Lee and Chien (1984) developed a semi-empirical approach, based on critical scaling theory (Stanley, 1971), for calculating the IFT between two equilibrium phases:

$$\sigma^{1/3.911} = [P_{\sigma l}(\rho_l)_m] - [P_{\sigma v}(\rho_v)_m] \quad \text{.....13}$$

for each component, the parachor is calculated from Eq. 14:

$$P_\sigma = A_C^{45/176}(V_C)_m / B \quad \text{.....14}$$

where $(V_c)_m$ is the molar critical volume of the component, and A_c is a constant, dependent on critical properties and the boiling temperature of component, calculated from the following expression:

$$A_C = P_C^{2/3} T_C^{1/3}(0.133\alpha_C - 0.281) \quad \text{.....15}$$

where P_c is the critical pressure of component, T_c is the critical temperature of component, and α_C is the Riedel parameter evaluated from the expression:

$$\alpha_C = 0.9076\left[1.0 + \frac{(\ln(P_C / P_a)(T_b / T_C))}{(1 - T_b / T_C)}\right] \quad \text{.....16}$$

where T_b is the boiling temperature of component, P_a is the atmospheric pressure, b is a constant which could be estimated from the component's IFT. For some pure hydrocarbon compounds, b, has been correlated to the critical compressibility factor (Z_c) as in Eq. 17:

$$b = 1.854426 Z_C^{-0.52402} \quad \text{.....17}$$

For multi-component fluids, the molar average mixing rule is used to calculate the values of the above parameters, both for the liquid and vapour phases.

Other predictive models (Brock and Bird, 1952; Hough and Stegemeier, 1961; Hugill and Welsenes, 1986) have also been used in the literature for IFT prediction. These models have more or less the same functional form, except that they employ different values of the critical exponent. The correlation of Firoozabadi et al (1988) can be used to approximate the parachor of pure hydrocarbon fractions from C_1 through C_6 and for C_{7+} fractions:

$$(P_{ch})_i = 11.4 + 3.23 M_i - 0.0022 (M_i)^2 \quad \text{.....18}$$

Katz and Saltman (1939) suggested the following expression for estimating the parachor for C_{7+} fractions as:

$$(P_{ch})_{C_{7+}} = 25.2 + 2.86 M_{C_{7+}} \quad \text{.....19}$$

3.3 Experimental Program

Some twenty different methods have been suggested in the literature for determining the boundary tension of adjoining phases. Surprisingly, only three or four have been commonly adopted in practice, namely the classical capillary rise, the drop weight, the spinning drop and the pendant drop. Padday (1969) in his excellent review and the book by Rusanov (1996) have discussed extensively the various techniques that have been used for measuring interfacial tensions.

This study incorporates the pendent drop technique for IFT measurements at various thermodynamic conditions. This method is probably the most convenient, versatile and

popular technique for high-pressure high-temperature (HPHT) and low IFT measurements (Akutsu et al. 2007). The experimental assembly is essentially made up of a temperature control system, a flow system and a photographic system. The photographic system consists of a stereo-zoom microscope with exposure controller and a fibre-optic light source. The HPHT experimental gear is shown schematically in **Fig. 10** and graphically in **Fig. 11**.

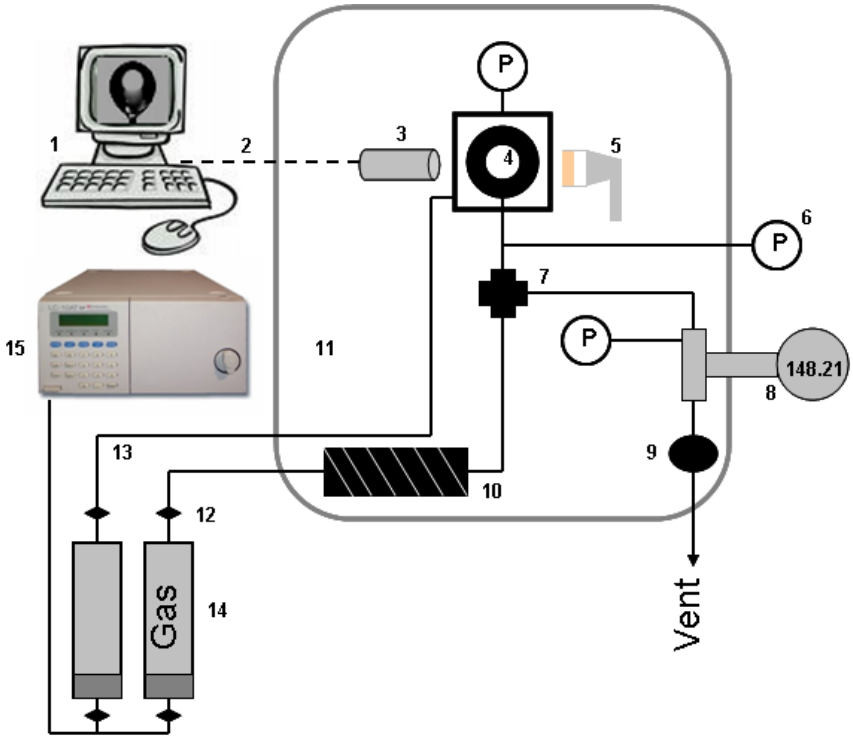

Fig. 10 - HPHT Pendant Drop Facility Schematic

Legend:

1: computer, 2: instrumentation lines, 3: microscope and capturing camera, 4: pendant drop cell, 5: fiberoptic light and diffuser, 6: pressure transducer, 7: two-way valve, 8: Sarasota density meter, 9: back-pressure regulator, 10: stainless steel coil, 11: temperature-controlled air bath, 12: one-way valve, 13: high-pressure 1/16" tubing, 14: fluid cylinders, 15: Shimadzu LC-20AT pump.

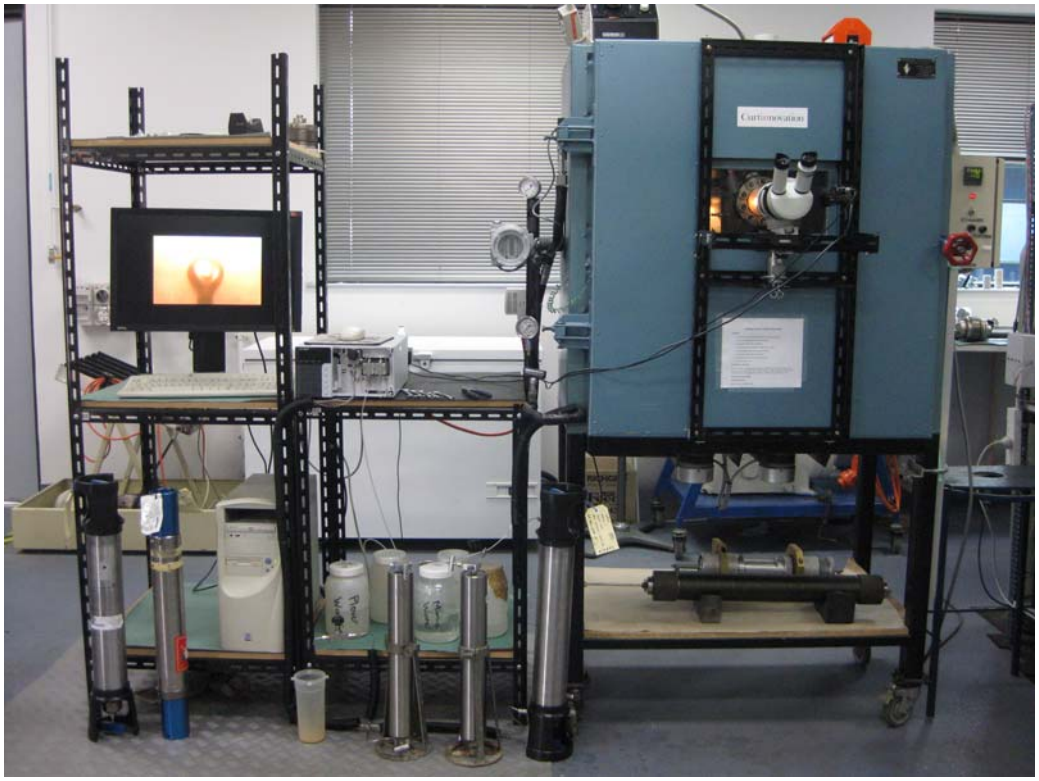

Fig. 11 - HPHT Pendent Drop Facility Photograph

The experimental chamber and illuminating systems were housed inside a precise temperature-control double-walled oven (supplied by Furnace Technologies). A very low heat conduction glass served as an access window for capturing images. A uniform deviation-free stainless-steel fine needle (1 mm outer diameter) was mounted inside the cell to permit the measurements of IFT's in the range of 1000 to 8000 psi. The IFT experimental chamber firmly rested on an extension vibration-free arm in the air bath. A built-in high speed stirrer was used to obtain a positive circulation of the air in the path. This fan was directing the air first along the heaters and then around the equilibrium cell.

3.3.1 Fluids

CO_2, CH_4 and N_2 gases used throughout these investigations were supplied by BOC Gases. They all had a reported purity of 99.99%. The brine was synthetically made based on water analysis from a local reservoir in Western Australia with molar concentrations of 0.00612 NaCl, 0.001199 KCl and 0.992681 distilled water. The condensate sample had a

calculated density of 0.8161 g/cc at 15 ^{o}C and a molecular weight of 175.8 g/mol. The composition of this sample is shown in **TABLE 1** (Appendix I). **TABLE 1** demonstrates that no methane or ethane components were present and that C_1-C_{10} forms 38.93 mole% of the sample. The density of the gases, brine and condensate at each test point was experimentally measured using a Sarasota density meter (component 8 in Fig. 10). The density meter was manufacture-calibrated. On the registration certificate, it is stated that the calibration is traceable to national standards and that the calibration accuracy is within $\pm 2E-6$ g/cc. These chemicals were employed without any further modification or purification.

3.3.2 Procedures, Precautions and Data Analysis

Preliminary air-water IFT measurements were conducted to calibrate the drop about the central vertical axis of the needle as well as to determine whether the IFT value for this 'reference' system matches the value within literature. The measured IFT value for this system was 73 dyne/cm which was in perfect agreement with the American Society for Testing and Materials standards at atmospheric conditions (ASTM, 2009). The experimental chamber was then prepared to carry out various investigations for this study. This preparation included cleaning the entire cell with mineral turpentine, flushing with air and then purifying and purging it with the test gas twice prior to performing any experiments. The high pressure optical cell was initially charged with brine and was then kept for an hour to heat up to test temperature. The test gas was subsequently injected through the needle from a Core Laboratory cylinder placed in the neighbourhood of the cell inside the oven in a highly controlled process to form the pendant drops. The thermofluid system was allowed to reach thermal and pressure equilibrium at the desired temperature before any data points were taken. The drop profile images were then photographed with the aid of a digital Watec colour camera (model WAT-202B) and captured through a computerised program as video clips and pictures for subsequent image analysis, digitisation and computation. This procedure was repeated for test gas and condensate IFT measurements.

The accuracy of the IFT measurements was a priority concern. The accuracy was therefore attained using the following 4-step quality control procedure:

1. The thermodynamic system was designed to ensure it remained vibration-free throughout the investigations,
2. The equilibrium pressure and temperature readings were monitored using high precision gauges,
3. The drop was allowed to remain at the tip of the needle for identifiable periods of time (around 15 minutes as an equilibration time) so as to make sure that only IFT and gravity forces were in action, and thus viscosity and inertia played no part in the shape of the drop,
4. Every single measurement was repeated at least 4 times to ensure data reliability.

The IFT values were calculated directly from measurements of parameters indicative of drop shape, such as the maximum diameter and the height of the position of maximum diameter above the base of the drop; adopting the following well-established equations by Andreas at al. (1938):

$$\gamma = \Delta\rho.g.d_e^2/H \quad \text{.....20}$$

$$H = f(d_s/d_e) \quad \text{.....21}$$

where $\Delta\rho$ is the density difference between the two phases in (g/cc), d_e is the unmagnified equatorial diameter of the drop in (cm), g is the gravitational constant (981 cm/s^2), d_s is the diameter of the drop at a selected horizontal plane corresponding to the height equal to the maximum diameter d_e in (cm) and H is the dimensionless drop shape factor which is a function of d_s/d_e as shown in Eq. 21 above. The corresponding H value for each data set was read from well-documented tables in Danesh (1998).

3.4 Results and Discussions

This section serves as the backbone of this chapter in that it presents the experimental results of fluid densities, IFT data points as well as the spreading coefficients at various pressure and temperature conditions. The density measurements are depicted as density-differences between each fluid pair as shown in **Fig. 12** and **Fig. 13**. The spreading coefficients compare the isothermal condensate-wetting behaviour for each injection gas under investigation.

3.4.1 Density Measurements

The densities of nitrogen, methane, carbon dioxide, condensate and brine were separately measured using the Sarasota density meter at two temperatures and various pressures. Rather than graphically displaying individual density values, Fig. 12 demonstrates the density-difference between each fluid pair at a temperature of 95 ^{o}C. This particular representation was deemed helpful as it makes appropriate links to Eq. 20. The labels on the graphs represent the order of subtraction, e.g. the condensate-CO_2 curve displays the data for condensate density minus CO_2 density at the corresponding pressure and temperature.

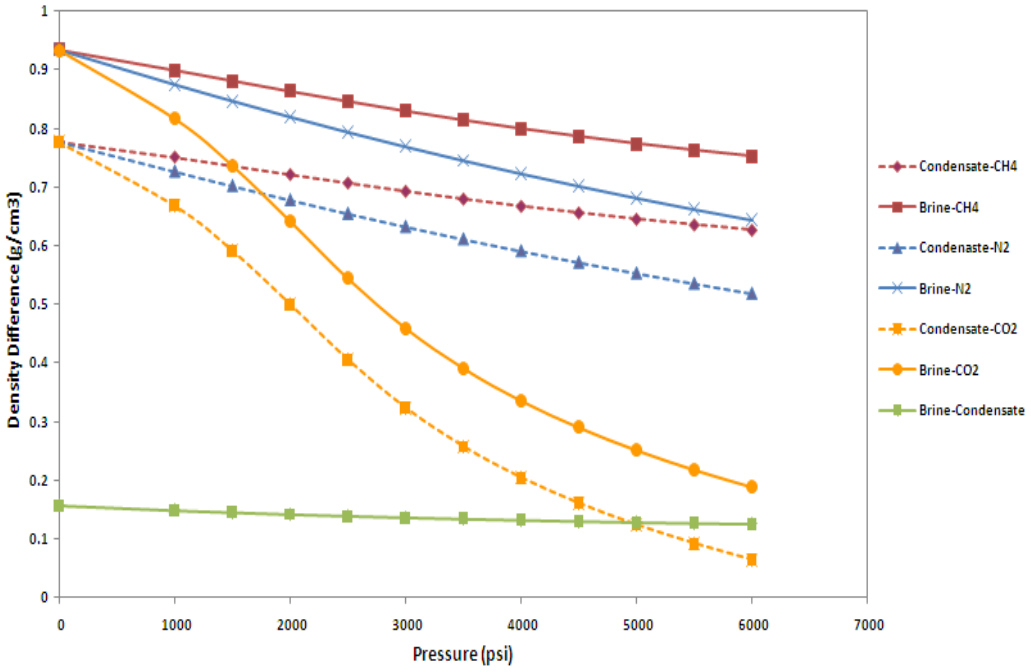

Fig. 12 - Density Difference as a Function of Pressure at 95 ^{o}C

Fig. 12 shows that (Al-Abri and Amin, 2010b):

1. Solid lines indicate that injection gases produce greater density-differences with brine than with condensate (dashed lies) for all test pressures. This indicates that brine is denser than condensate. The hierarchy of the density values would be expected to make brine segregate towards the bottom of the reservoir in an equilibrium three-phase fluid system,

2. Solid lines also indicate that injection gases result in almost the same density-difference with brine at atmospheric pressure and that this difference tends to decrease much faster with pressure in the brine-CO_2 system,
3. Dashed lines indicate that injection gases result in almost the same density-difference with condensate at atmospheric pressure and that this difference tends to decrease much faster with pressure in the condensate-CO_2 system,
4. Nitrogen and methane density-differences with both brine and condensate produce approximately linear trends but with different slopes. CO_2, however, produces a density-difference trend close to a third-order polynomial function with both brine and condensate,
5. Brine-condensate and condensate-CO_2 density-difference curves cross over at a pressure of 5000 psi.

Fig. 13 illustrates the effect of increasing the temperature to 160 ^{o}C on the density-difference values for all systems under investigation. The same comments apply to this graph as the previous one, except for the following three differences (Al-Abri and Amin, 2010b):

1. The density-differences shift downwards for all systems,
2. The brine-CO_2 and condensate-CO_2 show approximately straight lines at 160 ^{o}C,
3. There is no cross over between the brine-condensate and condensate-CO_2 density-difference curves in this graph.

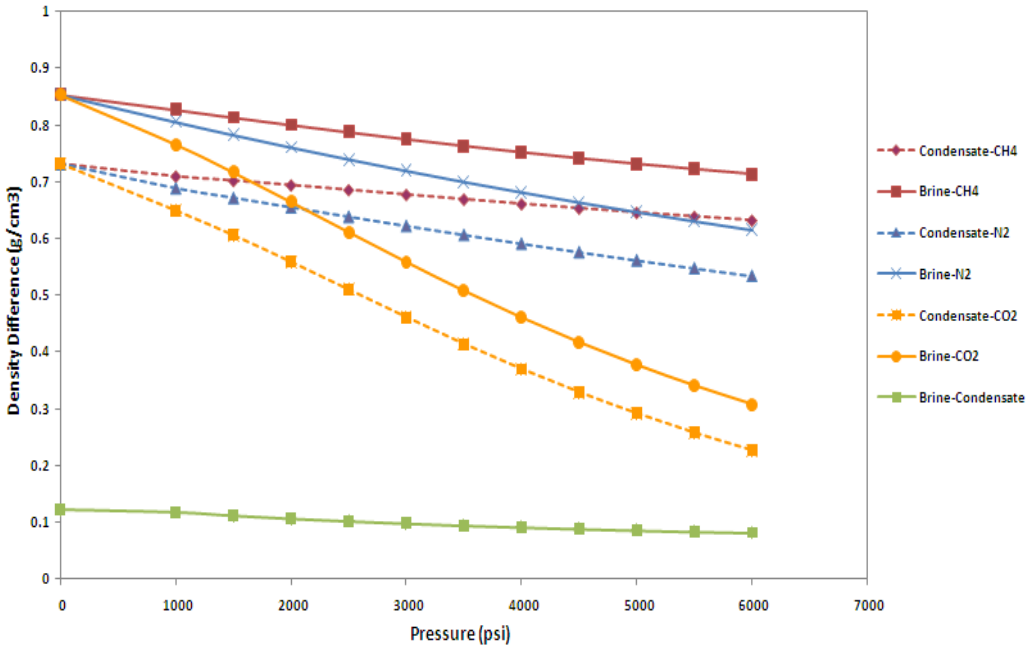

Fig. 13 - Density Difference as a Function of Pressure at 160 ^{o}C

3.4.2 IFT Measurements

Fig. 14 demonstrates that while pressure acts to reform the surface molecules of the gas drop and thus lowers the internal cohesions within the two adjoining phases of all pairs, the effect was more pronounced in the CO_2/brine system (solid green line). The gas drop capture in the brine medium was observed to have less physical volume with pressure for the three pairs resulting in a quantitative IFT decline with a comparatively steep decrease within the lower pressure range (Al-Abri and Amin, 2009). The N_2 drop, for example, was observed to experience a 9% decline in the IFT data when the pressure was increased six-fold (i.e. from 1000 psi to 6000 psi) for both test temperatures (solid and dashed blue lines). Fig. 14, in addition, illustrates that the magnitudes of the IFT values of the CH_4/brine system were approximately 6% lower each point than those of the N_2/brine system indicating relatively greater methane mixing and solubility in saline water as opposed to that of nitrogen at a given pressure and temperature (Al-Abri and Amin, 2010b). CO_2 miscibility into brine, interestingly, was found to increase a great deal with pressure as the IFT values drop almost 63% at both test temperatures (solid and dashed green lines).

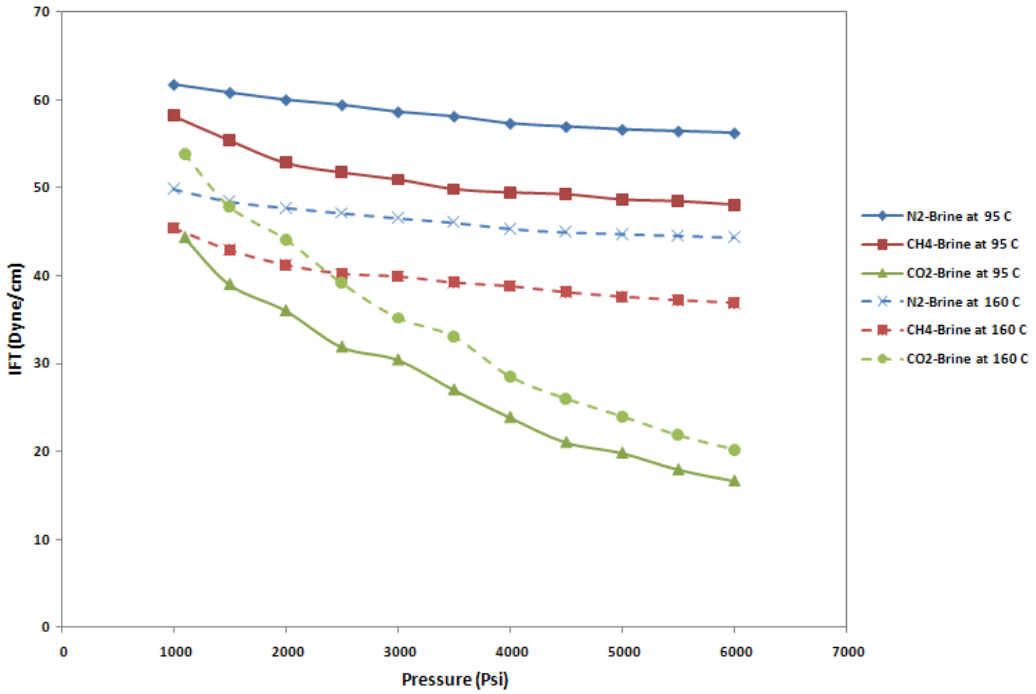

Fig. 14 - Gas-Brine IFT Behaviour at 95 ^{o}C (Solid Lines) and 160 ^{o}C (Dashed Lines)

The influence of temperature on the IFT behaviour deserves a careful examination and discussion. Temperature, as conventionally-known, tends to decrease the surface tension of any given system at any given pressure. This hypothesis suggests that the cohesive forces decrease as molecules vibrate at a higher frequency with temperature. This hypothesis is true for the N_2/brine and CH_4/brine systems. **Fig. 15** shows that the interface was more sensitive to temperature than pressure for aforementioned systems as the IFT magnitudes were 19% and 22% less respectively when test temperature was increased from 95 ^{o}C to 160 ^{o}C. The IFT behaviour was observed to be more temperature-dependent as opposed to pressure. Interestingly, for reasons related to the intermolecular bonding and the chemistry difference between fluid pairs under investigation, CO_2 responds differently to temperature. Fig. 15 shows that the IFT values increased around 18% when the temperature was increased from 95 ^{o}C to 160 ^{o}C at any test pressure (Al-Abri and Amin, 2010b).

The importance of these results arises when recognising that a great amount of reservoir water is usually left behind in the stratum following a waterflooding displacement scheme. Integrating these results with the other IFT data corresponding to the rest of the

present phases will offer the optimum design for a successful gas injection-enhanced recovery project. In addition, these results will play a key role in the design and execution of CO_2 geo-sequestration projects in saline aquifers that are usually immediately accessible and are found in all sedimentary basins.

Fig. 16 presents the gas fluid-condensate IFT results as a function of pressure and temperature. The blue curves show that pressure significantly reduces the IFT between the N_2 drop and the condensate. The IFT declined by a factor of 10 when the pressure was increased from 1000 psi to 6000 psi at 95 ^oC (solid blue line). The N_2 drop was observed to attain complete miscibility (zero IFT) with the condensate at 7400 psi at 95 ^oC. In addition, the red curves demonstrate a shift downwards in the IFT values for CH_4/condensate system by approximately 3 dyne/cm compared to the previous N_2/condensate system. This suggests that CH_4 exhibits more solubility with the condensate (Al-Abri and Amin, 2010b). These observations benchmark Sanger and Hagoort (1998) investigations on the efficiency of nitrogen to evaporate condensates compared to methane. The authors submit that the evaporation capacity of methane is more than 20 times higher than that of nitrogen.

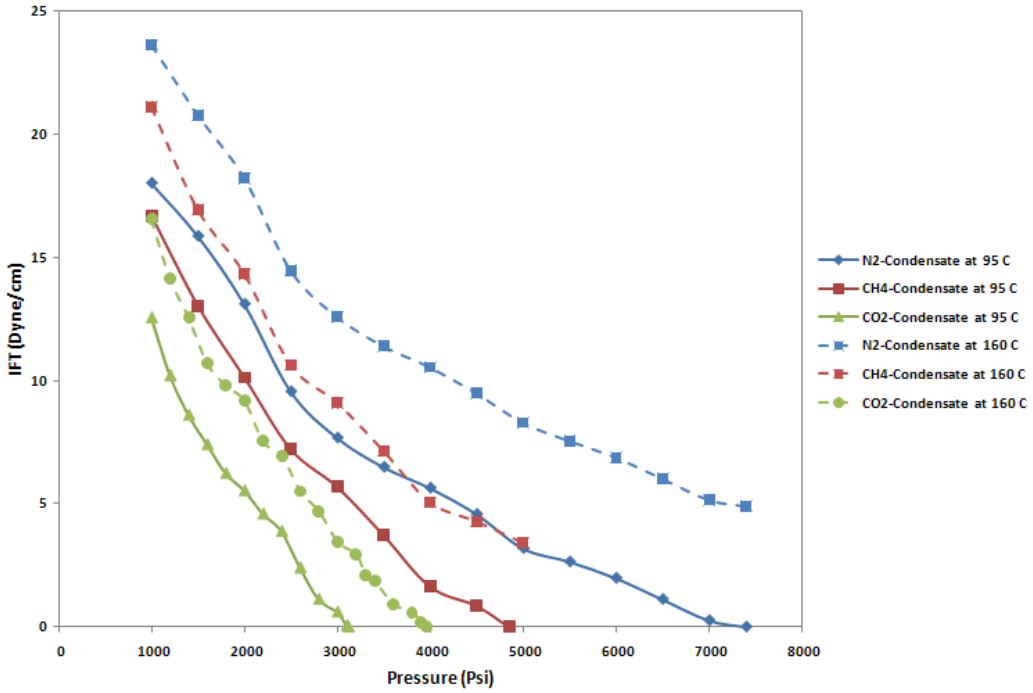

Fig. 15 - IFT Behaviour for all Test Gases with Condensate at 95 ^{o}C (Solid Lines) and 160 ^{o}C (Dashed Lines)

Furthermore, the CH_4/condensate system showed more response to pressure for a given temperature than the N_2/condensate fluid pair as the slope for this system is somewhat steeper. Methane and condensate become completely miscible (i.e. zero IFT) at 4780 psi at 95 ^{o}C; 2620 psi less than N_2 minimum miscibility pressure (MMP) at the same temperature. The green curves suggest that CO_2 becomes miscible with condensate at 3120 psi at 95 ^{o}C. This is a major advantage of the CO_2 miscible process as dynamic miscibility can be achieved at attainable pressures in a broad spectrum of reservoirs (Al-Abri and Amin, 2009; Al-Abri and Amin, 2010b). These observations provide a quantitative explanation for Ahmed et. al. (1998) studies on the effectiveness of lean gas, N_2 and CO_2 huff 'n' puff injection technique in removing the liquid accumulated in and around the wellbore. Ahmed et. al. (1998) reported that pure CO_2 is the most effective gas in reducing liquid dropout compared to others when injected at the same pressure.

Fig. 15 shows that the three systems respond in a similar fashion to temperature. The IFT between the N_2 drop and the condensate was observed to increase in excess of 20%

when the temperature was increased from 95 ^{o}C to 160 ^{o}C for any given pressure (solid and dashed blue lines). This suggests that N_2 mixing with the condensate decreases with temperature. The IFT profiles for CH_4 and CO_2 follow the same pattern; increase with temperature. CO_2 achieves complete miscibility with the condensate at 3960 psi at 160 ^{o}C. High temperatures, representative of abnormal or deep reservoirs, tend to increase the surface tension between the N_2 drop and condensate.

Fig. 16 illustrates the variation of condensate-brine IFT, with pressure and temperature. The IFT was observed to decrease with pressure and temperature (Al-Abri and Amin, 2009). The effect of pressure on IFT of pure liquid-hydrocarbons-water is generally small and can be neglected in most cases (Danesh, 1998).

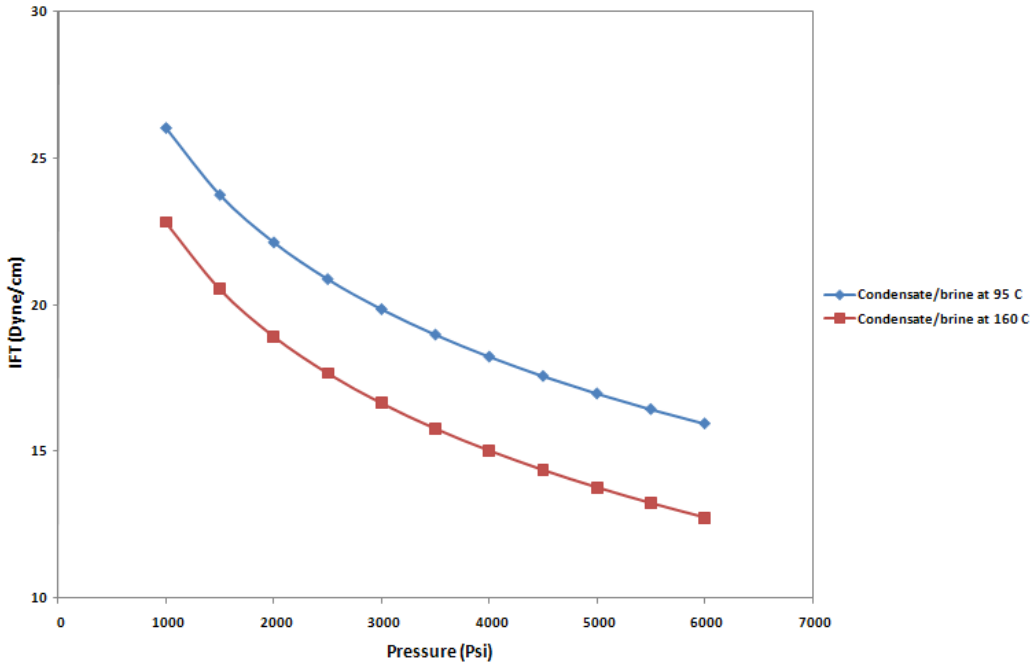

Fig. 16 - IFT Behaviour for Condensate with Brine at 95 ^{o}C (Blue Line) and 160 ^{o}C (Red Line)

3.4.3 Spreading Coefficients

This section investigates the 'balance' between the IFT of the three co-existing reservoir phases which, in turn, will determine the condensate recoveries in gasfloods. Rowlinson and Widom (1982) defined the spreading coefficient for a water-wet system as:

$$S = \gamma_{wg} - (\gamma_{wo} + \gamma_{og}) \quad \text{.....22}$$

where γ_{ij} is the IFT corresponding to each pair of the various phases normally present in the system.

The spreading coefficients of the fluid systems under investigation as a function of pressure and temperature are shown graphically in **Fig. 17**. It shows that all systems have positive spreading coefficients indicating the presence of continuous condensate films (in the centre of the pores) over the water films covering the rock grains. This will not only increase the condensate drainage phenomena (during gas injection) at lower pressure drops, but will also provide continuous 'conduits' that guide isolated condensate globules toward the production well, thereby resulting in minimal losses of the injected gas to the reservoir water (Al-Abri and Amin, 2009; Al-Abri and Amin, 2010b). On the other hand, negative values would have signified a lens-type discontinuous distribution of condensate between water and gas, thereby enabling gas-water contact and consequently lowering the condensate recoveries.

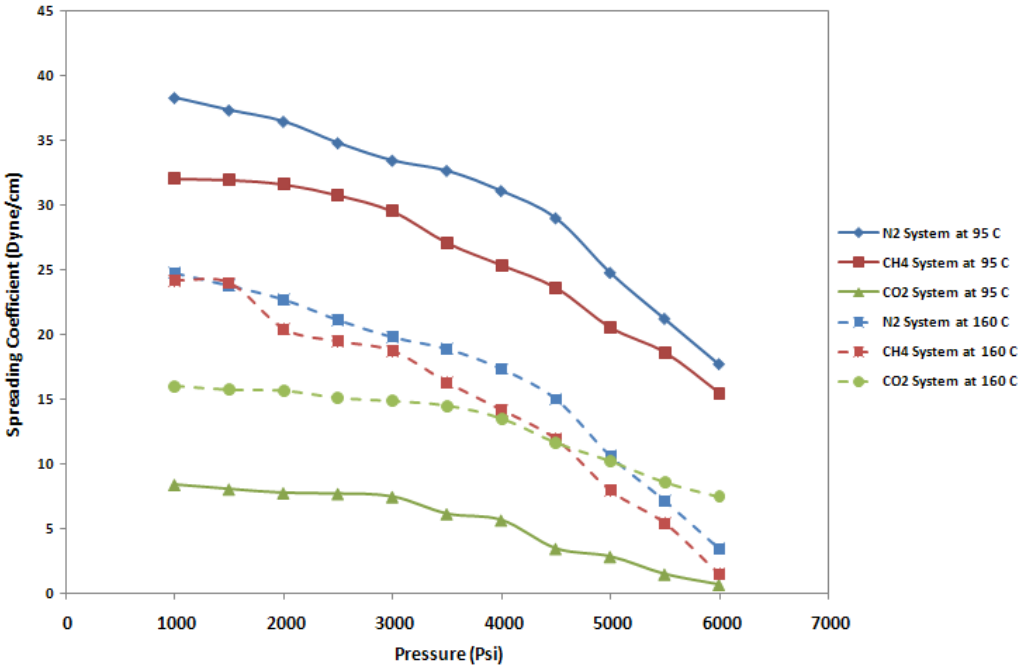

Fig. 17 - Spreading Coefficient as a Function of Pressure for all Systems

3.5 Conclusion

Complete with a considerable amount of experimental data and extensive references to literature on this specific topic, this chapter provides an important reading for petroleum and chemical engineers assessing the productivity of gas condensate reservoirs, and evaluating the distribution and flow characteristics of immiscible and miscible fluids through a porous structure. This chapter concludes that:

1. The hierarchy of the experimental density values of each of the injection gases with brine and condensate indicates that brine would segregate towards the bottom of the pore space in an equilibrium three-phase fluid system,
2. Nitrogen and methane density-differences with both brine and condensate show approximately linear trends but with slightly different slopes. Carbon dioxide, however, produces a density-difference trend close to a third-order polynomial function with both brine and condensate at 95 ^{o}C,
3. The density-differences tend to decrease for all systems when test temperature is increased to 160 ^{o}C,

4. The equilibrium IFT decreases with pressure for the CO_2-brine, CO_2-condensate, CH_4-brine, CH_4-condensate, N_2-brine, and N_2-condenaste systems. This indicates that gas solubility increases with pressure at a given temperature,
5. The drop interface of the N_2/brine and CH_4/brine systems was observed to be more sensitive to temperature than pressure as the IFT magnitudes were 19% and 22% lower respectively when temperature was increased from 95 ^oC to 160 ^oC,
6. Nitrogen, methane and carbon dioxide were observed to achieve complete miscibility with the condensate at 7400, 4780, and 3120 psi respectively at 95 ^oC,
7. The spreading coefficient remained positive throughout the tested pressure range at 95 ^oC indicating the presence of continuous condensate films (in the centre of the pores) over the water films covering the rock grains. These observations suggest the magnitude of the condensate drainage during gas injection as well as losses of injected gas to the reservoir water,
8. Gas injection at very low IFT (order of 10^{-2} dyne/cm) could effectively recover the condensate.

CHAPTER IV

EXPERIMENTAL RELATIVE PERMEABILITY MEASUREMENTS

Flow in porous media is a very complex phenomenon and cannot be described as explicitly as flow through pipes or conduits. It is rather easy to measure the length and diameter of a pipe and compute its flow capacity as a function of pressure; however, in porous media flow is different in that there are no clear-cut flow paths which lend themselves to measurement. This multiphase flow can be related to the relative permeability of each phase, fluid viscosities, pressure drop, capillary pressure, and permeability. Of these parameters, relative permeabilities are the least understood and the most difficult quantities to measure (Saraf and McCaffery, 1985). This chapter describes both qualitatively and quantitatively relative permeability, mobility ratio, displacement front stability, and recovery performance of CO_2 injection into gas condensate reservoirs.

4.1 Overview

Field and laboratory displacement data are conventionally reported as relative permeability owing to the many combinations of saturation that may exist for a single medium (Ahmed, 2000). Relative permeability is a lumping parameter that includes effects of wettability characteristics, heterogeneity of reservoir rock and fluids, fluids saturations and other micro and macro influences (Saraf and McCaffery, 1985; Honarpour et al., 1986; Mathiassen, 2003). Relative permeability graphical curves consist of three elements: (1) the end point fluid saturations, (2) the end point permeabilities, and (3) the curvature of the relative permeability functions. The end point saturations determine the movable saturation range and are directly related to the amount of recoverable hydrocarbons. The end points of relative permeabilities enter into the expression for the mobility ratio and will determine the sweep efficiency of a displacement process. The shape of the curves in between may also have an important bearing on recovery efficiency. The directions of the curves point out the saturation histories which are called drainage or imbibition. The drainage curve applies to processes where the wetting phase is decreasing in magnitude and vice versa for the imbibition processes.

Relative permeability data is a key factor that controls the gas condensate well deliverability (Shi, 2009). In general, two-phase relative permeabilities are measured in the laboratory in preference to the use of prediction procedures, and the experimental values obtained are subsequently used in reservoir simulations (Saraf and McCaffery, 1985). Measurement of three-phase permeabilities is seldom attempted, however, primarily because of the enormous experimental difficulties, and estimation of the data is made using one of the following models:

1. Corey or Brooks-Corey equations for drainage.
2. Naar-Wygal equations for imbibition.
3. Land's equations for both drainage and imbibition.
4. Stone's equations for both drainage and imbibition.

Because extensive experimental three-phase relative permeability data are not available, each of the models above has not been tested for more than one or two sets, so that presently it is difficult to recommend any one of them. However, Land's model, although computationally more demanding due to the integral nature of the equations, seems to hold greater promise because of a more sound physical basis (Schneider and Owens, 1970).

In the absence of a widely tested and accepted mathematical model, it is still considered advisable to measure relative permeabilities in the laboratory and use these (with a higher degree of confidence) in reservoir engineering calculations. Calculation of relative permeability from experimental data is straight forward and does not involve any questionable assumptions. However, the experiments are difficult to set up, requiring elaborate equipment due to the presence of end effects and the difficulties associated with obtaining saturation measurements (Saraf and McCaffery, 1985). This research work adopted the unsteady-state procedure in which the effluent production from the core sample was recorded during the course of the imposed displacement processes. The accuracy and reliability of the measured data was a top concern; and the following quality control procedures were maintained:

- The pressure gradient was large (scaling coefficients were greater than critical) to minimise capillary pressure effects,

- The pressure drop was small compared to total operating pressure so that the incompressible fluid assumption was valid,
- The core was homogenous,
- The driving force and fluid properties were held constant,
- All data was recorded digitally and automatically requiring minimal human intervention.

The results presented in this chapter are valuable for reservoir engineers to use in reservoir characterisation, understanding the behaviour of gas condensate reservoirs, and predicting recovery factors associated with CO_2 injection. These data are also critical input parameters for reservoir simulators. The injection scenarios and displacement thermodynamic conditions were chosen by a local operator in Western Australia.

4.2 Experimental Program

4.2.1 Core and Fluid Properties

All experiments were carried out on a reservoir sandstone core plug from a gas condensate field in the North Western Shelf of Australia. The core has the following petrophysical characteristics: 6.9 cm length, 3.8 cm diameter, 13.2% porosity, and 22 md effective permeability. The connate water saturation is believed to have remained constant during the course of the tests, as the core effective permeability remained unchanged and no water production was observed. Fluid properties were discussed in detail in **Section 3.3.1**. The PVT properties of the fluids were calculated using the Peng-Robinson EOS.

4.2.2 Design

The experimental design adopts the unsteady state procedure in which effluent production from the core sample was recorded during the course of the imposed displacement processes. This procedure holds many advantages over the steady-state design including: the process resembles more the mechanisms taking place in the reservoir, it provides better end-point data, is simpler experimentally, is substantially quicker, requires smaller amounts of fluids, and is cheaper than the steady-state experiments

(Honarpour et al., 1986). The HPHT coreflooding displacement facility is shown schematically in **Fig. 18** and graphically in **Fig. 19**. It consists of a high-pressure pump (LC-20AT Shimadzu), titanium accumulators with floating pistons, check valves and a back-pressure regulator (BPR), a core holder, a gas meter and a gas analyser, and an online data collection instrument synchronised to a laboratory PC. The pressure of the flooding fluids inside the titanium vessels was maintained by injecting or withdrawing water from the bottom of the cells. High-pressure steel tubing (1/8 in. internal diameter) carried the fluids to the appropriate injection ports in the core holder. The produced fluids were carried through the BPR first and then into a graduated measuring cylinder. The core holder, backpressure regulators, fluid accumulators and flow lines were accommodated inside a temperature-controlled, air-forced circulation oven. The simulated reservoir temperature of 95 ^{o}C was maintained with a thermocouple that possesses an accuracy deviation of 0.5 ^{o}C. Pressure transducers located at the inlet and outlet of the core were used to measure the pressure drop across the core. The transducers provided stable differential pressure data with an accuracy of 0.01 psi during the course of the tests. The composition of the produced gas was monitored on the spot and on a continuous basis by a CO_2 gas analyser (PEM tech gas analyser) and recorded on the integrator. The volume of produced gas was also measured by a flow meter.

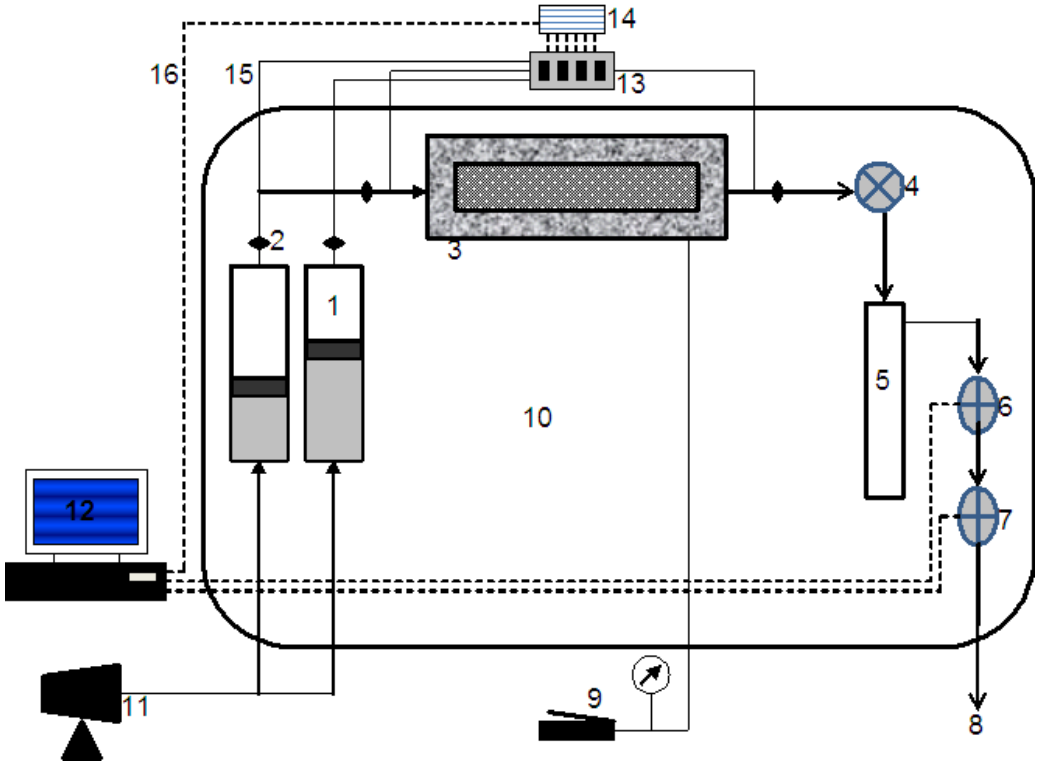

Fig. 18 - HPHT Coreflooding Facility Schematic

Legend:

1: HPHT fluid accumulators with floating pistons, 2: one-way valve, 3: core holder, 4: back pressure regulator, 5: separator, 6: gas flow meter, 7: gas analyser, 8: vent, 9: hand pump to control annulus pressure, 10: temperature-controlled oven, 11: Shimadzu pump, 12: laboratory computer, 13: pressure transducers, 14: data-taker™, 15: 1/8" high pressure tubing, and 16: instrumentation lines.

Fig. 19 - HPHT Coreflooding Facility Photograph

4.2.3 Procedures

Initial porosity and single phase permeability measurements were done prior to the establishment of connate water saturation. Conventional unsteady-state relative permeability curves were generated by initially saturating the core with condensate and then injecting CO_2 gas at predetermined flooding pressure. When the two phase flow occurred after gas breakthrough, the data required to calculate relative permeability were carefully measured. The Johnson, Bossler, and Naumann (JBN) method was used to construct the relative permeability curves versus saturation. The CO_2 injection continued until 10 pore volumes of injection (PVI).

4.3 Results and Discussions

This section reveals the results of two lines of concurrent investigations: experimental and numerical simulation. **Subsections 4.3.1 and 4.3.2** demonstrate the simulation analyses that were carried out to provide a better understanding of the role of fluid properties and phase behaviour on the displacement characteristics. Phase behaviour

and fluid properties determine the degree of components extractions and mass transfer, effectiveness of a displacement process and the stability of a flood front in field-scale processes (Al-Abri and Amin, 2010a; Al-Abri and Amin, 2010b; Creek and Sheffield, 1993; Cooney, 1966). The experimental results are illustrated in **Subsections 4.3.3, 4.3.4, and 4.3.5**, respectively investigating the IFT-dependent relative permeability and mobility ratio, velocity-dependent relative permeability, and composition-dependent relative permeability and mobility ratio.

4.3.1 Effect of Phase behaviour

Without exception, all enhanced recovery mechanisms should, in principle, be designed to handle complex fluid mixtures whose behaviour is strongly dependent on their chemical makeup and the prevailing pressure and temperature. This phase behaviour is of a prime consideration in the development and management of reservoirs, affecting all aspects of petroleum exploration and production. One of the most useful phase behaviour visualisations is the pressure-concentration envelope. The Aspen Hysys Simulation Package (AspenTech Co., 2009) was used to predict the thermodynamic state of the CO_2-condensate mixture at various injection pressures at a constant temperature of 95 ^{o}C. **Fig. 20** shows that the original condensate (0% CO_2) is a liquid at pressures above 3120 psi but splits into liquid and vapour below that pressure. A mixture containing 15 mole% CO_2 forms a single liquid phase above 3400 psi and a liquid and a vapour (CO_2 and light hydrocarbons) at lower pressures. Two liquids form at high pressures and CO_2 concentrations, a dense $SCCO_2$-rich phase and a condensate-rich liquid.

Fig. 20 also indicates that CO_2 is fairly soluble in condensates at typical reservoir pressures, but it is not miscible in all proportions at any reasonable pressure. The CO_2 mole fraction must, for instance, be nearly 0.55 before a second dense $SCCO_2$-rich phase appears at 5000 psi. Thus, when CO_2 is injected into the reservoir and contacts trapped condensate, at first it simply dissolves in the condensate droplets. This favourable phase behaviour relationship results in the swelling of condensate volume leading to improved recovery (Al-Abri and Amin, 2010a).

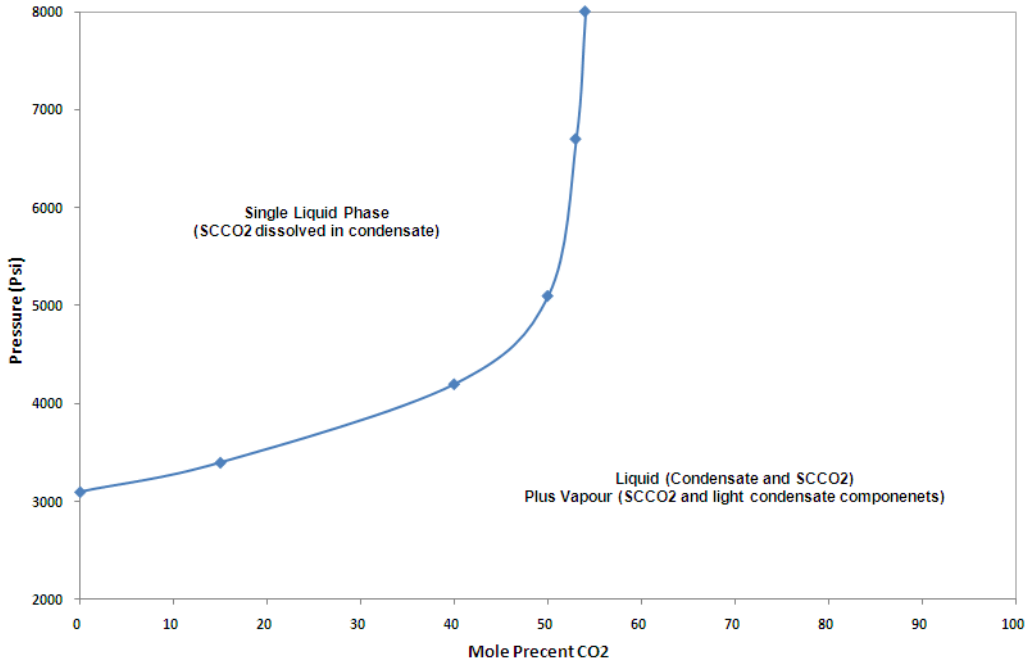

Fig. 20 - Phase Behaviour of Binary Mixtures of CO_2 and Condensate at 95 ^{o}C

4.3.2 Effect of Fluid Properties

The physical properties of CO_2 and condensate at various pressures were investigated utilising the PVTSim Package (Calsep Co., 2009). The simulator used the Peng-Robinson equation of state (EOS) to calculate the viscosity and density of each fluid at 95 ^{o}C. **Fig. 21** below shows the condensate-over-CO_2 density ratio (blue line) and viscosity ratio (red line) for the choice of pressures. The density ratio determines the relative buoyancy of CO_2 over the condensate. This is to say that when the density ratio is greater than unity then CO_2 would be expected to float above the liquid condensate droplets that would be pulled downwards towards the lower edge of the pore channels. This parameter is important as it controls the degree of gravity segregation. Fig. 21 suggests that gravity segregation would be expected to be more pronounced at lower injection pressures as the condensate remains the denser phase. This means that the CO_2 would mostly sweep-out the top part of the core sample leading to poor sweep efficiency. The viscosity ratio is another important design parameter that influences the stability of the flood front. The reduction in the condensate-over-CO_2 viscosity ratio with higher pressures would be expected to yield a stabilising effect on the front (Al-Abri and Amin, 2010a).

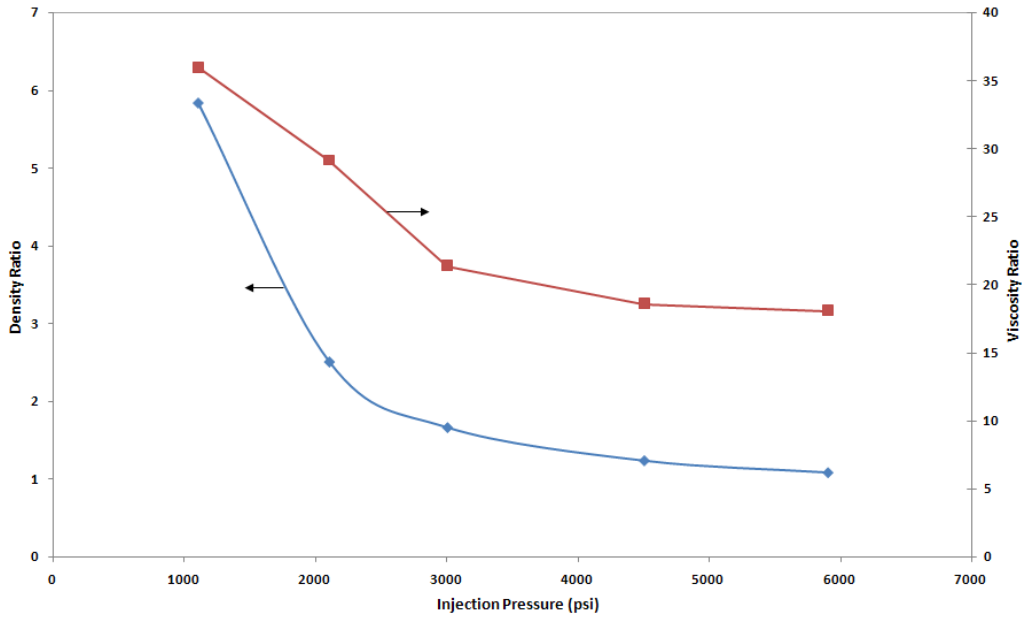

Fig. 21 - Condensate-CO_2 Density and Viscosity Ratios for all Injection Pressure Scenarios

4.3.3 Effect of Pore Pressure

This section demonstrates the effect of displacement pressure on condensate recovery and CO_2 breakthrough profiles. It reports coreflooding results as a function of pore volumes of gas injection (PVI) at a temperature of 95 ^oC, displacement velocity of 10 cm/hr and pore pressures of 1100, 2100, 3000, 4500 and 5900 psi. Although this velocity was chosen to be of particular relevance to real oil displacements by gas injection, its value is believed to be well above (3 orders of magnitude) the maximum flow velocity required for a completely stable gas injection process in oil-bearing formations. This low flow rate is required to overcome the tendency for CO_2 fingers to protrude into the condensate. Flow rates above this value would be expected to initiate unstable viscous fingers (Al-Abri and Amin, 2010a). The CO_2 is in the critical state at these pressure and temperature conditions, hereafter abbreviated as $SCCO_2$.

Fig. 22 below shows the percentage of condensate recovery factor as a function of PVI for the different displacement pressures. The dashed arrows indicate the percent of condensate recovery at breakthrough. In the 5900 psi miscible flood, breakthrough of $SCCO_2$ gas occurred at 0.62 PVI. Condensate production continued after breakthrough recovering 73.33 and 77.20% of the original condensate in place (OCIP) at 1.2 and 2.2 PVI

respectively. The condensate production was very slow after 1.5 PVI. The ultimate production was 78.9% OCIP at 6 PVI. In the 3000 psi near-miscible flood, breakthrough of gas occurred at 0.54 PVI. Condensate production increased to 64.16 and 68.74% of OCIP at 1 and 2 PVI respectively. The final production was 69.72% OCIP at 6 PVI. In the 1100 psi immiscible flood, breakthrough of $SCCO_2$ gas occurred at 0.21 PVI. Condensate production continued after breakthrough recovering 22.91 and 23.83% of the OCIP at 0.8 and 4 PVI respectively. The ultimate condensate recovery in all cases did not increase appreciably after breakthrough. Condensate recoveries at 0.10 PVI, for example, were 13.74, 13.31, 12.57, 9.92 and 9.65% OCIP for 1100, 2100, 3000, 4500 and 5900 psi injection pressures respectively. Lower displacement pressures yield relatively better condensate recovery at the start of the flooding programme (4.09% OCIP total difference at 0.10 PVI). This is not surprising as the CO_2 solubility in condensate is expected to be less at lower pressures. Although injection at high (i.e. miscible) pressures may seem to result in less recovery per PVI at the beginning, it actually produces the optimal ultimate and breakthrough recoveries (Al-Abri and Amin, 2010a).

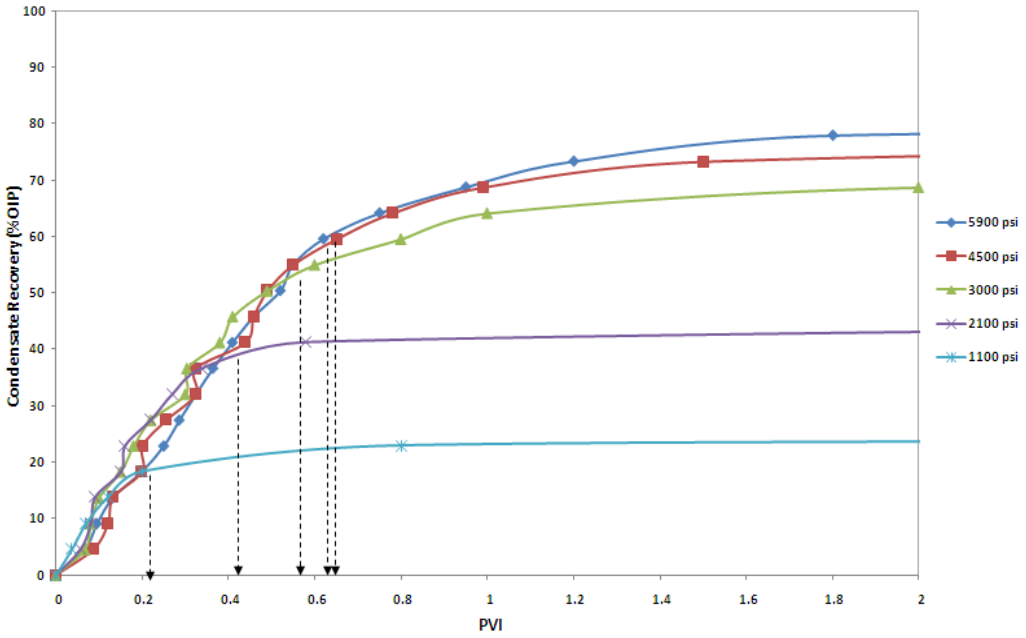

Fig. 22 - Pressure-Dependent Condensate Recovery Profiles

The $SCCO_2$ mole precent produced after breakthrough is demonstrated graphically as a function of PVI in **Fig. 23**. $SCCO_2$ breakthrough was observed to occur at 0.62, 0.60, 0.54, 0.41, 0.21 PVI corresponding to condensate recoveries of 59.70, 59.41, 53.12, 38.51 and 18.33% OCIP for 5900, 4500, 3000, 2100 and 1100 psi injection pressures respectively. Higher injection pressures were seen to result in a delayed gas breakthrough (0.41 PVI total difference).

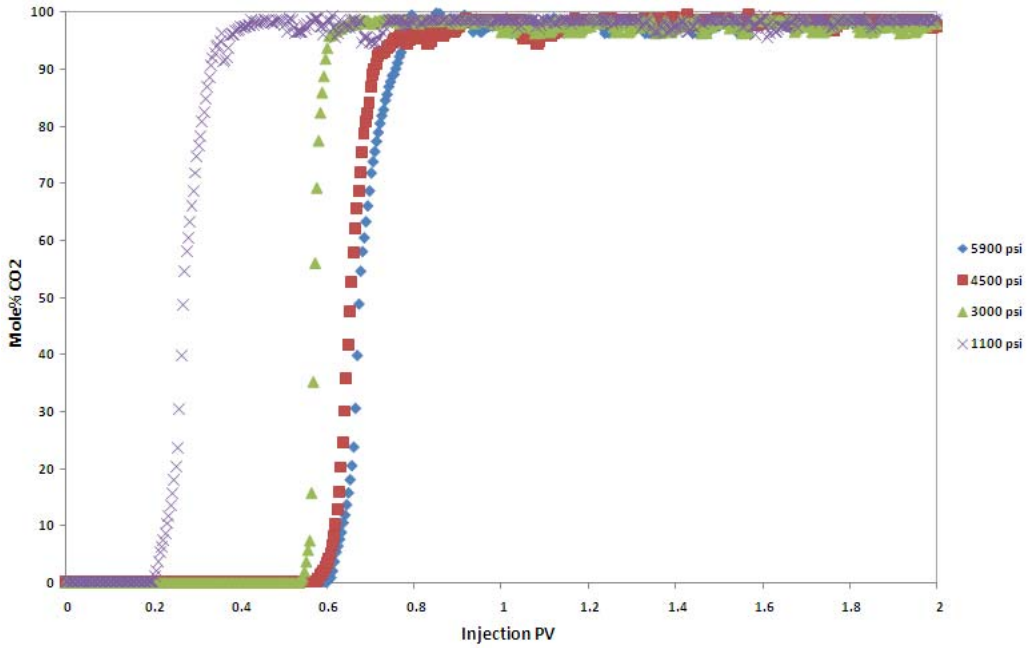

Fig. 23 - Mole Percent CO_2 Production as a Function of PVI

Fig. 24 presents the ultimate and breakthrough condensate recovery factor for various $SCCO_2$ injection pressures at constant flooding velocity and temperature of 10 cm/hr and 95 ^oC, respectively. The graph indicates that high injection pressures lead to high ultimate recovery of condensate. The sweep efficiency, which is a measure of the effectiveness of any EOR process, increases from 23.4 to 78.9 % OCIP when pressure increases from 1100 to 5900 psi. This sharp increase is contingent on the amount of mixing that occurs between the reservoir condensate and injected gas at miscible flooding conditions in particular (Walsh and Orr, 1990; Johns et al., 2002; Jessen et al., 2004; Garmeh et al., 2007). Fig. 24 also shows that the percentage difference in condensate recovery between the ultimate and breakthrough curves tends to be more pronounced as

miscible or near-miscible conditions are approached. This is an interesting observation as it may indicate the degree of the flood-front stabilities and subsequent sweep efficiency.

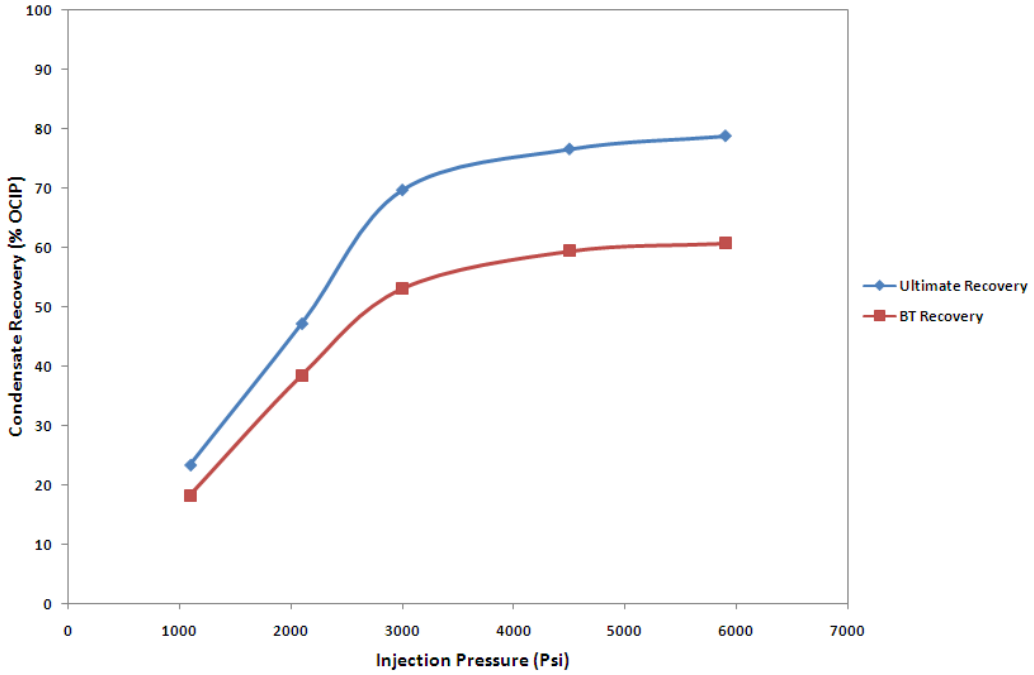

Fig. 24 - Pressure-Dependent Ultimate and Breakthrough Condensate Recoveries

Injection pressures not only decrease appreciably the condensate/CO_2 viscosity ratios (Fig. 21) and thus provide better mobility ratios, but they also reduce significantly the interfacial tension (IFT) and thus increase the capillary number. **Fig. 25** shows both the residual condensate saturation and the injection pressure as functions of IFT. It highlights that more residual condensate saturation (S_{or}) existed at lower flooding pressures possibly due to capillary instabilities that come into play at the flood front, but mostly due to the efficiency of the displacement process.

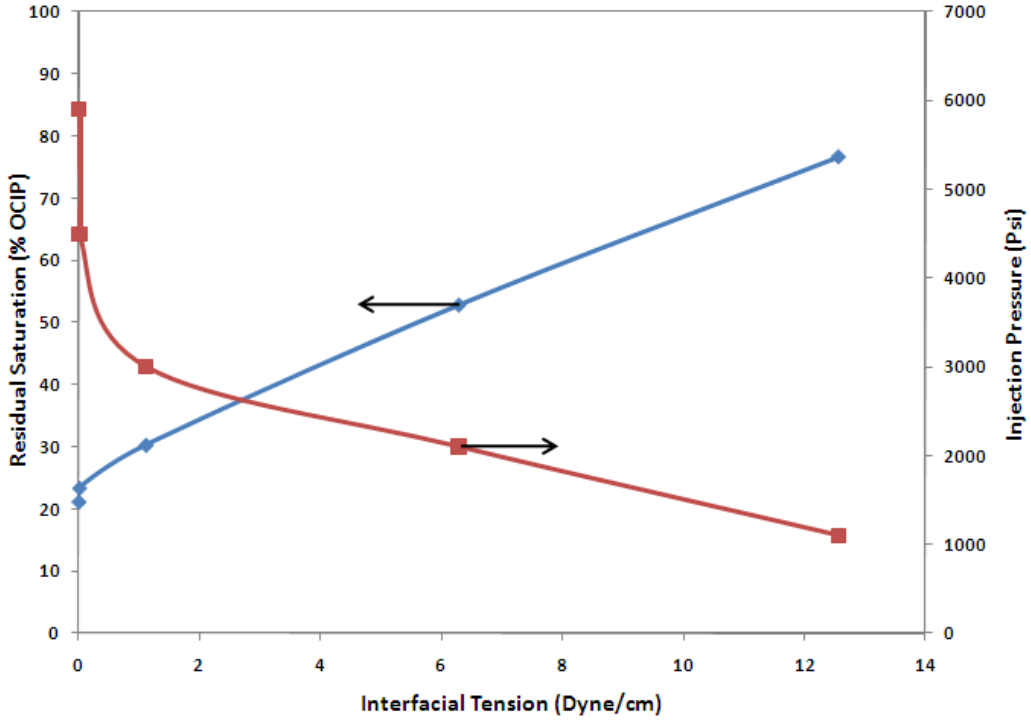

Fig. 25 - IFT-Dependent Residual Saturation for all Injection Pressure Scenarios

The pressure-dependent relative permeability curves associated with $SCCO_2$ injection are shown graphically as a function of the total fluid saturation inside the core in **Fig. 26**. The irreducible water saturation (S_{wi}) for core sample was 23.3% PV. The graphs illustrate that critical gas saturations and residual condensate saturations are pressure-dependent. Critical gas saturations varied from around 0.065 to 0.11, and residual condensate saturations changed from 76.6 to 21.2% PV for injection pressures of 2100 and 5900 psi, respectively. Fig. 26 also suggests that as the displacement pressure increases the capillary number improves resulting in higher relative permeability values. This lowers the residual saturations of the condensate and thus improves the recovery efficiency (Al-Abri and Amin, 2010a).

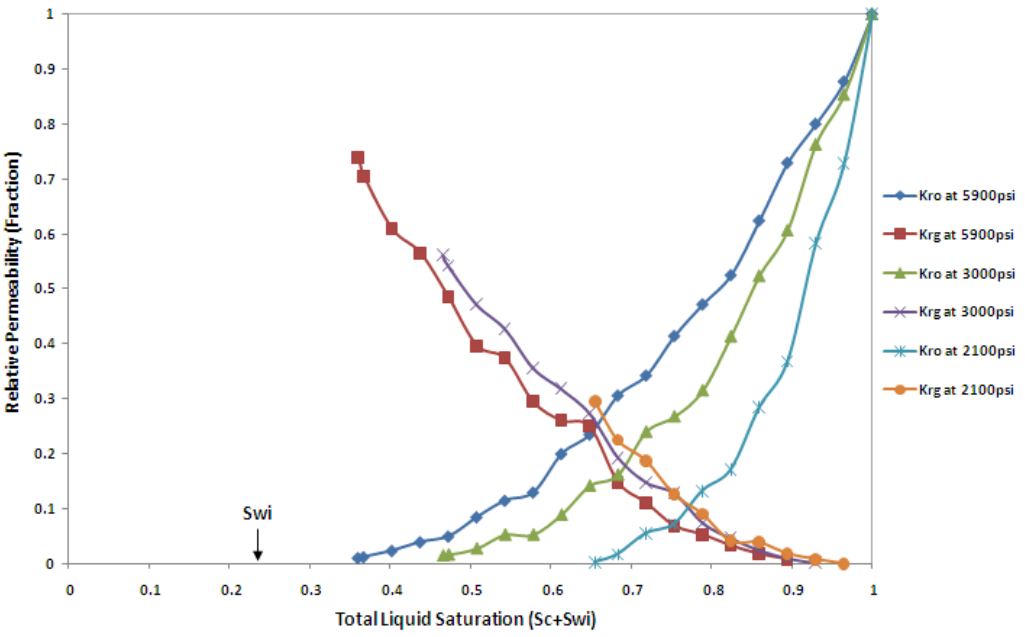

Fig. 26 - CO_2 and Condensate Composition-Dependant Relative Permeability

The relative permeability relationships which determine the flow behaviour of reservoir fluids in porous media strongly depend on the IFT at high pressure conditions. High pressure conditions (i.e. low IFTs) cause the networks of the two fluids to break up at the pore scale level. Ultimately, a mixture bank is formed at the flood front and, at that point, each fluid flows everywhere in proportion to its saturation in the sample, a behaviour that is commonly described by relative permeability curves illustrated in Fig. 26 above. This figure explains the condensate recovery efficiency improvement as miscibility conditions are approached (refer to Fig. 24).

Fundamentally all EOR processes aim to provide favourable mobility ratios for stable displacement fronts (typically M<1). The mobility ratio is a dimensionless group that serves as a benchmark for frontal drives. The mobility ratio affects both areal and vertical sweep, with sweep efficiencies decreasing as the mobility ratio increases for a given volume of fluid injected. High mobility ratios stimulate the degree of flow instability through the formation of viscous fingers (Perrine, 1961). Heterogeneities in the porous strata are not really friendly to mobility ratios as once a heterogeneity is encountered, a portion of the displacing fluid will travel with a greater local velocity and protrude past the rest of the front. If the width of the protrusion exceeds a critical width for finger formation

described by Gardner and Ypma (1984) and if the dispersion is not sufficient to suppress it, a viscous finger will begin to grow. Finger growth continues because of the low resistance flow path created by the low viscosity region in the finger. Habermann (1960) showed evidence that several fingers can merge or coalesce together to form a larger finger (**Fig. 27**).

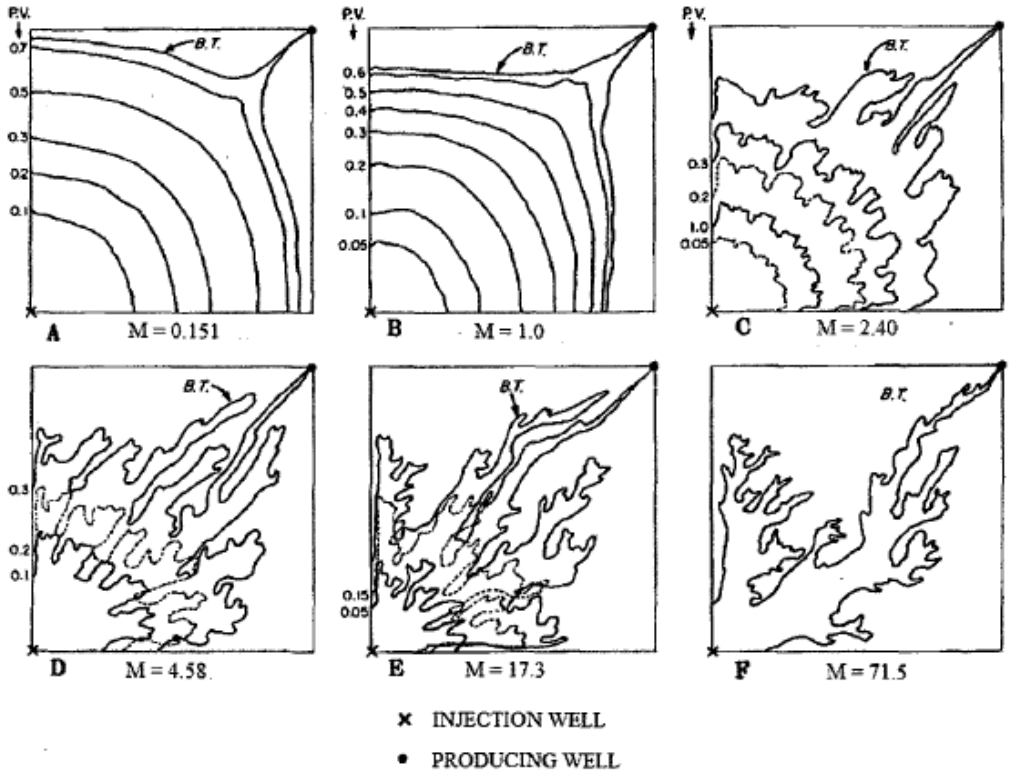

Fig. 27 - Viscous Fingering in Quarter Five-Spot as a Function of Mobility Ratio (Lewis, 2008)

Fig. 28 shows that at the cut-off criteria for a stable flow (M=1), $SCCO_2$ injection has already displaced 43%, 34% and 14% of OCIP at flooding pressures of 5900, 3000 and 1100 psi respectively. This illustrates that most of the OCIP is recovered at favourable mobility ratios (M<1). Miscible displacements cause a single phase to flow at the transition zone. The mobility ratio in such cases becomes the ratio of the displaced fluid viscosity to that of the displacing fluid. Fig. 4.28 also demonstrates that the magnitudes of the mobility ratios build up fairly quickly in the immiscible floods leading to poor sweep efficiencies.

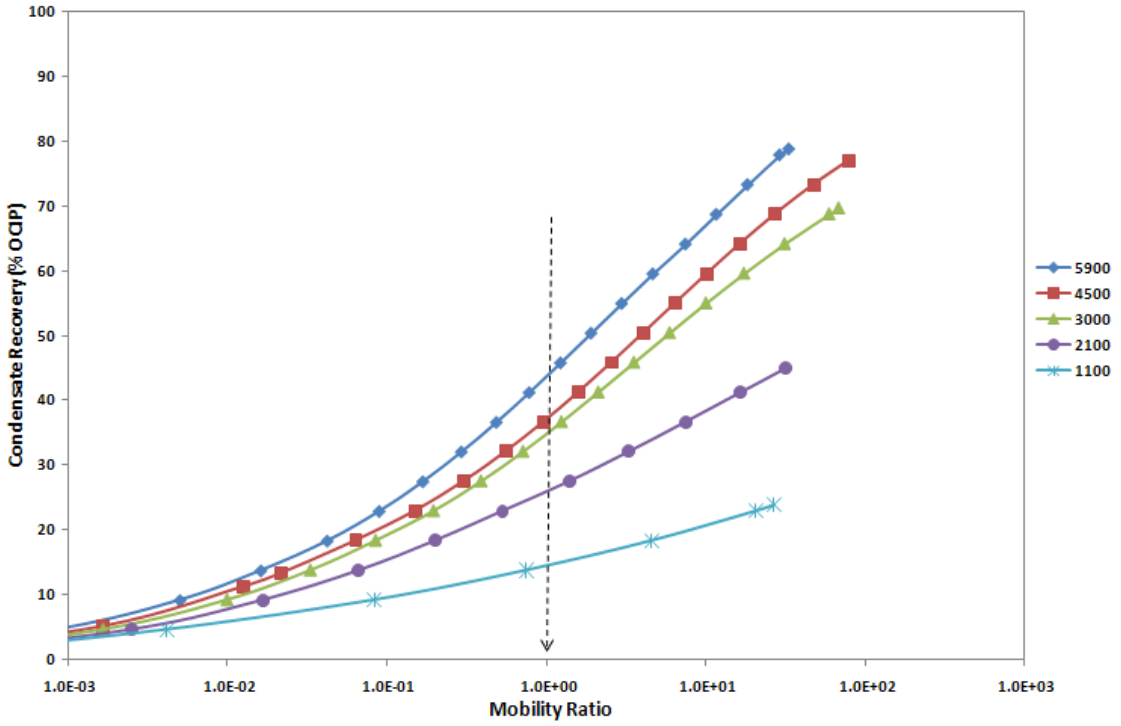

Fig. 28 - Percent Condensate Recovery as a Function of Mobility Ratios for all Injection Scenarios

4.3.4 Effect of Injection Rate

This section investigates the rate-dependent relative permeabilities and recovery profiles. These investigations were conducted at 5900 psi, 95 ^{o}C, and injection velocities of 10, 7, 5, 2 and 1 cm/hr; equivalent to typical field interstitial velocities of around 8, 5.5, 4, 1.6 and 0.8 ft/day. **Fig. 29** below shows the percent condensate recovery factor as a function of the gas injection pore volume PVI for the different flow rates. The dashed arrows indicate the condensate recovery percent at breakthrough. In the 10 cm/hr flood, breakthrough of $SCCO_2$ gas occurred at 0.62 PVI. Condensate production continued after breakthrough recovering 73.33 and 77.2% of the original condensate in place (OCIP) at 1.2 and 2.2 PVI respectively. The condensate production was very slow after 1.5 PVI. The ultimate production was 78.9% OCIP at 6 PVI. In the 7 cm/hr flood, breakthrough of gas occurred at 0.66 PVI. Condensate production increased to 68.7 and 77.9% of OCIP at 0.86 and 1.3 PVI respectively. The final production was 86.16% OCIP at 6 PVI. The ultimate condensate recovery in all cases did not increase appreciably after breakthrough.

Condensate recoveries at 0.6 PVI, for example, were 58.36, 61.87, 65.16, 69.25 and 72.29% OCIP for 10, 7, 5, 2 and 1 cm/hr injection velocities respectively. The slower the flow rate of displacement the better the condensate recovery becomes (13.93% OCIP total difference).

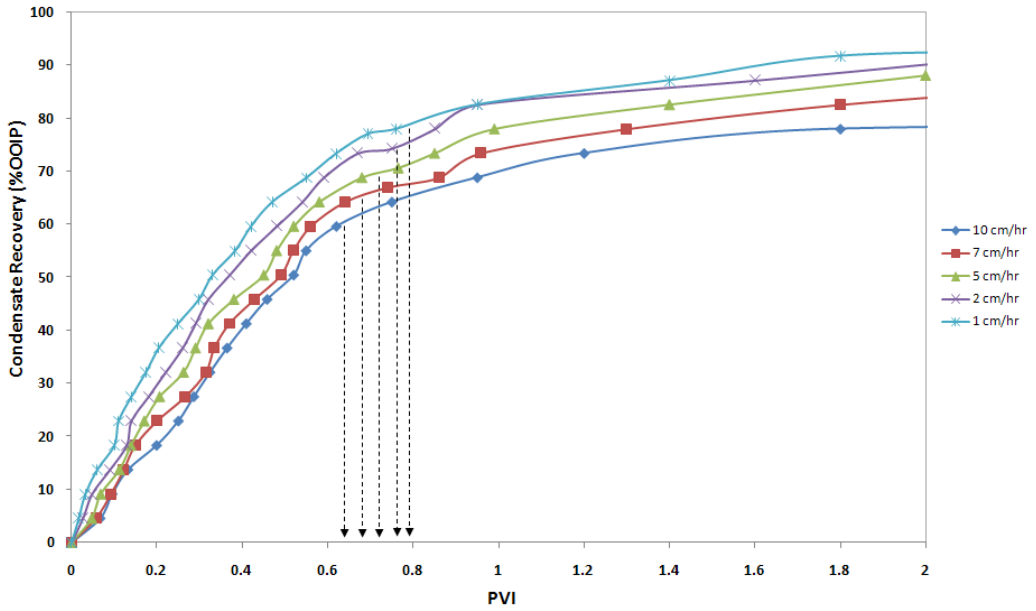

Fig. 29 - Condensate Recovery Comparison for all Injection Velocities

The $SCCO_2$ mole precent produced after breakthrough is demonstrated graphically as a function of PVI in **Fig. 30**. $SCCO_2$ breakthrough was observed to occur at 0.62, 0.66, 0.69, 0.75, 0.78 PVI corresponding to condensate recoveries of 59.7, 67.2, 70.5, 74.65 and 77.1% OCIP for 10, 7, 5, 2 and 1 cm/hr injection velocities respectively. Slower injection velocities delayed the gas breakthrough (0.16 PVI total difference).

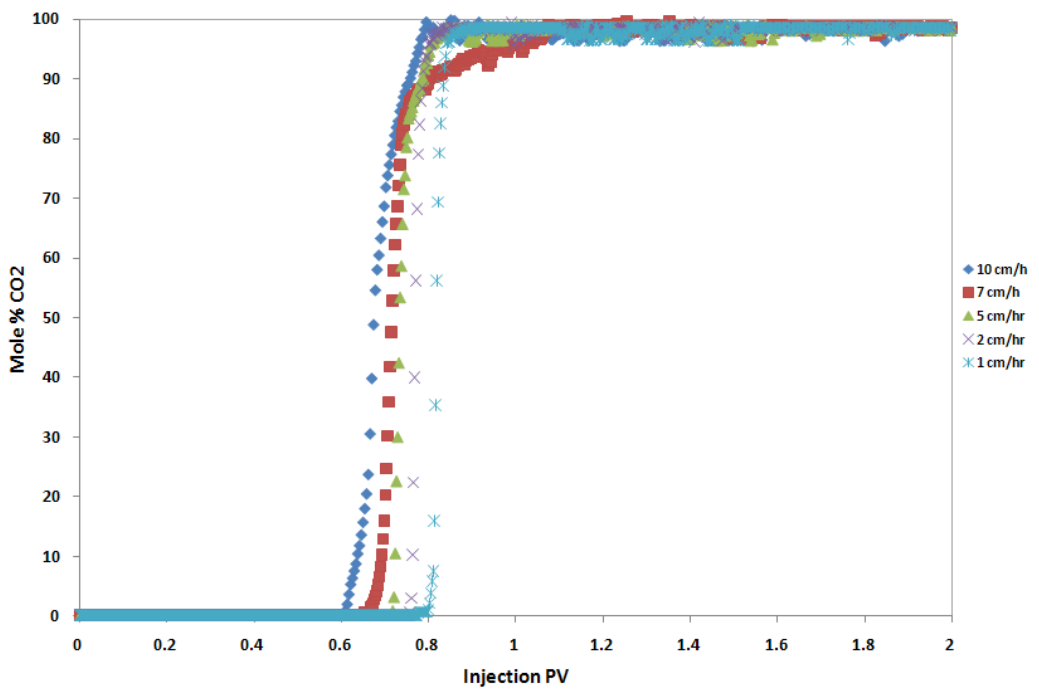

Fig. 30 - Mole Percent CO_2 Production as a Function of PVI

Fig. 31 presents the ultimate and breakthrough condensate recovery factor for various $SCCO_2$ injection rates at flooding pressure and temperature of 5900 psi and 95 ^oC, respectively. The graph indicates that slower frontal velocities corresponding to lower injection rates lead to higher ultimate recovery of condensate. The sweep efficiency increases from 78.9 to 92.6% OCIP when frontal velocity decreases from 10 to 1 cm/h, respectively. These results are consistent with prior experimental and numerical studies of drainage in flowcells (Ferer et al., 2004; Ji et al., 2002).

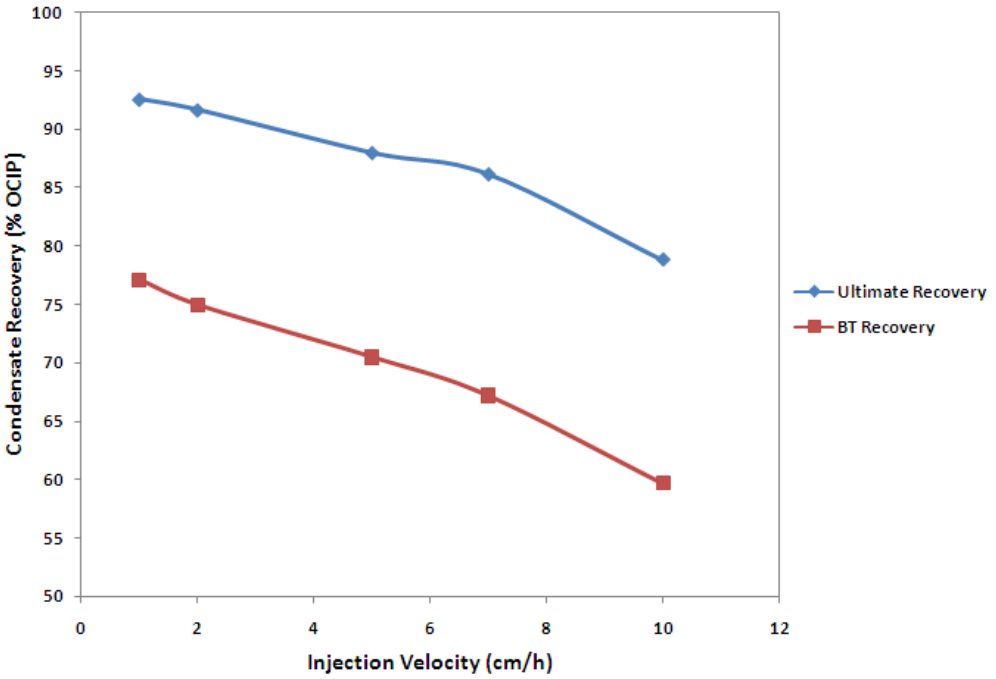

Fig. 31 - Ultimate and Breakthrough Condensate Recovery Comparison for all Injection Velocities

Crandall (2007) has numerically studied the effect of injection flow rate on the invading air mass distribution through a water-saturated porous section, when wettability and viscosity ratios were kept constant. Crandall's flowcell models confirm that an increase in the injection velocity leads to narrower fingers, indicating lower precentage saturation of the invading fluid with increasing injection rates (**Fig. 32**).

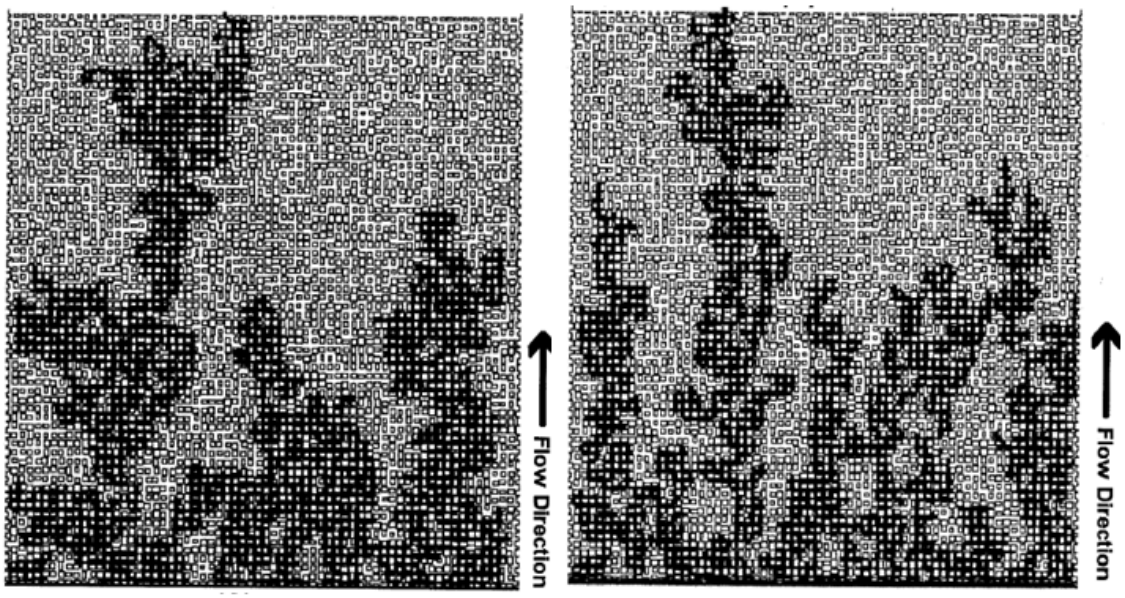

Fig. 32 - Breakthrough Simulation Images of Two Different Velocities of Air (Black) Penetrating Water

Crandall (2007) stated that injecting above the critical value for stable displacements changes the distribution profiles from capillary fingering to more dendritic fingers. The fractal dimension of the air increased as the velocity and thus the capillary number decreased. He has also pointed out that air saturation inside the porous section decreased from 23.2% to 18.4% to 16.4% with injection velocities of 1, 5 and 10 cm/s, respectively. In a similar manner the $SCCO_2$ is expected to behave when conducting rate-sensitivity analysis. The precent saturation of the less-viscous invading fluid quantifies how this will affect the utilisation of $SCCO_2$ in condensate recovery processes.

The rate-dependent relative permeability curves associated with $SCCO_2$ injection are shown graphically as a function of the total fluid saturation inside the core in **Fig. 33**. The graphs illustrate that critical gas saturations and residual condensate saturations are rate-dependent. Critical gas saturations varied from around 0.11 to 0.14, and residual condensate saturations changed from 21.2 to 7.42% PV for injection velocities of 10 and 1 cm/hr, respectively. The graphs also suggest that displacement rates affect the condensate relative permeability more than the CO_2 curves. As the displacement velocities increase

viscous forces tend to have an influence on the behaviour of the two phase flow resulting in seemingly decreased phase mobilities and increased residual saturations (Al-Abri et al., 2009).

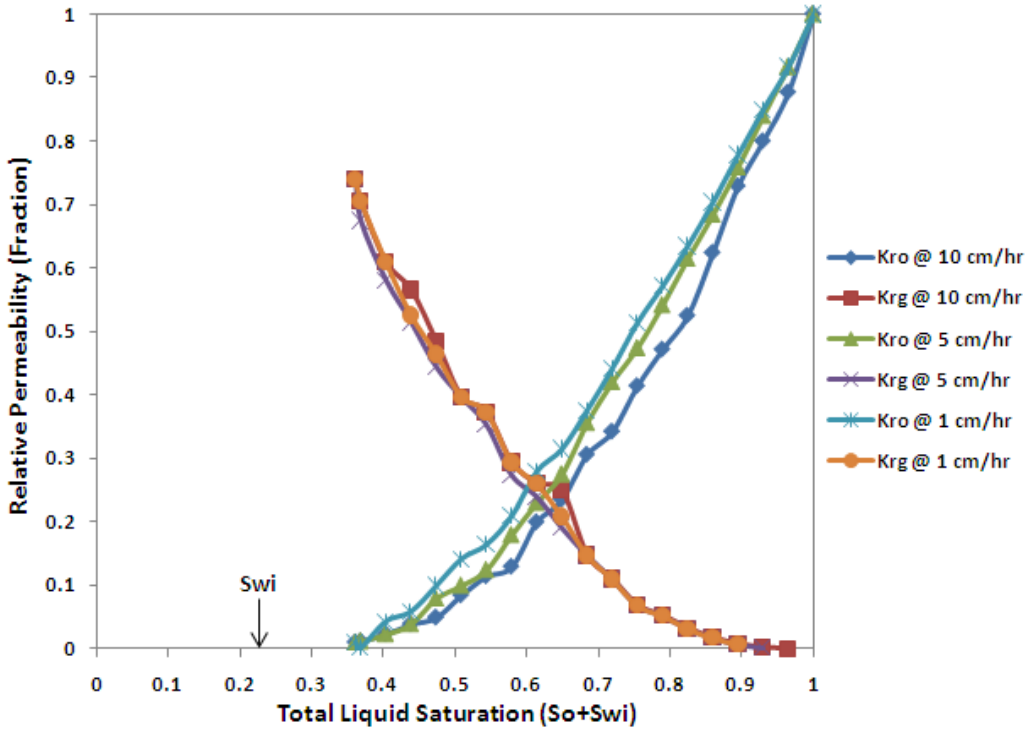

Fig. 33 - CO_2 and Condensate Rate-Dependant Relative Permeability

4.3.5 Effect of Injection Composition

This section examines the effect of methane contaminants with the injection CO_2 on the sweep efficiency and mobility ratio. These investigations were done at flooding conditions of 95 ^oC temperature, 5900 psi pressure, 10 cm/hr displacement velocity and various methane concentrations. The recovery of condensate as a function of CO_2 concentration in the injection displacing gas is displayed graphically in **Fig. 34**. The graph shows that the maximum condensate recovery is obtained when injecting pure supercritical CO_2, with recoveries reaching 80% of the condensate-in-place (CIP). Pure injection of CH_4 (i.e. zero CO_2 concentration) gives the lowest recovery of around 45%. In other words, more S_{or} exists at lower concentrations of CO_2 in the injection gas for reasons related to efficiency of the displacement process. The chart also illustrates that the condensate

recovery at CO_2 breakthrough of pure supercritical CO_2 injection exceeds 60% of CIP whereas pure CH_4 injection results in gas breakthrough recovery of less than 24%. The recovery of the supercritical CO_2-CH_4 mixtures distribute proportionally in between those ends. Another interesting observation is that the *breakthrough* recovery of pure supercritical CO_2 injection is higher than the *ultimate* recovery of pure CH_4 injection into the same core and at same flooding conditions (Al-Abri et al., 2010a; Al-Abri et al., 2010b).

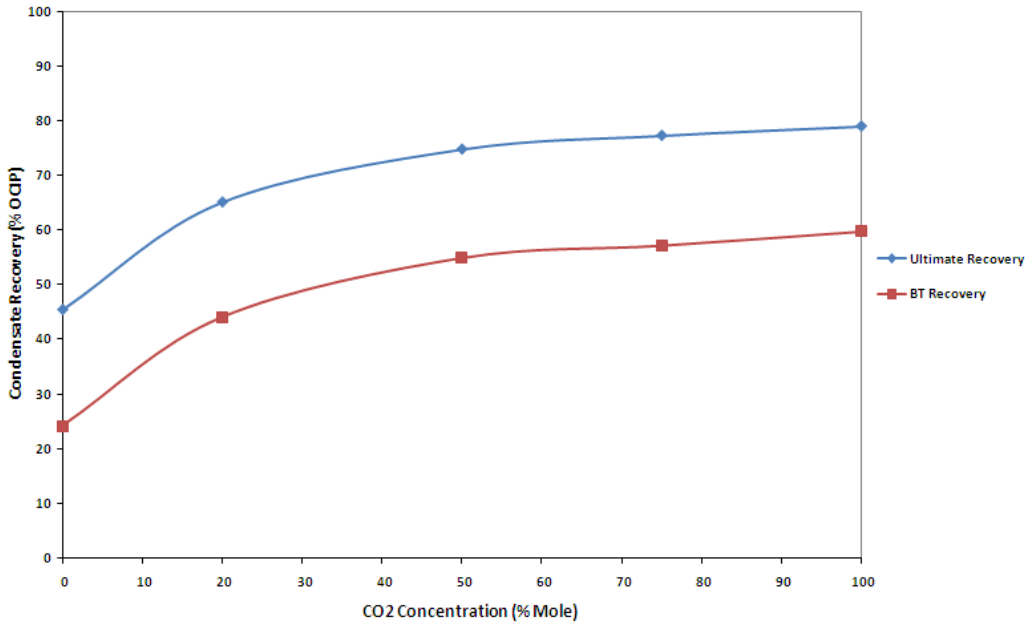

Fig. 34 - Condensate Recovery at Different Concentrations of CO_2 and CH_4

The relative permeability of the condensate and injection gas as a function of total liquid saturation is illustrated in **Fig. 35**. The lowest water saturation (i.e. irreducible water saturation) established in situ was 23.3% of pore volume. The graphs show that a small saturation of the injection gas inside the core drastically reduces the relative permeability of the condensate. Following the initial gas dissolution and the subsequent condensate swelling and vaporisation, the condensate starts to move towards the production terminal at relatively low saturation of injection gas. This saturation, often referred to as critical gas saturation, is observed to decrease slightly (4% total difference in saturation) when moving from pure CO_2 injection to mixtures to pure CH_4 injection. The graph also illustrates that the flow of condensate ceases at the irreducible oil saturation plus the irreducible water

saturation. This value is observed to increase when injecting pure CH_4 leaving more quantities of residual condensate left behind. These end point saturations determine the movable saturation range for the corresponding gas injection. The end points of relative permeabilities of each injection scenario enter into the expression for the mobility ratio that determines the sweep efficiency of each displacement process. The relative permeability curves improve as the CO_2 concentration in the injection gas increases. This improvement is attributed to the fact that mobility ratios decrease and thus provide more stable displacement fronts (Al-Abri et al., 2010a).

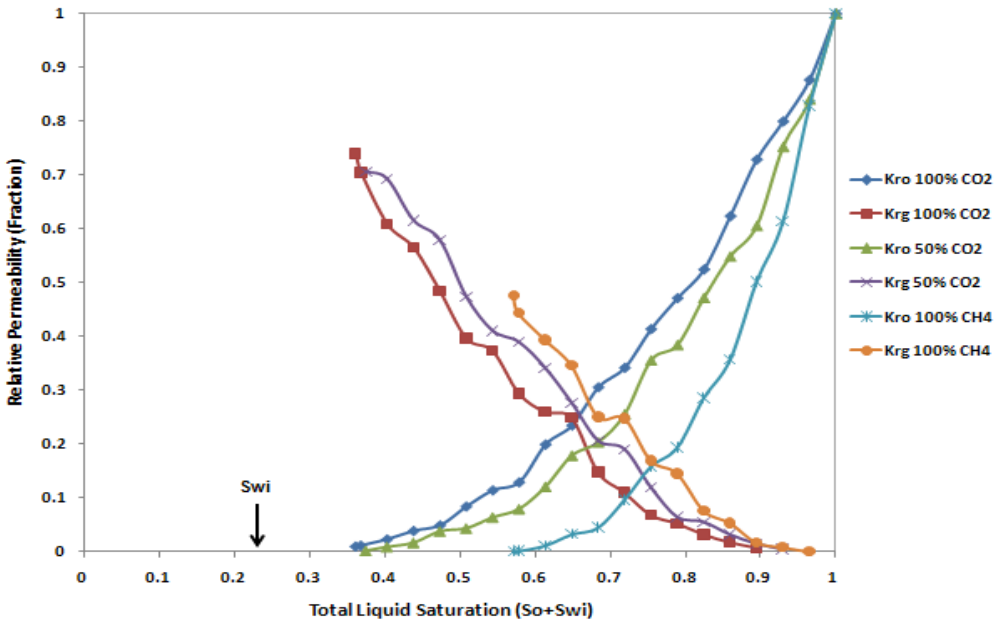

Fig. 35 - CO_2 and Condensate Composition-Dependant Relative Permeability

It is always beneficial to compare the mobility ratio at various conditions so as to understand the degree of flow stabilities. **Fig. 36** shows that at the cut-off criteria for a stable flow (M=1), pure $SCCO_2$ injection displaces 43% of OCIP as opposed to 33% in the 50-50% CO_2/CH_4 mixture to around 20% following the injection of pure methane.

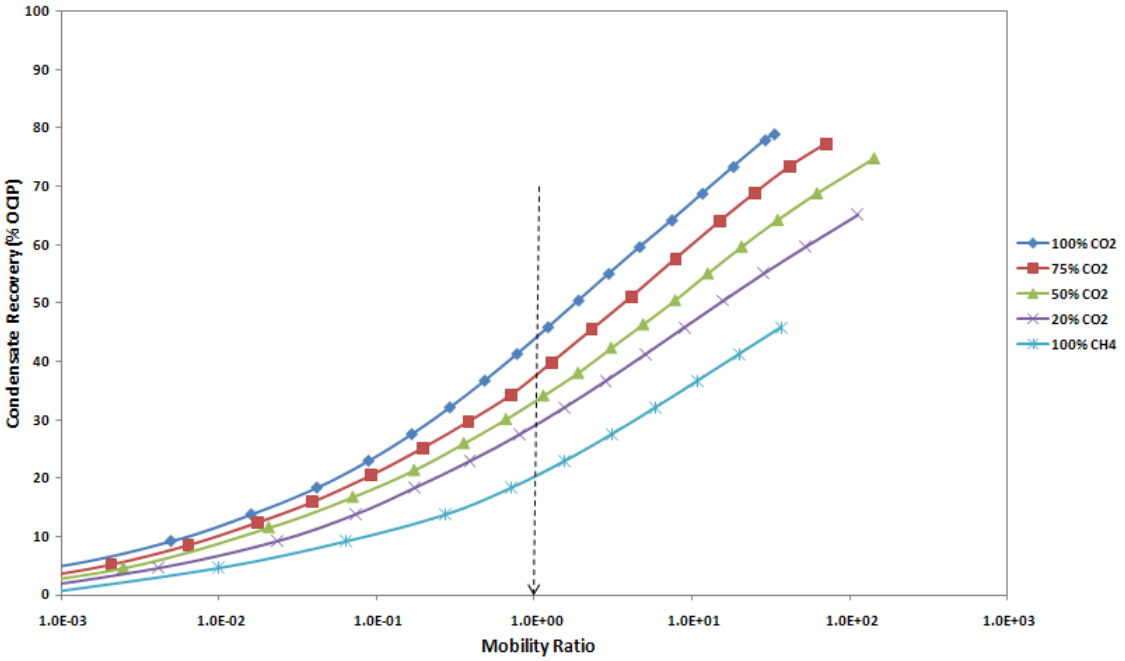

Fig. 36 - Composition-Dependent Mobility Ratios

4.4 Conclusion

This chapter has discussed the influence of phase behaviour, fluid properties, displacement pressure, gas injection composition, and injection flow rate on the efficiency of condensate production. Favourable phase behaviour relationships stimulate the swelling of the condensate volume leading to improved recovery. Fluid properties are responsible for gravity segregation and displacement frontal stability. Gravity segregation would be expected to be more pronounced at lower injection pressures as the condensate remains the denser phase leading to poor sweep efficiencies. CO_2 injection at high pressures provides a stabilising effect on the flood front and thus a better mobility ratio.

The injection pressure was found to be a key factor governing the development of miscible displacement conditions in the reservoir. Miscible displacements not only delayed injection gas breakthroughs but also improved the ultimate condensate sweep efficiency. The sweep efficiency, for instance, increased from 23.4% to 78.9% OCIP at 1100 and 5900 psi flooding pressures respectively. This sharp increase is contingent on the amount of mixing that occurs between the reservoir condensate and injected gas at miscible flooding conditions in particular. Furthermore, relative permeability data was found to increase with

displacement pressure leading to lower residual condensate saturations. The rapid buildup of mobility ratios in the immiscible displacements may indicate the formation of viscous fingers.

The chapter has also shown that slower displacement rates produce better condensate recovery and later breakthrough of CO_2. This negative rate coupling is directly related to phase trapping and mobilisation of condensate fluids. High injection rates may indicate the growth of narrow dendritic fingers that displace lower pore volumes for a certain volume of gas injection. The condensate relative permeability was found to change appreciably whereas the CO_2 relative permeability change was found to be limited. Higher displacement rates simulate higher CO_2 injection rates or faster radial rates encountered close to production wells, and vice-versa for lower injection rates.

The effect of methane contaminants in the injection gas on the sweep efficiency was also investigated. The relative permeability curves showed that a small saturation of the injection gas inside the core drastically reduces the relative permeability of the condensate, and that this effect becomes more pronounced as methane concentration in the injection gas increases. The condensate recovery was more than double for the pure CO_2 injection as opposed to pure methane injection at a unity mobility ratio.

CHAPTER V

NUMERICAL SIMULATION OF CO_2 INJECTION INTO FRACTURED GAS CONDENSATE RESERVOIRS

Much current practice in predicting hydrocarbon recovery is based on numerical simulation, because simulation can solve problems that quantitatively describe the flow of multiple phases in a heterogeneous reservoir. This chapter intends to provide answers to the *'what if questions'* that may arise anytime throughout the production life of a reservoir and particularly during the exploratory stage of a certain field. This is not uncommon as the reservoir data required for production forecasting is often imperfect, incomplete and hence uncertain (Caldwell and Heather, 1991; Murtha, 1993; Moffat and Williams, 1998; Tamhane et al., 1999). This uncertainty in reservoir data translates to uncertain numerical simulations and production forecasts. The chapter therefore demonstrates numerically the relative significance of:

1. Various reservoir fluid thermodynamic conditions (reservoir composition and fluid pressure),
2. Several development strategies (natural depletion, CO_2 injection, injection flow rate, and WAG).

on the recovery performance of both natural gas and liquid condensate. The chapter presents also the mathematical basis for the 3D three-phase, dual-porosity, and finite-difference set of equations for simulating gas injection into naturally fractured gas condensate reservoirs.

5.1 Overview

More than sixty percent of the world's remaining oil reserves are hosted by intensely fractured porous rocks such as the carbonate sequences of Iran, Iraq, Oman, or offshore Mexico (Beydoun, 1998). The high contrast of capillarity between the matrix and the fractures makes a significant difference in the recovery performance of fractured and non-fractured reservoirs (Lemonnier and Bourbiaux, 2010). Simulation of naturally fractured reservoirs is a challenging task from both a reservoir description and a numerical

standpoint (Selley, 1998). Fractures exist in nearly all reservoir rock formations, ranging in size from millimetres to kilometres (Selroos et al., 2002). Flow of fluids within the reservoir is primarily through the high-permeability, low effective-porosity fractures surrounding individual matrix blocks. The matrix blocks contain the majority of the reservoir pore volume and act as source or sink terms to the fractures. The rate of recovery of oil and gas from a fractured reservoir is a function of several variables, including size and properties of matrix blocks and pressure and saturation history of the fracture system. Specific mechanisms controlling matrix/fracture flow include water/oil imbibitions, oil imbibitions, gas/oil drainage, and fluid expansion.

5.2 Reservoir Simulator

Tempest 6.6 (Roxar Co., 2010) was utilised to create a hypothetical simulation model in order to evaluate the performance of various reservoir fluid thermodynamic conditions, injection design variables, and economic recovery factors of CO_2 injection into a heterogeneous, anisotropic, faulted and fractured gas condensate reservoir. This simulator is finite-difference compositional that takes into account mass transfer, molecular diffusion, components extraction and dynamic phase behaviour relationships. Gas injection schemes into gas condensate reservoirs in particular are inherently compositional as the injection gas is rarely in full equilibrium with the in situ residents (Lemonnier and Bourbiaux, 2010). The Todd-Longstaff model was utilised in the simulations to calculate the effective phase permeabilities and fluid mobilities and thus to control the displacement front expansion (Todd and Longstaff, 1972; Wu et al., 1989; Sorbie et al., 1994; Thiele et al., 1996).

Tempest 6.6 provides a dual porosity model (DPORO) for simulation of fractured reservoirs. The DPORO model makes use of two simulation cells to represent a single volume of physical space by associating one cell with the matrix flow and one with the fracture flow. The solver assumes the first $N_z/2$ layers of the grid to form the matrix cells whereas the fracture cells form the second $N_z/2$. Non-neighbour connections between the two parts of the grid, constructed automatically by Tempest, allow flow between the matrix and fracture cells. The simulation input file incorporates the relevant experimental interfacial tension and relative permeability data as well as published CO_2 solubility data (Chang et al., 1998; Zhenhao and Rui, 2003). Section 5.2.1 presents the 3D three-phase,

dual-porosity, finite-difference model for simulating naturally fractured reservoirs. The formulation is implicit in pressure, water saturation, and gas saturation or saturation pressure for both matrix/fracture flow and fracture flow.

5.2.1 Matrix/Fracture Transport Equations

The simulator assumes that the reservoir consists of a continuous fracture system filled with discontinuous matrix blocks. The primary flow in the reservoir occurs within the fractures with local exchange of fluids between the fracture system and matrix blocks. The simulator assumes also that each block has known properties and geometric shape. The following subsections present the equations describing finite-difference three-phase 3D flow in the fracture system.

5.2.1.1 Fracture Flow Equations

Water:

$$\Delta[T_w(\Delta p_w - \gamma_w \Delta D)] + \lambda_w(p_{wm} - p_w) - q_w = \frac{V_b}{\Delta t}\delta(\phi b_w S_w) \quad \text{.....23}$$

Oil:

$$\Delta[T_o(\Delta p_o - \gamma_o \Delta D)] + \lambda_o(p_{om} - p_o) - q_o = \frac{V_b}{\Delta t}\delta(\phi b_o S_o) \quad \text{.....24}$$

Gas:

$$\Delta[T_g(\Delta p_g - \gamma_g \Delta D)] + \lambda_g(p_{gm} - p_g) + \Delta[T_o R_s(\Delta p_o - \gamma_o \Delta D)] + \lambda_o R_s(p_{om} - p_o) - q_g = \frac{V_b}{\Delta t}\delta(\phi b_g S_g + \phi b_o R_s S_o) \quad \text{.....25}$$

The $\lambda\ (p_m - p\ )$ terms represent matrix/fracture fluid exchange and act as source or sink terms in the fracture system.

5.2.1.2 Matrix/Fracture Flow Equations

Water:

$$-\lambda_w(p_{wm} - p_w) = \frac{V_b}{\Delta t}\delta(\phi b_w S_w)m \quad \text{.....26}$$

Oil:

$$-\lambda_o(p_{om}-p_o)=\frac{V_b}{\Delta t}\delta(\phi b_o S_o)m \quad \text{……...……...27}$$

Gas:

$$-\lambda_g(p_{gm}-p_g)-\lambda_o R_s(p_{om}-p_o)=\frac{V_b}{\Delta t}\delta(\phi b_g S_g+\phi b_o R_s S_o) \quad \text{…...……....28}$$

The transmissibilities between the matrix and fracture blocks are calculated as follows for the water equation:

$$\lambda_w=0.001127\,\sigma k_{rw}\left(\frac{kV_b}{B_w\mu_w}\right)_m \quad \text{……..……29}$$

The coefficient σ is a geometric factor that occurs for the surface area of the matrix blocks per unit volume and a characteristic length associated with matrix/fracture flow (Warren and Root, 1963).

Eqs. 23 through to 28 represent six equations in 12 unknowns. Six additional equations–three for the fracture and three for the matrix expressing the sum of saturations are:

$$S_w+S_o+S_g=1 \quad \text{……..……....30}$$

and capillary pressure relationships,

$$P_{cwo}=p_o-p_w \quad \text{……..……...31}$$

and

$$P_{cgo}=p_g-p_o \quad \text{……...…….....32}$$

complete the set of 12 model equations.

5.2.1.3 Fracture Flow Terms

Fracture flow terms are evaluated implicitly as follows for the oil phase fracture flow term.

$$\Delta[T_o(\Delta p_o-\gamma_o\Delta D)]=\Delta[T_o(\Delta p_o-\gamma_o\Delta D)]^k+\Delta[T_o^k(\Delta\delta p-\Delta\delta p_{cgo})]+(\Delta p-\Delta p_{cgo}-\gamma_o\Delta D)^k\,\delta T_o \quad \text{…...…….....33}$$

where

$$\delta P_{cgo} = \frac{\partial P_{cgo}}{\partial S_g} \delta S_g \quad \text{.....34}$$

and

$$\delta T_o = \frac{\partial T_o}{\partial S_g} \delta S_g + \frac{\partial T_o}{\partial S_w} \delta S_w, \; p \le p_s \quad \text{.....35}$$

or

$$\delta T_o = \frac{\partial T_o}{\partial p_s} \delta p_s + \frac{\partial T_o}{\partial S_w} \delta S_w, \; p > p_s \quad \text{.....36}$$

Relative permeabilities and PVT properties all are evaluated at upstream conditions using latest iterate values of pressure, saturations, and saturation pressure.

5.2.1.4 Matrix/Fracture Flow Terms

Matrix/fracture flow terms in Eqs. 26, 27, and 28 are calculated implicitly in a manner similar to the fracture flow terms with two exceptions: the $\partial T_o / \partial p_s$ derivatives are not included for flow above the bubble point, and special considerations are given to upstream relative permeabilities when flow is from the fracture to the matrix since flow is governed essentially by matrix properties. Relative permeability to water is limited to matrix k_{rw} evaluated at zero P_{cwo}.

$$k_{rw} = k_{rw}(P_{cwo} = 0) S_{wf} \quad \text{.....37}$$

The term S_{wf} accounts for the fractional coverage of a grid block by water. Oil relative permeability is calculated as

$$k_{ro} = k_{ro}(S_w, S_g)_m S_{of} \quad \text{.....38}$$

where $K_{ro}(S_w, S_g)_m$ is evaluated using Stone's equation:

$$k_{ro} = (k_{rw} + k_{row})(k_{rg} + k_{rog}) - (k_{rw} + k_{rg}) \quad \text{.....39}$$

Gas relative permeability is calculated at a matrix gas saturation of one minus residual oil to gas and minus irreducible water saturation,

$$k_{rg} = k_{rg}(1 - S_{org} - S_{wc}) S_{gf} \quad \text{.....40}$$

For flow from the matrix to the fracture, matrix saturations are used to evaluate relative permeabilities and capillary pressures from input values.

5.3 Reservoir Model

5.3.1 Model Description and Initialisation

The geological model incorporates 26 x 48 x 50 non-orthogonal grids; representing reservoir dimensions of 10,240 x 12,600 x 3,650 ft in the X, Y, and Z directions respectively. It includes 3 fractured and partially communicating compartments. The model encompasses 4 injection wells and 2 production wells. The reference depth datum was set to 6500 ft subsurface. The reservoir exists above a moderately supportive aquifer. **TABLE 2** shows the base case properties of the simulation model.

TABLE 2. PETROPHYSICAL CHARACTERISTICS OF THE BASE CASE SIMULATION MODEL

No. of blocks	26 x 48 x 50								
Average matrix x-permeability (md)	36.5								
Average matrix y-permeability (md)	38.5								
Average matrix z-permeability (md)	1.5								
Average matrix porosity (%)	10.5								
Datum depth (ft)	6,500								
Datum pressure (psi)	3,000								
Components	N_2	CO_2	C_1	C_2	C_3	C_4	C_5	C_6	C_{7+}
Initial fluid composition	0.00	0.02	0.55	0.15	0.10	0.10	0.05	0.02	0.01
Temperature (c)	95								
Hydrocarbon pore volume (reservoir ft^3)	2,148E+6								
Total pore volume (reservoir ft^3)	7,690E+6								
Fracture x-permeability (md)	100*36.5								
Fracture y-permeability (md)	100*38.5								
Fracture z-permeability (md)	20*1.5								
Fracture porosity (%)	99								
Bottomhole pressure (psi)	1,200								
Water injection rate (stb/d)	0								
CO_2 injection rate (kscf/d)	1,800								

Average aquifer influx rate (mstb/d)	3
Simulation start time (date)	01 January 2010
Simulation end time (date)	01 January 2020

Fig. 37 demonstrates the matrix porosity distribution in the model. Porosity in general is a measure of the potential storage volume for porous media. Matrix porosity varies randomly between a minimum of 1.3E-5 to a maximum of 34%. Fracture porosity was set as 99%.

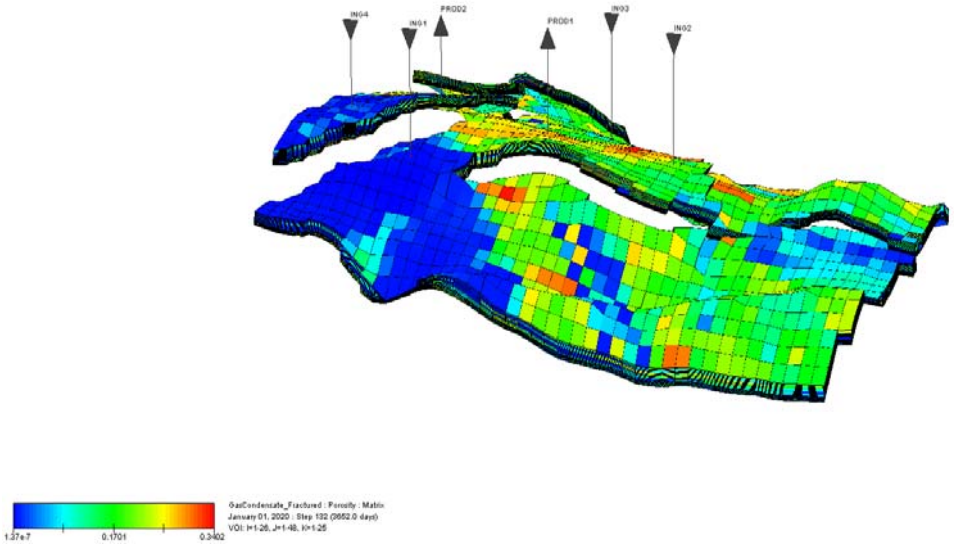

Fig. 37 - Matrix Porosity Distribution in the Model

Fig. 38 shows the matrix x-permeability distribution in the model. X-matrix permeability varies from 10 to 780 md. Fractures typically do not have much volume, but by joining pre-existing pores, they enhance permeability significantly. Fracture permeability can be a major controlling factor of the flow of fluids in many naturally fractured reservoirs. Fracture x-permeability was set as 100 times the average x-permeability of the matrix (36.5 md).

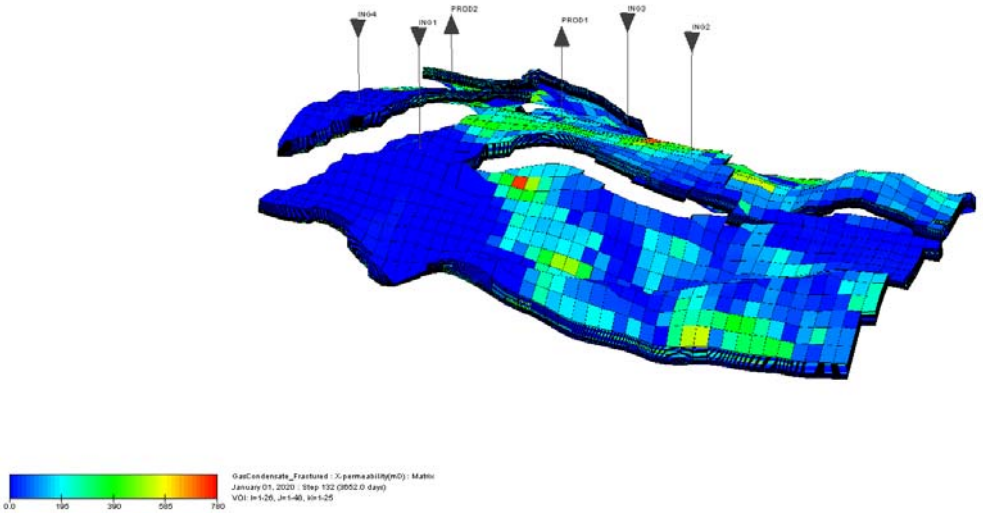

Fig. 38 - Matrix X-Permeability Distribution in the Model

Figs. 39 and **40** respectively depict the water and methane saturations in the base case model. This shows that the reservoir sits on top of a big aquifer. The aquifer supports the reservoir with an average influx of 3 mstb/d. Methane saturation forms 55% of the original composition of the reservoir fluid.

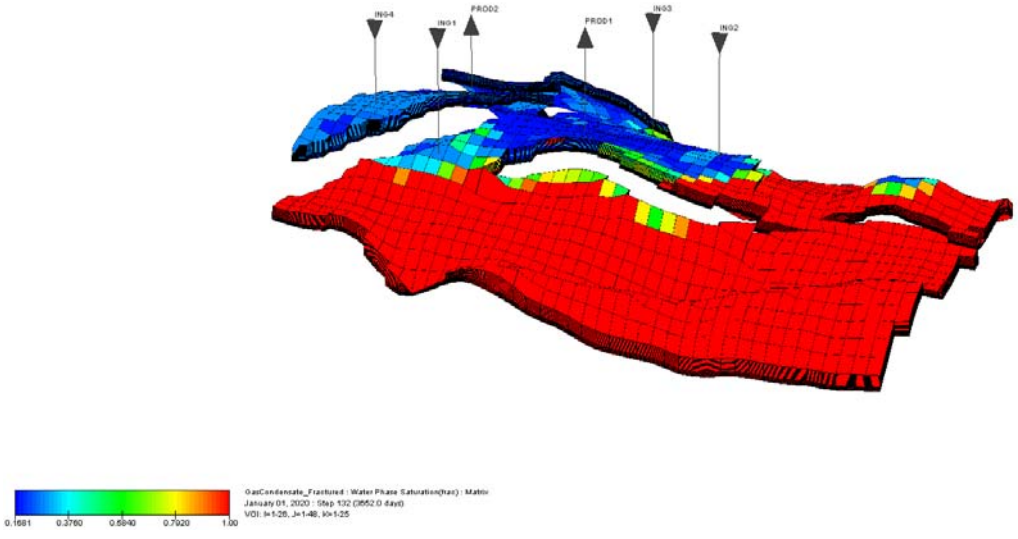

Fig. 39 - Water Saturation Distribution in the Model

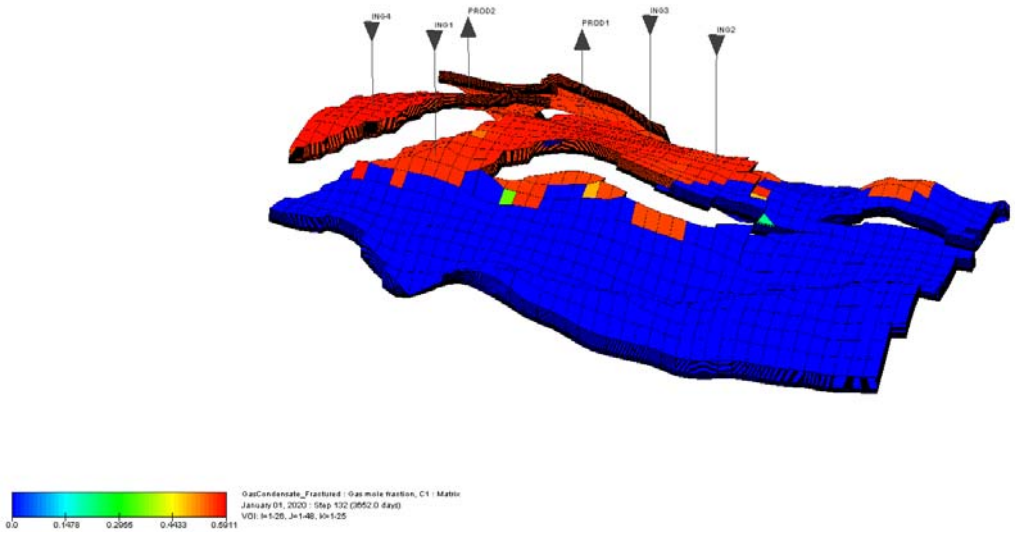

Fig. 40 - Methane Saturation Distribution in the Model

The production wells are completed in the fracture zone to allow for maximum hydrocarbons drainage. The production mode is set at a constant bottomhole pressure in order to observe the three-phase flow of natural gas, and condensate as well as injection gas. This production scheme permits the comparison of different injection pressures (and thus different capillary numbers) on the overall recovery performance.

5.3.2 Model Assumptions

- Non-Darcy flow effects are not considered.
- Capillary pressure is not considered.
- Near wellbore effects are accurately represented by a refined grid.
- Phase equilibrium is accurately calculated by the equation of state (EOS).
- A reduced permeability zone (skin) is not considered.
- No compositional gradient is considered.

5.4 Results and Discussions

This section presents the sensitivity analysis of various injection/production scenarios as well as reservoir thermodynamic parameters. The simulation throughputs are interpreted and compared based on the reservoir cumulative condensate production, cumulative natural gas production, CO_2 percentage breakthrough, water cut percentage, average reservoir pressure, condensate in place and natural gas in place.

5.4.1 Natural Depletion

Natural depletion is most certainly one of the important drive mechanisms in which the reservoir is virtually totally enclosed by imporous media and the only production energy comes mostly from the reservoir system itself. Predication of the natural depletion recovery behaviour becomes a major issue in gas condensate reservoirs in particular. **Fig. 41** shows the condensate production rate (CPR) and the condensate production total (CPT) for different reservoir initial pore pressures. During the first 6 months of production, the CPR declines from 59.91 to 3.98, from 20.19 to 1.63, and from 2.92 to 0.26 mstb/d at 5900, 3000, and 2100 psi initial pore pressure respectively. The relatively higher condensate production rates at 5900 psi compared to that of 3000 psi or 2100 psi are attributed to the large pressure drawdown that exists between reservoir pressure and the constant bottomhole pressure (1200 psi). The simulator also predicts a CPT of 5.97, 2.18, and 0.27 mmstb at the end of the 10 year simulation period at the aforementioned pressures respectively. The natural depletion performance of these systems is a result of the competition between gravity, capillary and viscous forces. The relatively higher flow rates at 5900 psi encourage viscous forces to overcome the holding effect of the gravity and capillary forces and thus drive the condensate to the production wells.

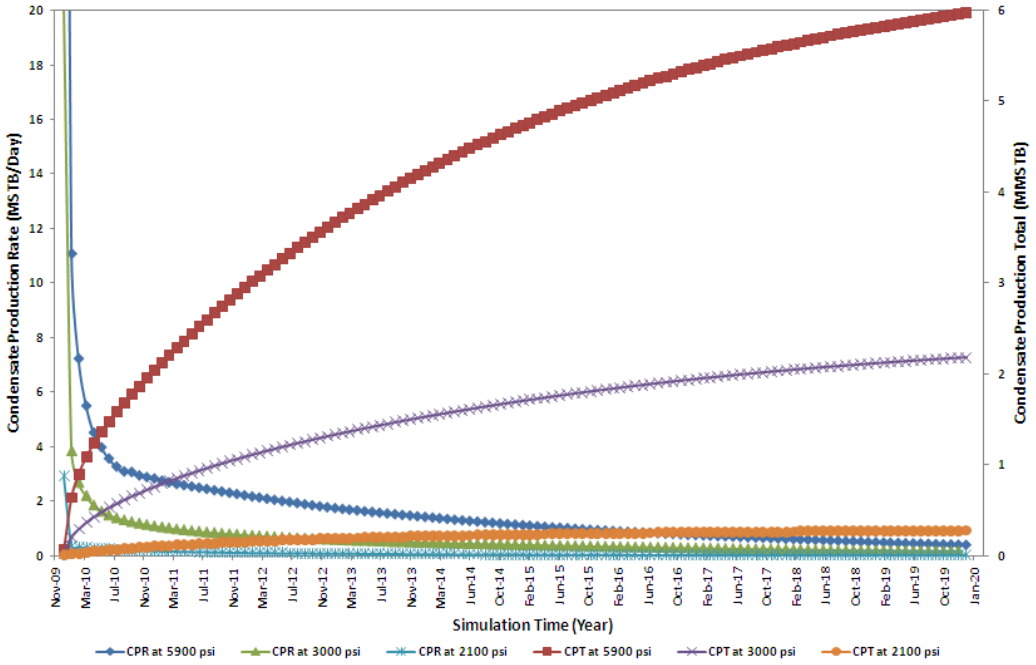

Fig. 41 - Condensate Production Behaviour during Natural Depletion

Fig. 42 shows the natural gas production rate (NGPR) and the natural gas production total (NGPT) for the three different pore pressures. The productivity index of the production wells increases with the production flow rate and thus with the initial reservoir pore pressure. The reservoir starts to produce at 1618.63, 885.29, and 501.49 mmscf/d at 5900, 3000, and 2100 psi initial pore pressure respectively. These flow rates decrease sharply as the production continues. The cumulative natural gas production is almost three-fold at 5900 psi compared to that at 2100 psi.

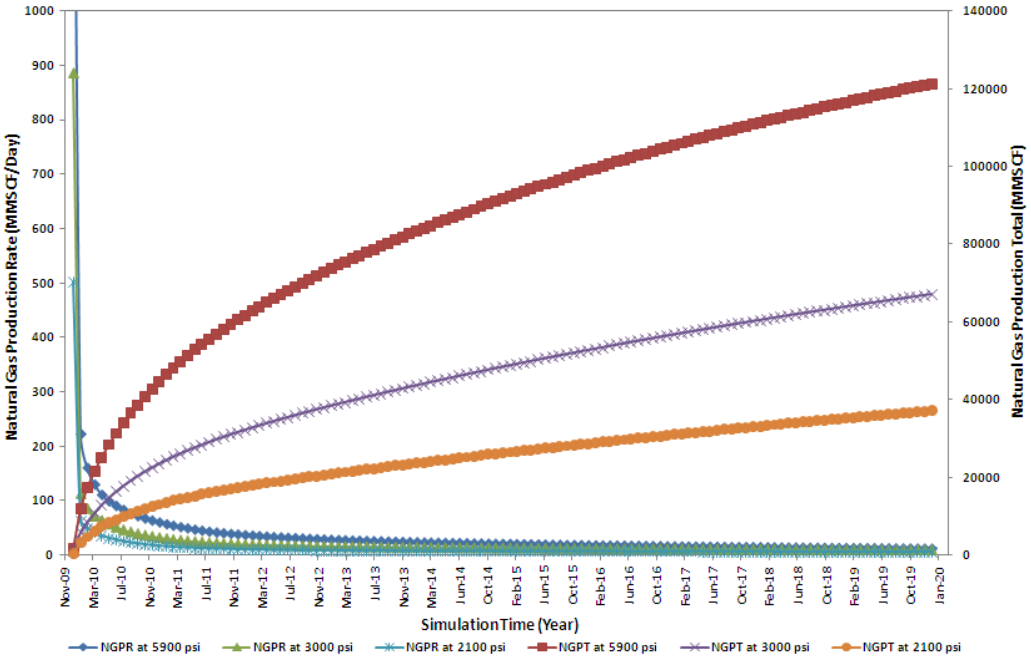

Fig. 42 - Natural Gas Production Behaviour during Natural Depletion

Fig. 43 shows some noteworthy results. The reservoir initially has 36.95, 28.35, and 21.09 mmstb condensate in place (CIP) at 5900, 3000, and 2100 psi respectively. These quantities reduce to 31.06, 26.22, and 20.92 mmstb at the end of the 10 year simulation period. The latter figures are shocking as they mean that massive volumes of condensate will be left behind in the reservoir and thus lost to production. Similarly, only small fractions of the natural gas in place will be produced at the three different pressures and the rest will remain as residual. The residual quantities are higher as the initial reservoir pressure increases. This makes the situation even worse as most of the gas condensate reservoirs exist at high pressures (Wall, 1982; Roussennc, 2001).

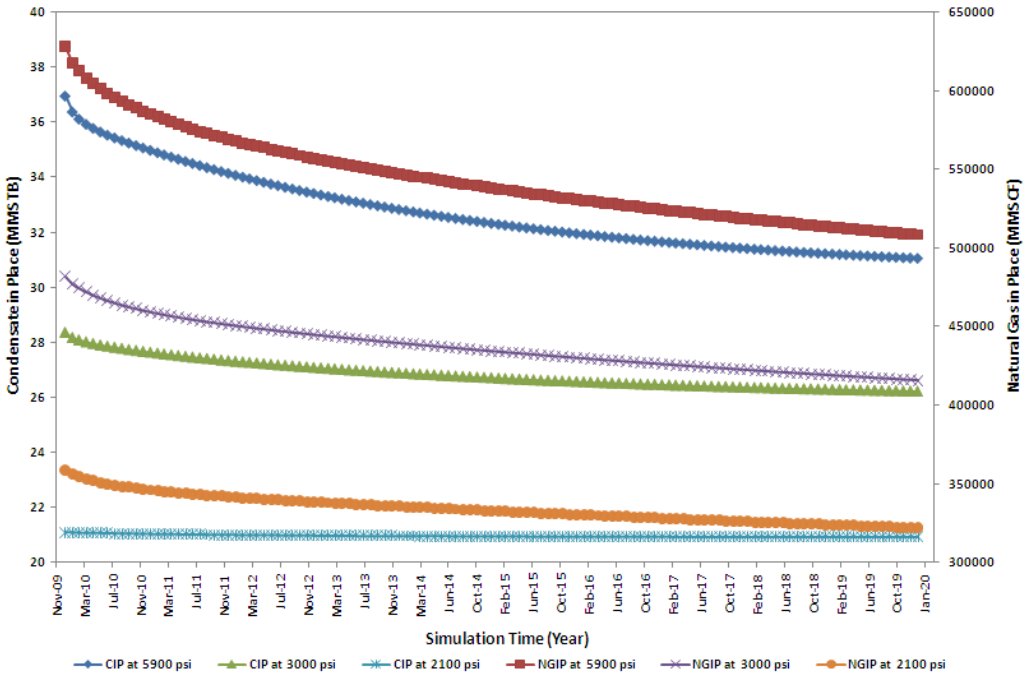

Fig. 43 - Natural Gas and Condensate in Place

Fig. 44 illustrates the change in the average reservoir pressure (ARP) as well as the overall recovery factor (RF). The ARP drops by 949.47, 348.53, and 166.95 psi at the end of the simulation period of 5900, 3000, and 2100 psi cases respectively. The RF requires some special attention. Only 12.86% of the natural gas and condensate resources is recovered in 10 years at 2100 psi initial reservoir pressure. This figure increases to 24.43 and 43.06% at 3000 and 5900 psi respectively. These figures are not satisfactory for reservoir engineers and suggest that something has to be done to boost the production performance. The inefficient natural depletion of gas condensate resources has always been a major concern in the petroleum industry.

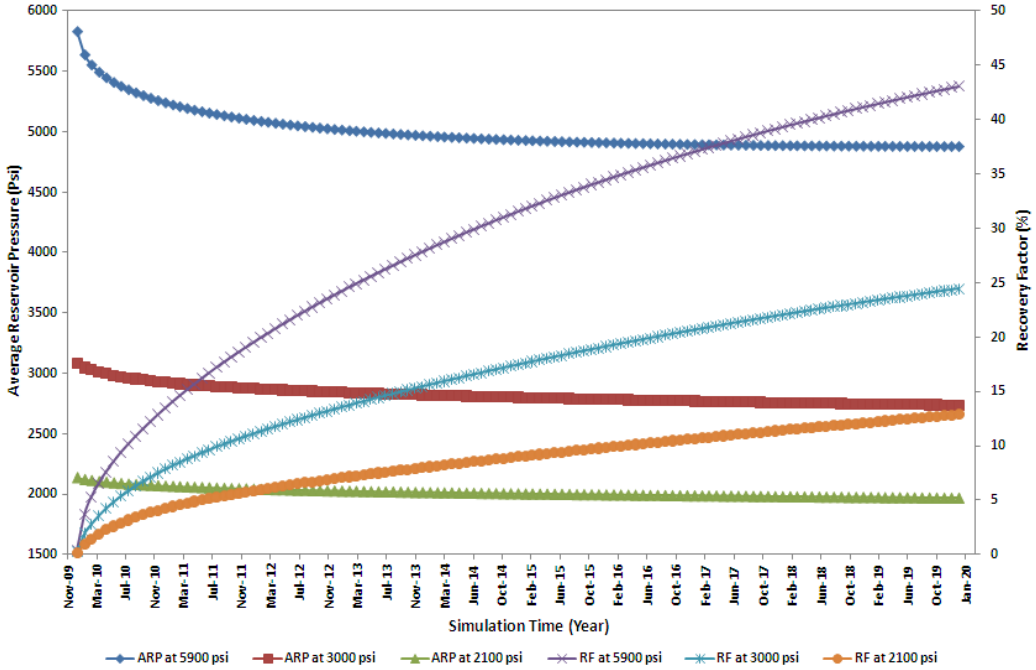

Fig. 44 - Average Reservoir Pressure and Recovery Factor

5.4.2 Waterflooding

Waterflooding has been practiced as an art in the petroleum industry to displace liquid hydrocarbons. This section investigates what if waterflooding is used to maximise the recovery from such reservoirs? Does CO_2 really increase the ultimate recovery over waterflooding? **Fig. 45** shows the behaviour of the CPT and NGPT throughout the 10 year simulation time. It illustrates that waterflooding the reservoir at rates of 400 and 200 bbl/d produces ultimate recoveries of 2.25 and 2.22 mmstb CPT, and 68043 and 67622 mmscf NGPT. The base case (BC) CO_2 injection yields better CPT and NGPT of 2.71 and 73859 mmscf.

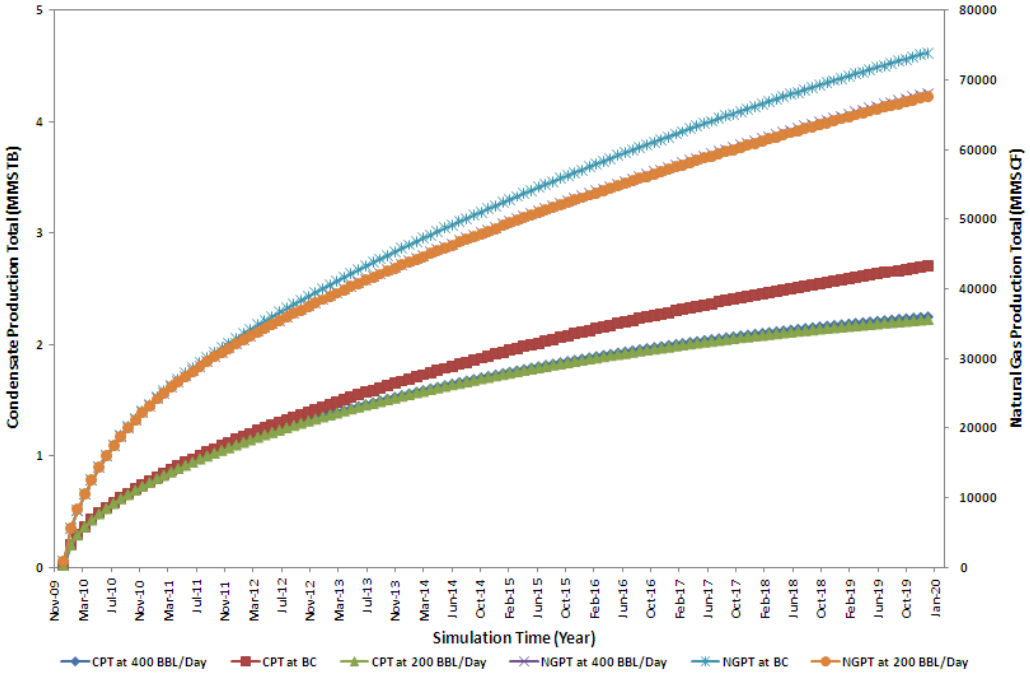

Fig. 45 - Condensate and Natural Gas Production Behaviour during Waterflooding

Fig. 46 presents the temporal behaviour of the water cut and recovery factor as a percentage. The reservoir will produce less than 1.2% water (percent to total liquid production) in 2020 at both waterflooding scenarios. Waterflooding increases the incremental recovery of both natural gas and liquid condensate by only around 0.5% of the 3000 psi natural depletion case. This may not justify the economics of the process. The other disadvantage of waterflooding gas condensate reservoirs is the bypassing and trapping of gas and liquid condensate, which can result in up to 50% of the gas being unrecovered (Dake, 1983; Fisherman and Prior, 1983).

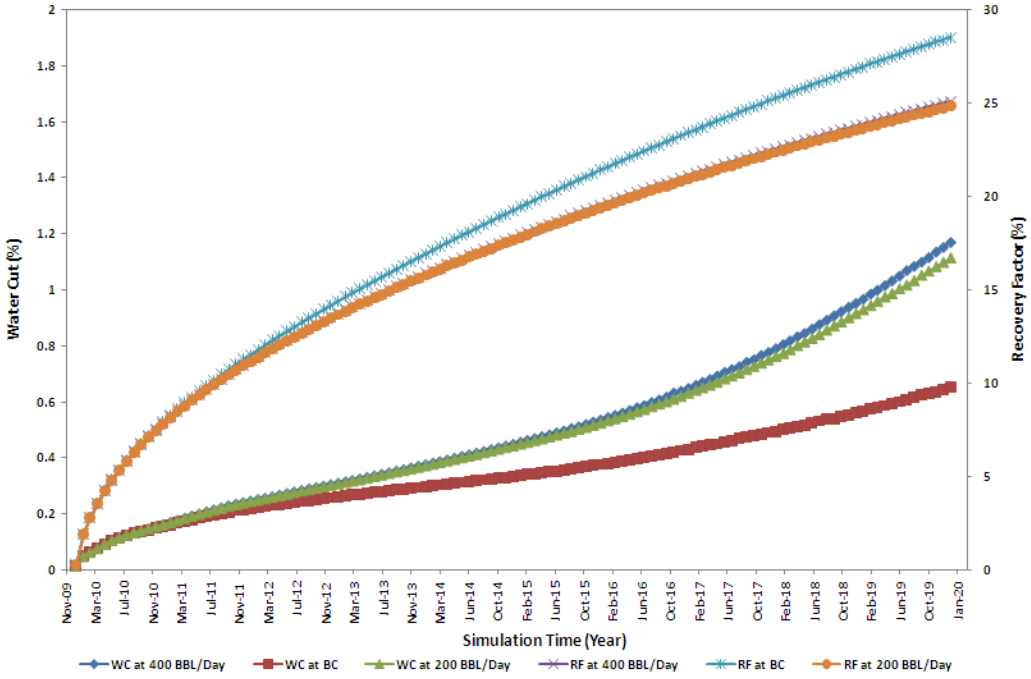

Fig. 46 - Percent Water Cut and Recovery Factor during Waterflooding

5.4.3 Continuous Gas Injection (CGI-FRS): Flow Rate Sensitivity

This section introduces the concept of continuous CO_2 injection into fractured gas condensate reservoirs at various flow rates. Getting a good glimpse of the CO_2 recovery mechanism is the natural first step in understanding the impact of injection flow rate on the production performance. The injected CO_2 travels faster through the fracture network as all the injection and production wells are completed in the fracture zone. The CO_2 interacts with the natural gas through conventional dispersion and diffusion processes. However, once the CO_2 front encounters a condensate grid cell, physical components extraction and condensate swelling takes place. The encountered condensate volume will immediately become saturated with injection gas sitting in the fracture. The matrix condensate that has been partially (or completely) saturated with CO_2 has a different composition to the original condensate. This compositional difference causes molecular diffusion of all components in the condensate phase. Some of the swollen free condensate might enter the fracture, either being dissolved completely into the fracture gas, or moving as a free phase in the fracture together with the fracture gas.

This section investigates the impact of varying the CO_2 injection rate around the base case value (1800 kscf/d) on the recovery performance. **Fig. 47** shows that the CPT at the end of the simulation period reaches 2.94, 2.70, and 2.44 mmstb at 2700, 1800, and 900 kscf/d injection rates respectively; while the NGPT for the same flow rates are respectively 75706, 73859, and 71268 mmscf. This suggests that there is a positive rate coupling between the condensate and natural gas production totals and injection flow rate. Further, the cumulative condensate production increases in excess of 19% in the BC scenario compared to that of the corresponding natural depletion at 3000 psi shown in Fig. 41. CO_2 injection also accelerates the condensate and natural gas productions. The total condensate production for instance after 5 years of production was 1.69 and 1.91 mmstb during natural depletion at 3000 psi and BC CO_2 injection respectively.

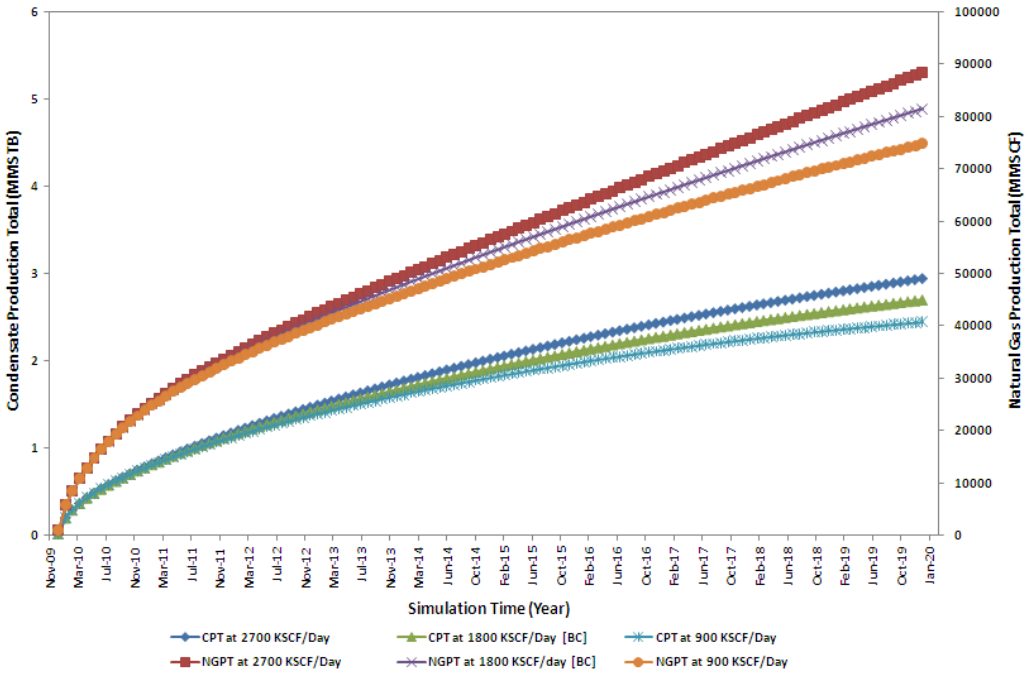

Fig. 47 - Condensate and Natural Gas Production Behaviour during CGI-FRS

Although the experimental and simulation work suggest that higher injection rates above the critical value result in lower recovery in a core plug scale (Crandall, 2007; Al-Abri et al, 2009), the simulation models captured greater CO_2 saturation and distribution at higher injection rates at full field scales. This suggests that in addition to the mixing that is

caused by diffusion, mixing is also introduced by local variations in the flow velocity of the fluids in the porous media. This velocity induced mixing is generally referred to as dispersion (Perkins and Johnston, 1963).

Fig. 48 illustrates the CO_2 breakthrough as a percentage of the produced natural gas at any given time. It shows that the CO_2 breaks through six months after the commencement of injection. This is not surprising as the CO_2 follows the easiest pathway in the reservoir i.e. through fractures. However, the cumulative CO_2 percent at the end of the 10 year simulation period does not exceed 15% in all cases. Fig. 48 also illustrates the total recovery factor of each injection rate; with recoveries of 30.14, 28.52, and 26.66% at 2700, 1800, and 900 kscf/d injection rates respectively.

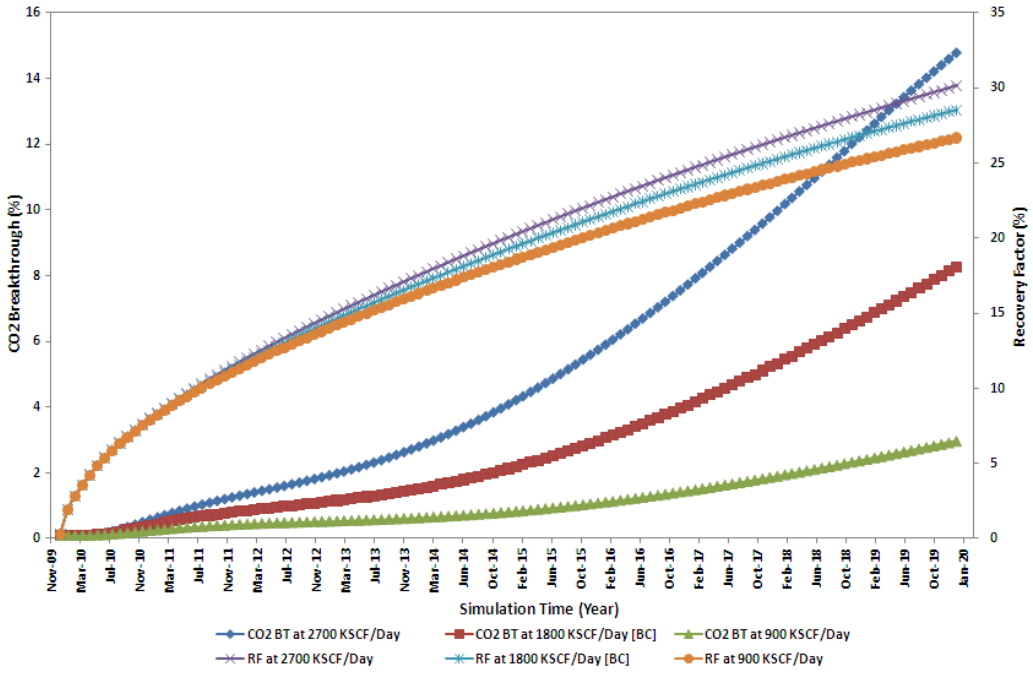

Fig. 48 - Percent CO_2 Produced and Recovery Factor during CGI-FRS

5.4.4 Continuous Gas Injection (CGI-PPS): Pore Pressure Sensitivity

This section investigates the effect of reservoir pore pressure on the condensate and natural gas recovery performance. The CO_2 injection rate was maintained at the BC value (1800 kscf/d). **Fig. 49** depicts both the condensate production total (CPT) and the natural gas production total (NGPT) to be strongly related to the initial reservoir pore pressure.

The CPT at the end of the injection period approaches 6.51, 2.70, and 0.51 mmstb for 5900, 3000 (BC), and 2100 psi initial reservoir pore pressures respectively. Similarly, the NGPT after 10 years of injection reaches 128256, 73859, and 43266 mmscf for the aforesaid pressures respectively.

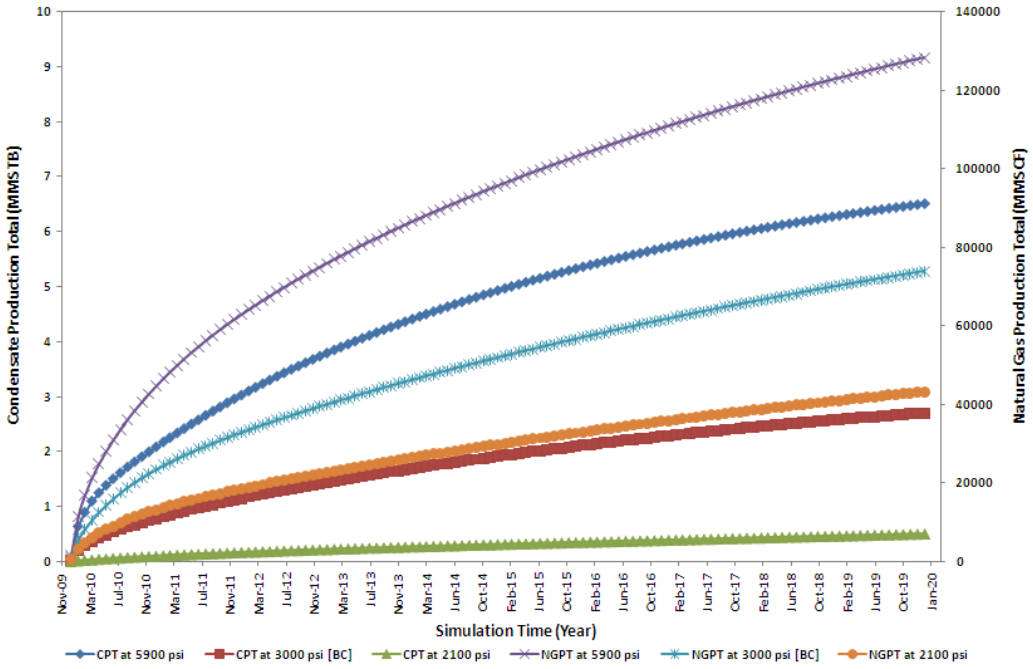

Fig. 49 - Condensate and Natural Gas Production Behaviour during CGI-PPS

The reservoir produces more condensate and natural gas at higher pore pressures for a couple of reasons:

1. More hydrocarbon volumes exist in the reservoir at high pore pressures; with gas pore volumes of 1900, 1916, and 2165 $mmft^3$ and condensate pore volumes of 41, 41, and 0 mmbbl at 2100, 3000, and 5900 psi respectively. This would indicate that the reservoir is capable of producing greater surface volumes from higher initial pressures for a certain pressure drawdown,
2. The recovery mechanism at the three displacement pressures is significantly different. The CO_2 displaces the condensate immiscibly at 2100 psi resulting in residual saturations staying behind the flood front. The displacement processes are schematically illustrated in **Fig. 50** for the miscible and

immiscible displacements. The reduction in interfacial tension and capillary forces as well as the presence of favourable solubility and phase behaviour relationships increase the efficiency of the miscible CO_2 injection process.

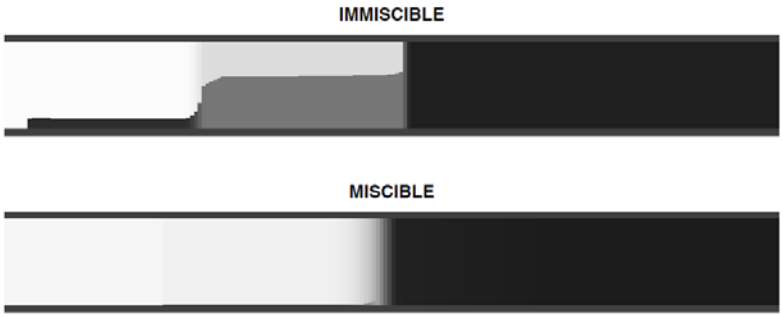

Fig. 50 - CO_2 Displacement Process Schematic

Fig. 51 shows that the injected CO_2 breaks through at almost the same time in all scenarios (6 months after the commencement of injection). The produced CO_2 percentage in the natural gas stream, however, tends to increase more rapidly in the immiscible displacement. This is not surprising as the CO_2 would be expected to inter-finger through the reservoir to the production wells at lower displacement pressures. The favourable CO_2 solubility relationships with the condensate at 5900 psi as well as the existence of a more stable displacement front make the injected CO_2 show a later breakthrough behaviour compared to other cases. The recovery factor changes significantly in the three cases; with values of 15.95, 28.52, and 46.95% at 2100, 3000, and 5900 psi respectively.

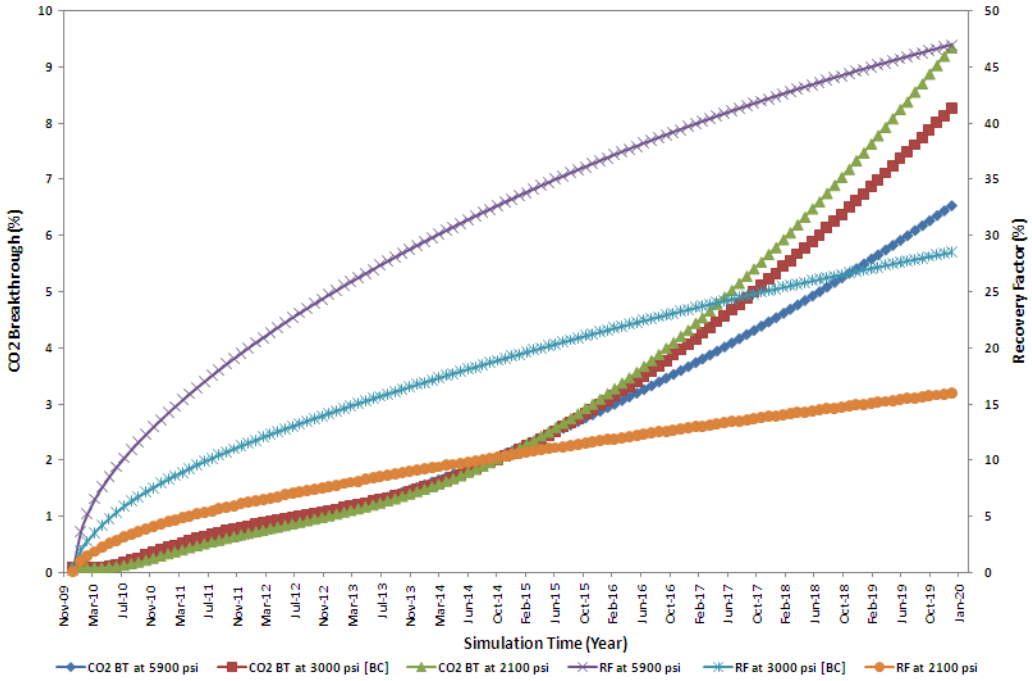

Fig. 51 - Percent CO_2 Produced and Recovery Factor during CGI-PPS

5.4.5 Gas Injection After Waterflooding (GAW)

This section intends to examine the production behaviour following GAW. **Fig. 52** displays the simulation results of two scenarios: CO_2 injection after initial three years of waterflooding (GA3W), and CO_2 injection after initial six years of waterflooding (GA6W). These injection procedures were considered to see whether waterflooding would actually provide a stabilising effect on the CO_2 flood front in a fractured gas condensate reservoir. The CPT and NGPT production curves show that the lower water injection period at the beginning the better the recovery performance. In fact, pure CO_2 injection still produces the best natural gas and condensate recovery. However, GA3W or GA6W may prove practical from an economic point of view.

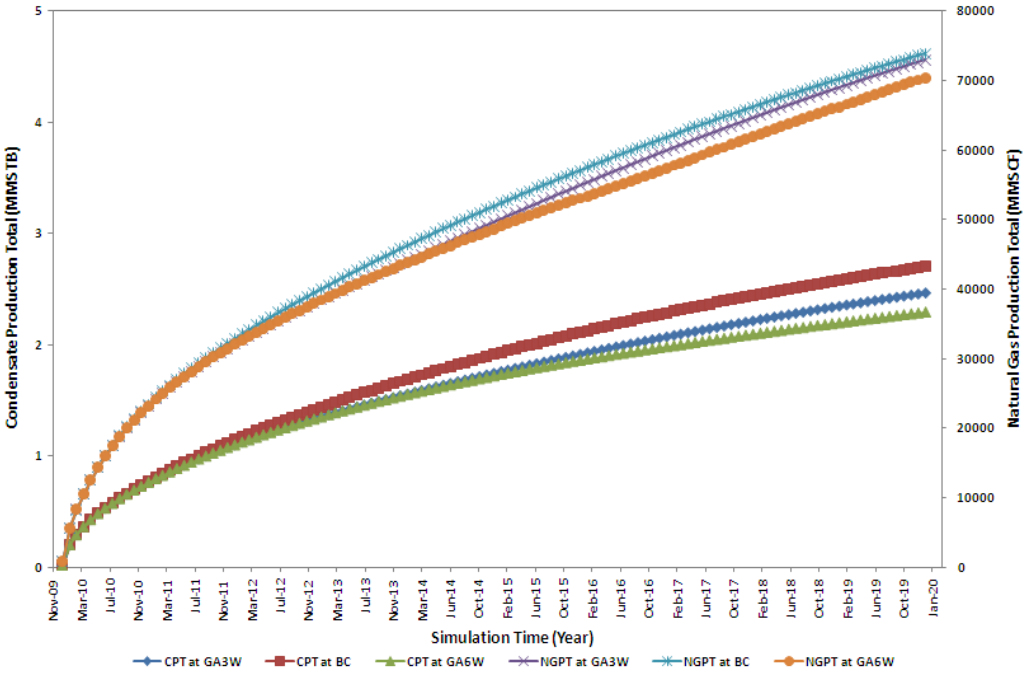

Fig. 52 - Condensate and Natural Gas Production Behaviour during GAW

In either case, the heterogeneity of the reservoir causes the dominant transport mechanisms during waterflooding to be layer-flow rather than piston flow. This before and after waterflooding behaviour was visualised using experimental micromodels by Sohrabi et al. (2007). They show that the slow thickening of water films at the sides and corners of the oil filled pores is a direct consequence of a capillary dominated flow regime. **Fig. 53** shows that the oil is divided into two types following gas injection from the same end as the water i.e. bottom up. The first type is oil in the form of some filaments surrounded with thick water layers. This oil is not seen by the incoming gas. The second type is thick oil ganglia in contact with the gas channel; formed by fluid redistribution or by local oil transfer brought about by the gas injection.

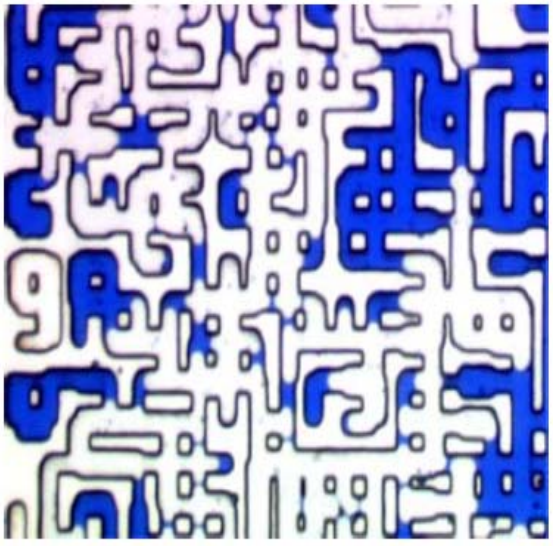

(a) before waterflooding

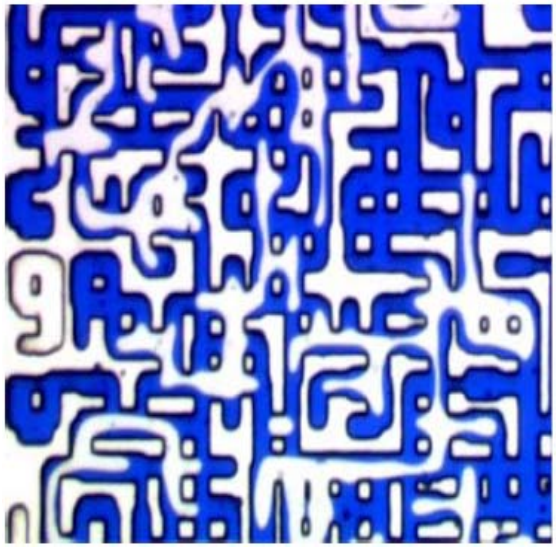

(b) after waterflooding

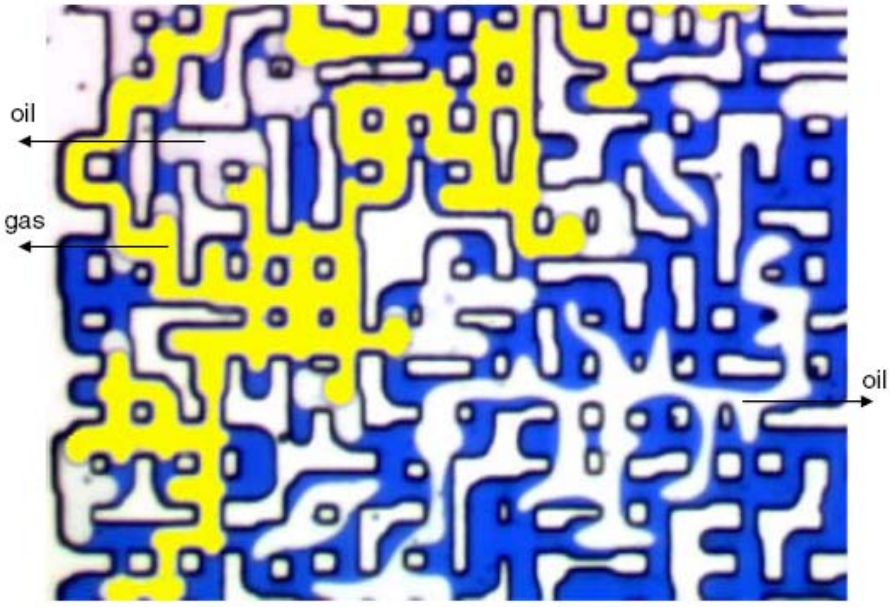

(c) during gas injection

Fig. 53 - Micromodel Visualisations of Gas Injection

Fig. 54 illustrates the reservoir water cut and recovery factor percentages. Water cut remains low throughout the 10 year production period and stays less than 1%. Water cut is highest when the reservoir is waterflooded for 6 years before gas injection is commenced. The ultimate recovery factor increases from 25.88 to 27.30 to 28.52% when the reservoir is developed through WA6W, WA3W, and BC continuous CO_2 injection respectively.

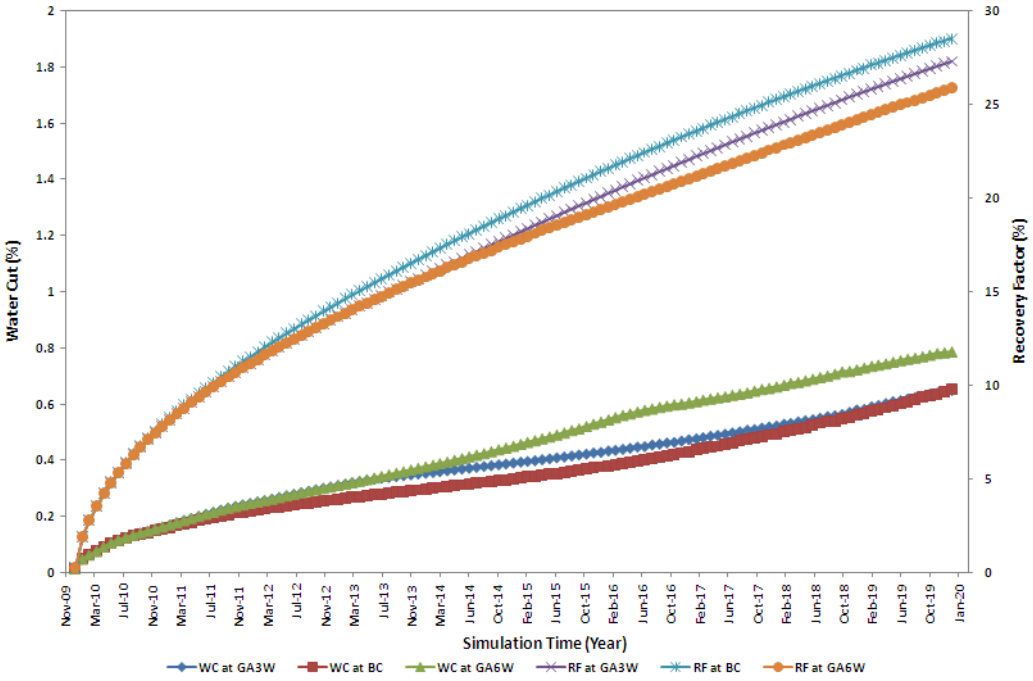

Fig. 54 - Percent Water Cut and Recovery Factor during GAW

5.4.6 Water Alternating Gas Drive (WAG)

The WAG process consists of alternate injections of water and gas for periods of time to theoretically provide better sweep efficiency and reduce gas channelling from injector to producer. Water injection serves to drive the mobilised hydrocarbons (with lower viscosity and increased volume) towards the production wells, thus resulting in a waterflood at an improved mobility ratio. The WAG process also reduces the mobility ratio of CO_2 as water blocks the CO_2 invaded zones and slows down its advancement, thereby preventing its rapid production. This section investigates two WAG scenarios: the reservoir is initially waterflooded for 1 year and then on/off alternate CO_2/water injection three times until the reservoir is again waterflooded for the rest of the simulation time (WAG1), whereas the second scenario is to waterflood the reservoir for 3 years and then on/off alternate CO_2/water injection three times (WAG3). WAG1 and WAG3 produce better results than pure waterflooding but prove not as good as GAW.

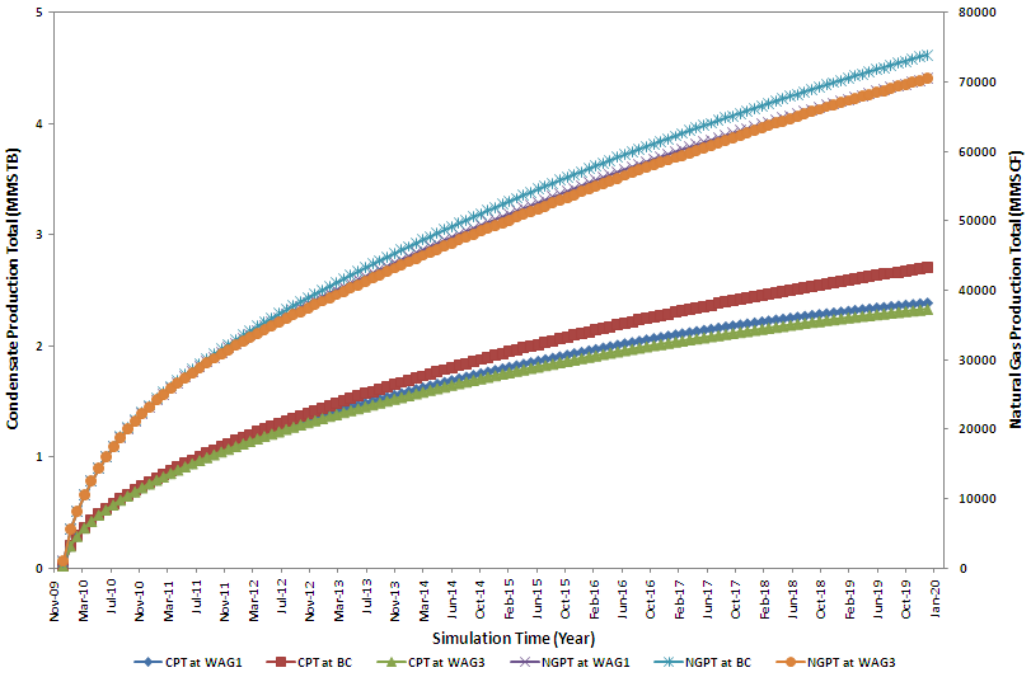

Fig. 55 - Condensate and Natural Gas Production Behaviour during WAG

Fig. 56 illustrates that WAG1 and WAG3 yield very similar recovery factors; with magnitudes relatively less than those of GAW but more than pure waterflooding. Water cut values also remain below 1% with the WAG1 scheme having sharper increase at the end.

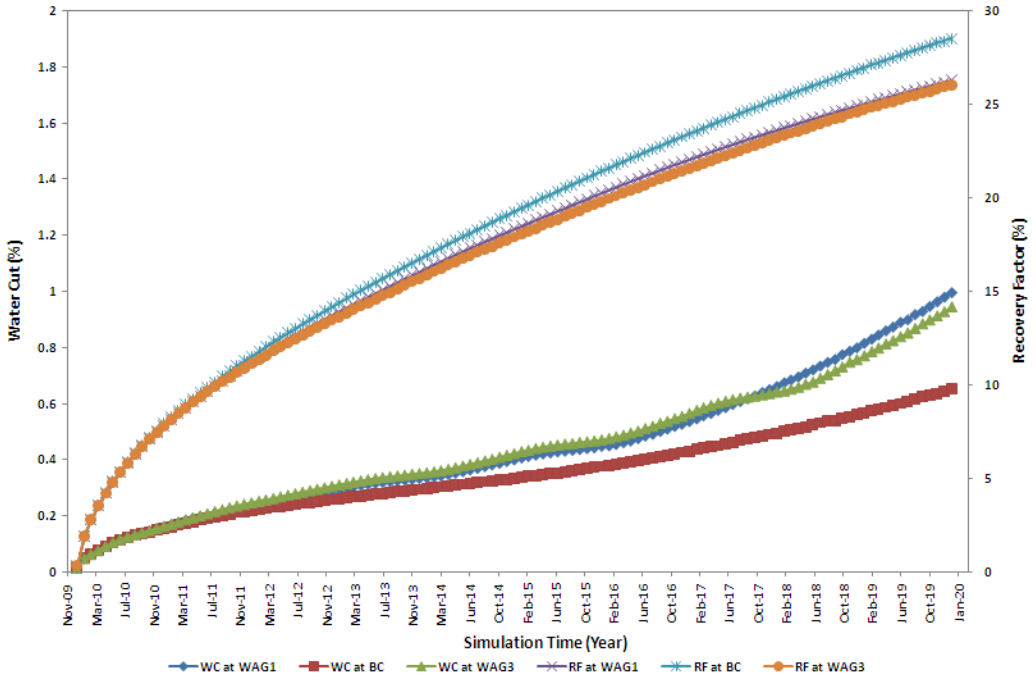

Fig. 56 - Percent Water Cut and Recovery Factor during WAG

5.4.7 Reservoir Composition

In petroleum engineering, and specifically in reservoir engineering, the main issue is one of the physical behaviour and characteristics of the petroleum fluids. The composition of the fluid clearly has a significant impact on the behaviour and properties and thus on the recovery of these fluids. This section investigates three different compositions: COMP3 that consists predominantly of methane and other short-chain components, COMP2 is the base case composition, and COMP1 that consists of relatively smaller fractions of light components and more heavy ends. **TABLE 3** shows the components of the three compositions.

TABLE 3. SIMULATION FLUID COMPOSITIONS

Components	**N_2**	**CO_2**	**C_1**	**C_2**	**C_3**	**C_4**	**C_5**	**C_6**	**C_{7+}**
COMP1	0.00	0.02	0.50	0.15	0.14	0.10	0.05	0.02	0.02
COMP2	0.00	0.02	0.55	0.15	0.10	0.10	0.05	0.02	0.01
COMP3	0.00	0.02	0.60	0.20	0.10	0.05	0.025	0.0025	0.0025

Fig. 57 shows the phase envelopes for the three compositions. The reservoir will experience retrograde thermodynamic conditions when the pressure reaches the dewpoint line of the corresponding composition. The extent of condensation under isothermal pressure reduction varies considerably and is to a large extent related to the temperature difference between the critical temperature of the fluid and the reservoir temperature (black dashed line). COMP3 would be expected to experience greater condensate formation and thus condensate blockage.

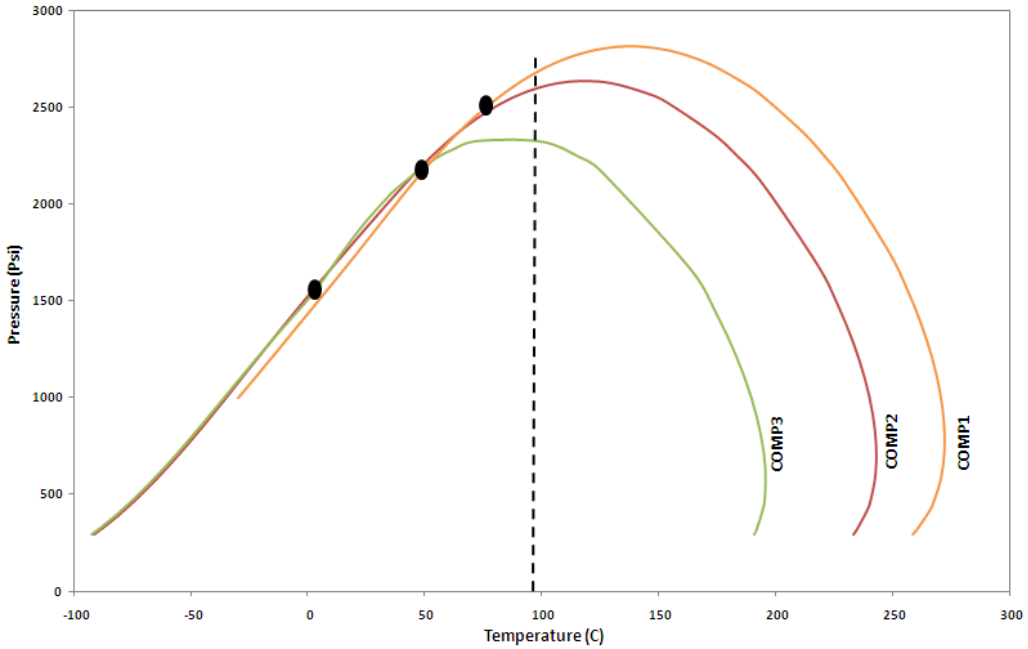

Fig. 57 - Phase Envelopes Showing Thermodynamic Simulation Conditions

The role of the CO_2 as a vaporising agent will be more critical in COMP3 compared to the others as greater formation damage would be expected to form in this case. **Fig. 58** demonstrates that CO_2 injection into the same fractured reservoir but having different compositions, produces 2.45, 2.71 and 2.84 mmstb CPT for COMP1, COMP2 and COMP3 respectively. The NGPT for these cases is 79424, 73859, 68433 mmscf respectively.

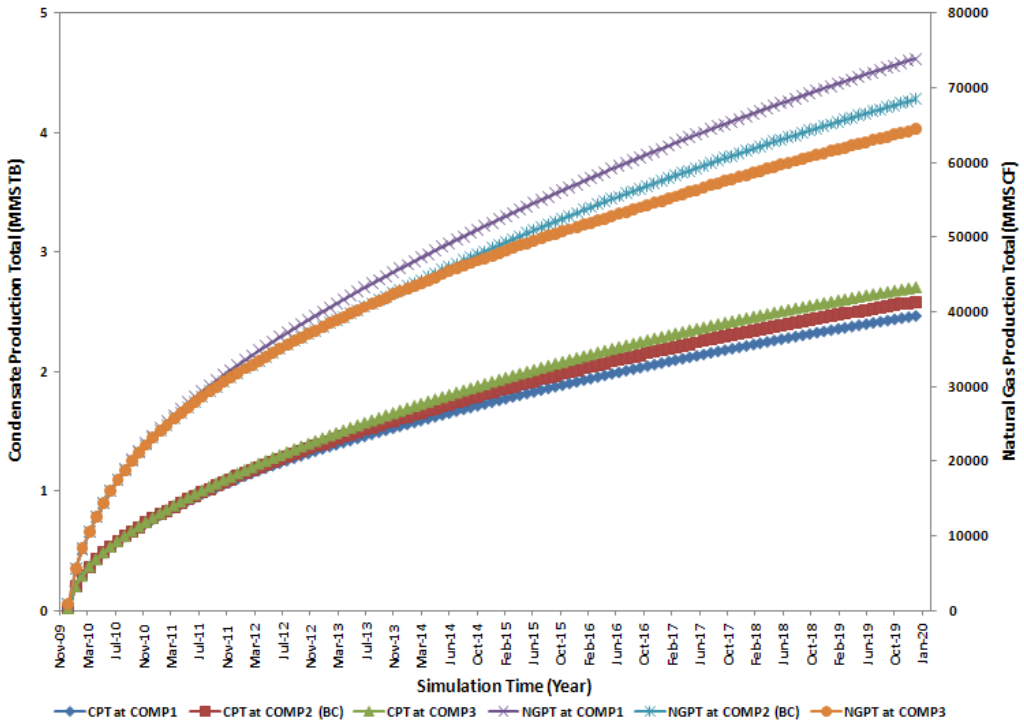

Fig. 58 - Condensate and Natural Gas Production Behaviour for Different Reservoir Compositions

Fig. 59 shows the CO_2 breakthrough and recovery factor profiles in percentages. The CO_2 still breaks through at almost the same time for the three compositions (i.e. 6 months after the commencement of injection). However, the CO_2 percentage builds up relatively faster in COMP3 as lower net pore volume would be there in the reservoir following greater condensate dropout. The recovery factors vary slightly. Hydrocarbons recoveries are relatively higher for leaner fluids than richer fluids because less condensate blockage is formed in the production of lean gases.

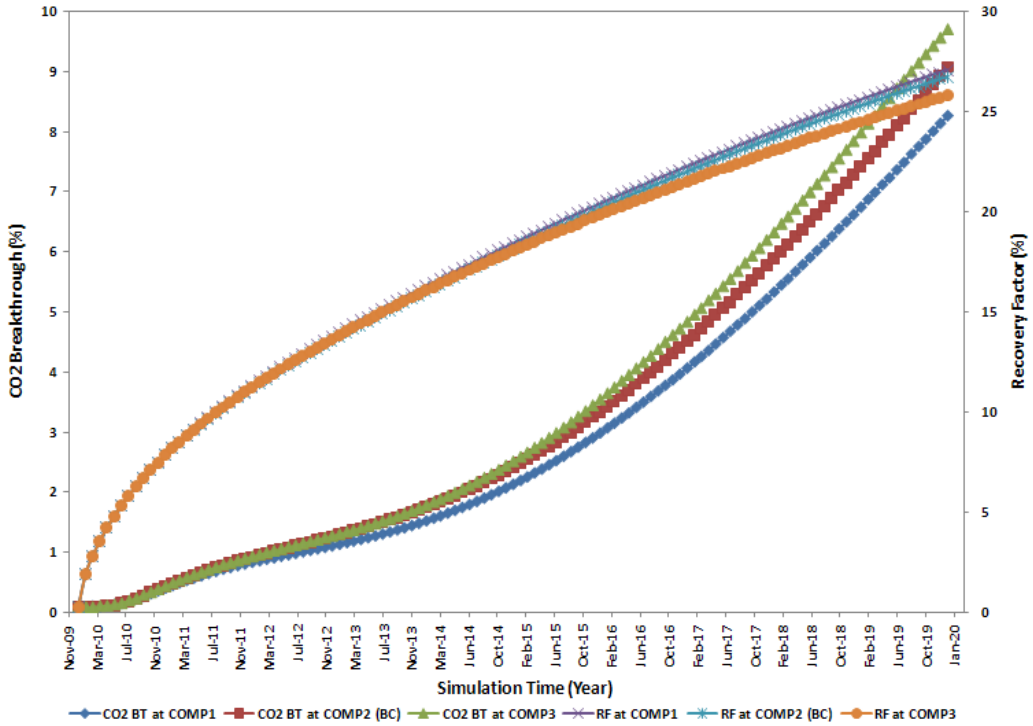

Fig. 59 - Percent Water Cut and Recovery Factor for Different Reservoir Compositions

5.5 Conclusion

This chapter has numerically investigated the impact of several development processes (natural depletion, CO_2 injection, injection flow rate, and WAG) as well as reservoir fluid thermodynamic conditions (initial reservoir composition, and initial pore pressure). The relative significance of each of these sensitivity runs on the production performance is shown in **TABLE 4** below.

TABLE 4 shows that initial pore pressure determines the reservoir productivity during natural depletion. The drawdown between reservoir pressure and the constant bottomhole pressure (1200 psi) increases as the initial pore pressure increases; resulting in higher condensate and natural gas recoveries. When the reservoir pore pressure was set at 3000 psi, waterflooding was found to increase the incremental recovery factor by only 0.5%. This may not justify the economics of the process. The other disadvantage of waterflooding gas condensate reservoirs is the bypassing and trapping of gas and liquid condensate, which can result in up to 50% of the gas being unrecovered (Dake, 1983; Fisherman and Prior, 1983).

The continuous CO_2 injection was found to increase the recoveries appreciably; with the recovery factor increasing with CO_2 injection rate. The CO_2 interacts with the natural gas through conventional dispersion and diffusion processes. However, once the CO_2 front encounters a condensate grid cell, physical components extraction and condensate swelling takes place. The encountered condensate volume will immediately become saturated with injection gas sitting in the fracture. The matrix condensate that has been partially (or completely) saturated with CO_2 has a different composition than the original condensate. This compositional difference causes molecular diffusion of all components in the condensate phase. Some of the swollen free condensate might enter the fracture, either being dissolved completely into the fracture gas, or moving as a free phase in the fracture together with the fracture gas. The characteristics of the base case model are highlighted in orange in TABLE 2.

When the CO_2 injection rate was maintained at the base case value (1800 KSCF/Day), this constant injection was found to be a strong function of the initial reservoir pore pressure. The displacement mechanisms change from immiscible condensate displacements at 2100 psi to near-miscible at 3000 psi to completely miscible at 5900 psi. Gas injection after waterflooding (GAW) and water alternating gas injection (WAG) were investigated to see whether these injection schemes would actually provide better sweep efficiency and reduce gas channelling from injector to producer. Contrary to common understanding, these schemes do not provide the optimum recoveries from fractured gas condensate reservoirs but they still can be practical from an economic point of view. In addition, the composition of the reservoir fluid was clearly found to have a significant impact on the behaviour and properties and thus on the recovery of these fluids.

TABLE 4. SENSITIVITY RESULTS OF VARIOUS DEVELOPMENT PROCESSES AND RESERVOIR CONDITIONS

	Sensitivity Description	**Sensitivity Cases**	**CPT (MMSTB)**	**NGPT (MMSCF)**	**RF (%)**
1	Natural Depletion	2100 psi	0.28	37144	12.86
		3000 psi	2.18	66998	24.43
		5900 psi	5.97	121234	43.06
2	Waterflooding	200 BBL/Day	2.22	67623	24.84
		400 BBL/Day	2.25	68043	25.08
3	Continuous Gas Injection: Flow Rate Sensitivity (CGI–FRS)	900 KSCF/Day	2.44	71268	26.67
		1800 KSCF/Day	2.71	73859	28.52
		2700 KSCF/Day	2.94	75706	30.14
4	Continuous Gas Injection: Pore Pressure Sensitivity (CGI–PPS)	2100 psi	0.51	43266	15.95
		3000 psi	2.71	73859	28.52
		5900 psi	6.51	128256	46.95
5	Gas Injection After Waterflooding (GAW)	GA3W	2.46	72921	27.30
		GA6W	2.29	70394	25.88
6	Water Alternating Gas Injection (WAG)	WAG1	2.38	70456	25.82
		WAG3	2.33	70466	26.04
7	Reservoir Composition	COMP1	2.45	79424	29.28
		COMP2	2.71	73859	28.52
		COMP3	2.84	68433	25.81

CHAPTER VI

CONCLUSIONS AND RECOMMENDATIONS

Gas condensate reservoirs are increasingly becoming commonplace. The displacement mechanisms in such systems are known to be distinctively different to those in conventional gas/oil reservoirs. Because CO_2 injection into gas condensate reservoirs has been conceptually proposed to be a promising technology from economical and environmental standpoints, quantitative understanding of interfacial interactions and fluid dynamics has been lacking. This is the main purpose of this research work. This chapter presents the main technical conclusions and potential recommendations for future studies.

6.1 Conclusions

The technical goal of this research work was to better understand, by means of experiments and numerical simulation, the interplay among viscous, gravitational, and capillary forces during CO_2 injection into gas condensate reservoirs. Rather than analysing the individual effect of each of these forces alone, this study investigates the parameters that gauge multiphase flow through porous media such as interfacial tensions, relative permeabilities, mobility ratios, and residual saturations after drainage with CO_2.

Chapter III evaluated the effectiveness of carbon dioxide (CO_2), methane (CH_4), and nitrogen (N_2) injection into gas condensate reservoirs through laboratory interfacial tension (IFT) and spreading coefficient measurements at various pressure and temperature conditions. The chapter concludes that:

1. The hierarchy of the experimental density values of each of the injection gases with brine and condensate indicates that brine would segregate towards the bottom of the pore space in an equilibrium three-phase fluid system,
2. N_2 and CH_4 density-differences with both brine and condensate show approximately linear trends but with slightly different slopes. CO_2, however, demonstrates a density-difference trend close to a third-order polynomial function with both brine and condensate at 95 ^oC,

3. The density-differences tend to decrease for all systems when test temperature is increased to 160 ^{o}C,
4. The equilibrium IFT decreases with pressure for the CO_2-brine, CO_2-condensate, CH_4-brine, CH_4-condensate, N_2-brine, and N_2-condenaste systems. This indicates that gas solubility increases with pressure at a given temperature,
5. The drop interface of the N_2/brine and CH_4/brine systems was observed to be more sensitive to temperature than pressure as the IFT magnitudes were 19% and 22% lower respectively when temperature was increased from 95 ^{o}C to 160 ^{o}C,
6. N_2, CH_4 and CO_2 were observed to achieve complete miscibility with the condensate at 7400, 4780, and 3120 psi respectively at 95 ^{o}C,
7. The spreading coefficient remained positive throughout the tested pressure range at 95 ^{o}C indicating the presence of continuous condensate films (in the centre of the pores) over the water films covering the rock grains. These observations suggest the magnitude of the condensate drainage during gas injection as well as losses of injected gas to the reservoir water,
8. Gas injection at very low IFT (order of 10^{-2} dyne/cm) could effectively recover the condensate.

Chapter IV evaluated the efficiency of CO_2 injection into gas condensate reservoirs through recovery performance and mobility ratio measurements; with special emphasis on the rate-dependent, IFT-dependent, and injection gas composition-dependant relative permeabilities. The chapter concludes that:

1. Phase behaviour is of a prime consideration in the development and management of gas condensate reservoirs. Favourable relationships stimulate the swelling of the condensate volume leading to improved recovery,
2. Fluid properties are responsible for gravity segregation and frontal stability and thus the macroscopic displacement efficiency. Lower injection pressures experience a higher degree of gravity segregation as the condensate remains the denser phase leading to poor sweep efficiencies. CO_2 injection at high

pressures provides a stabilising effect on the flood front and thus a better mobility ratio,

3. Interfacial tension (IFT), displacement flow rate, injection gas composition, mobility ratio and viscosity ratio were found to affect both condensate and CO_2 relative permeability values,
4. Miscible displacements not only delayed injection gas breakthroughs but also improved the ultimate condensate sweep efficiency. Furthermore, relative permeability data was found to increase with displacement pressure leading to lower residual condensate saturations. The rapid buildup of mobility ratios in the immiscible displacements indicates the formation of viscous fingers,
5. Slower displacement rates produce better condensate recovery and later breakthrough of CO_2. This negative rate coupling is directly related to phase trapping and mobilisation of condensate fluids. High injection rates indicate the growth of narrow dendritic fingers that displace lower pore volumes for a certain volume of gas injection. The condensate relative permeability was found to change appreciably whereas the CO_2 relative permeability change was found to be limited to a narrow range,
6. The relative permeability curves showed that a small saturation of the injection gas inside the core drastically reduces the relative permeability of the condensate, and that this effect becomes more pronounced as methane concentration in the injection gas increases. The condensate recovery was more than double for the pure CO_2 injection as opposed to pure methane injection at a unity mobility ratio.

Chapter V evaluated the behaviour of CO_2 injection on a field scale through numerical simulations in heterogeneous, anisotropic, fractured and faulted systems. The study also investigated the performance of various reservoir fluid thermodynamic conditions, injection design variables, and economic recovery factors associated with CO_2 injection. The chapter concludes that:

1. Initial pore pressure determines the reservoir productivity during natural depletion. The drawdown between reservoir pressure and the constant

bottomhole pressure (1200 psi) increases as the initial pore pressure increases; resulting in higher condensate and natural gas recoveries,

2. Waterflooding increases the incremental recovery factor of the natural depletion process by only 0.5%. This may not justify the economics of the process. The other disadvantage of waterflooding gas condensate reservoirs is the bypassing and trapping of gas and liquid condensate, which can result in up to 50% of the gas being unrecovered (Dake, 1983; Fisherman and Prior, 1983),
3. Continuous CO_2 injection was found to increase the natural gas and condensate recoveries appreciably; with the recovery factor increasing with CO_2 injection rate,
4. Gas injection after waterflooding (GAW) and water alternating gas injection (WAG) could be considered for an economical exploitation,
5. The composition of the reservoir fluid was clearly found to have a significant impact on the behaviour and properties and thus on the recovery of these fluids.

6.2 Recommendations

Computerised Tomography Scanned (CTS) images would reveal the magnitude of bypassing for the immiscible displacements and for the unfavourable viscosity ratio corefloods. CTS images would be very helpful in order to identify the saturation profiles in all experiments to be contacted and prove the dominant role of the IFT, viscosity ratios and capillary end effects for low flow rates.

The IFT effect should also be investigated for a heterogeneous core. Heterogeneities could be identified using CTS images. Results for different flow rates, viscosity ratios and IFT should be compared with the respective ones from the homogeneous core of this study. Wettability is definitely a factor affecting the experimental data. Oil-wet and mixed cores should be employed to investigate the IFT and flow rate effects on relative permeability. Imbibition experiments would provide information on how relative permeability curves depend on the saturation path and reveal hysteresis phenomena.

Of course, the ultimate future work is the application of the findings of this work in the field with actual fluids and flow conditions. This work can be used to offer predictive values of relative permeability and, with the help of the non-Darcy coefficient, can aid greatly in the matching of actual field flow behaviour. This notion can allow the optimisation of field operations and, by extension, it can also allow for the optimisation of near-well geometry such as perforation schemes, well completions and reservoir-to-well contact, such as hydraulic fracturing. While these ideas are outside the scope of this work they are certainly intimately connected and their engineering is a highly recommended future direction.

REFERENCES

Adamson, J. A., and Flock, D. L. (1962). Prediction of Miscibility. *Canadian Petroleum Technology*, 72-77.

Afidick, D., Kaczorowski, N. J., & Bette, S. (1994). *Production Performance of Retrograde Gas Reservoir: A Case Study of the Arun Field*. Paper presented at the SPE Asia Pacific Oil and Gas Conference, Melbourne, Australia, 7-10 November.

Ahmed, T. (2000). *Reservoir Engineering Handbook* (second edition). Houston, Texas: Gulf Professional Publishing.

Ahmed, T. (2007). *Equations of State and PVT Analysis.* Houston, Texas: Gulf Publishing Company.

Ahmed, T., Evans, J., Kwan, R., & Vivian, T. (1998). *Wellbore Liquid Blockage in Gas Condensate Reservoirs.* Paper presented at the SPE Eastern Regional Meeting, Pittsburgh, 9-11 November.

Akutsu, T., Yamaji, Y., Yamaguchi, H., Watanabe, M., Smith, R., & Inomata, H. (2007). Interfacial Tension between Water and High Pressure CO_2 in the Presence of Hydrocarbon Surfactants. *Fluid Phase Equilibria, 257,* 163-168.

Al-Abri, A., & Amin, R. (2009). *Experimental Investigation of Interfacial Interactions of Condensate/Brine/SC-CO_2 Systems at High Pressure and High Temperature Conditions.* Paper presented at the International Petroleum Technology Conference, Doha, Qatar, 7-9 December.

Al-Abri, A., & Amin, R. (2010a). Phase Behaviour, Fluid Properties and Recovery Efficiency of Immiscible and Miscible Condensate Displacements by $SCCO_2$ Injection: Experimental Investigation. *Transport in Porous Media*. In Press.

Al-Abri, A., & Amin, R. (2010b). Interfacial Tension Effects of Hydrocarbon and Non-Hydrocarbon Gas Injection into Gas Condensate Reservoirs. *Chemical Engineering and Technology.* In Press.

Al-Abri, A., Sidiq, H., & Amin, R. (2009). Experimental Investigation of the Velocity-Dependent Relative Permeability and Sweep Efficiency of Supercritical CO_2 Injection into Gas Condensate Reservoirs. *Natural Gas Science and Engineering, 1,* 158-164.

Al-Abri, A., Sidiq, H., & Amin, R. (2010a). Enhanced Natural Gas and Condensate Recovery by Carbon Dioxide and Methane Flooding. *Petroleum Science and Technology*. In Press.

Al-Abri, A., Sidiq, H., & Amin, R. (2010b). Mobility Ratio, Relative Permeability and Sweep Efficiency of Supercritical CO_2 and Methane Injection to Enhance Natural Gas and Condensate Recovery: Coreflooding Experimentation. *Natural Gas Science and Engineering*. In Press.

Al-Anzi, H. (2003). *Experimental Measurements of Gas Blockage and Treatments in Low and High Permeability Cores.* PhD Dissertation. University of Texas at Austin.

Al-Anzi, H. A., Sharma, M. M., & Pope, G. (2004). *Revaporisation of Condensate with Methane Flood*. Paper presented at the SPE International Petroleum Conference, Puebla, Mexico, 8-9 November.

Al-Anzi, H. A., Walker, J. G., Pope, G. A., Sharma, M., & Hackney, D. F. (2003). *A Successful Methanol Treatment in a Gas Condensate Reservoir: Field Application*. Paper presented at the SPE Production and Operations Symposium, Oklahoma, 22-25March.

Ali, J. K., McGualey, P. J., & Wilson, C. J. (1997). *The Effects of High Velocity Flow and PVT Changes Near the Wellbore on Condensate Well Performance.* Paper presented at the SPE Annual Technical Conference and Exhibition, San Antonio, Texas, 3-5 October.

Andreas, J. M., Hauser, E. A., & Tucker, W. B. (1938). *Boundary Tension by Pendant Drops*. Paper presented at the 50th Colloid Symposium, Cambridge, Massachuetts.

Austad, T., & Standnes, D. (2003). Spontaneous Imbibition of Water into Oil-Wet Carbonates *Journal of Petroleum Science and Engineering 39*(3-4), 363-376.

Ayyalasomayajula, P., Silpngarmlers, N., Berroteran, J., Sheffield, J., & Kamath, J. (2003). *Condensate Relative Permeability Data for Well Deliverability Predictions for a Deep Marine Sandstone Reservoir*. Paper presented at the SCA.

Ayyalasomayajula, P., Silpngarmlers, N., & Kamath, J. (2005). *Well Deliverability Predications for a Low-Permeability Gas Condensate Reservoir* Paper presented at the SPE Annual Technical Conference and Exhibition, Dallas, Texas, 9-12 October.

Bahramian, A., Danesh, A., Gozalpour, F., Tohidi, B., & Todd, A. (2007). Vapour-Liquid Interfacial Tension of Water and Hydrocarbon Mixture at High Pressure and High Temperature Conditions. *Fluid Phase Equilibria, 252*, 66-73.

Bardon, C., & Longerson, D. G. (1980). Influence of Very Low Interfacial Tensions on Relative Permeability. *SPE Journal, 20*(10), 391-401.

Barnum, R. S., Brinkman, F. P., Richardson, T. W., & Spillette, A. G. (1995). *Gas Condensate Reservoir Behaviour: Productivity and Recovery Reduction due to Condensation*. Paper presented at the SPE Annual Technical Conferecne and Exhibition, Dallas, Texas, 22-25 October.

Batycky, J. P., & McCaffery, F. G. (1978). *Low Interfacial Tension Displacement Studies.* Paper presented at the 29th Annual Technical Meeting of CIM, Calgary, Canada.

Bear, J. (1972). *Dynamics of Fluids in Porous Media*. New York City. American Elsevier Publishing Company.

Beydoun, Z. (1998). Arabian Plate Oil and Gas: Why So Rich and So Prolific? *Petroleum Geology 21*(2), 74-81.

Blunt, M., Fayers, F. J., & Orr, F. M. J. (1993). Carbon Dioxide in Enhanced Oil Recovery. *Energy Convers. Mgmt., 34*(9-11), 1197-1204.

Boom, W., Wit, K., Zeelenberg, J. P., Weeda, H. C., & Maas, J. G. (1996). *On the Use of Model Experiments for Assessing Improved Gas Condensate Mobility Under Near-Wellbore Flow Conditions.* Paper presented at the SPE Annual Technical Conference and Exhibition, Denver, Colorado, 6-9 October.

Bourbiaux, B. J., & Limborg, S. G. (1994). *An Integrated Experimental Methodology for a Better Prediction of Gas Condensate Flow Behaviour.* Paper presented at the 69th SPE Annual Technical Conference and Exhibition, New Orleans, LA, 25-28 September.

BP (June 2010). Statistical Review of World Energy. *Online Article*, 50. Retrieved from http://www.bp.com/productlanding.do?categoryId=6929&contentId=7044622

Brock, J., & Bird, R. (1952). Surface Tension and the Principles of Corresponding States. *AICHEJ, 56*, 996-999.

Caldwell, R. H., & Heather, D. I. (1991). *How to Evaluate Hard-to-Evaluate Reserves*. Paper presented at the SPE Hydrocarbons and Economic Evaluation Symposium, Dallas, Texas, 11-12 April.

Chang, Y., Coats, B. K., & Nolen, J. S. (1998). A Compositional Model for CO_2 Floods including CO_2 Solubility in Water *SPE REE, 1*(2), 155-160.

Chen, H., Wilson, S. D., & Monger-McClure. F. (1999). Determination of Relative Permeability and Recovery for North Sea Gas Condensate Reservoir *SPE REE*, 939-402.

Chopra, A. K., & Carter, R. D. (1986). Proof of the Two-Phase Steady-State Theory for Flow through Porous Media. *SPE Formation Evaluation*.

Cooney, D. (1966). Effect of Mass Transfer on Stability of Miscible Displacement Fronts in Porous Media. *Ind. Eng. Chem., 5*(3), 426-430.

Crandall, D. (2007). *Two-Phase Flow in Porous Media and Fractures.* PhD Dissertation, Clarkson University, Potsdam, New York.

Creek, J. L., & Sheffield, J. M. (1993). Phase Behaviour, Fluid Properties, and Displacement Characteristics of Permian Basin Reservoir Fluid/CO_2 Systems. *SPE REE, 8*(1), 34-42.

Cullick, A. S., Lu, H. S., Jones, L. G., Cohen, M. F., & Watson, J. P. (1989). *WAG May Improve Gas Condensate Recovery.* Paper presented at the Gas Technology Symposium, Dallas, Texas, 7-9 June.

Dake, L. P. (1983). *The Hierarchy of Production Methods for Offshore Gas Condensate Fields.* Paper presented at the Conference on North Sea Gas Condensate Reservoirs and their Development, London, UK.

Danesh, A. (1998). *PVT and Phase Behaviour of Petroleum Reservoir Fluids.* Amsterdam, The Netherlands. Elsevier Science and Technology Books

Danesh, A., Henderson, G. D., & Peden, J. M. (1989). *Experimental Investigation of Retrograde Condensation in Porous Media at Reservoir Conditions*. Paper presented at the SPE Annual Technical Conference and Exhibition, Houston, Texas, 2-5 October.

Danesh, A., Henderson, G. D., & Peden, J. M. (1991). Experimental Investigation of Critical Condensate Saturation and its Dependence on Interstitial Water Saturation in Water-Wet Rocks. *SPE REE,* 336-342.

Dawe, R. A., & Grattoni, C. A. (2007). Fluid Flow Behaviour of Gas Condensate Near-Miscible Fluids at the Pore Scale. *Petroleum Science and Engineering, 55,* 228-236.

Dindoruk, B., & Firoozabadi, A. (1996a). *Crossflow in Fractured/Layered Media Incorporating Gravity, Viscous, and Phase Behaviour Effects: Part II - Features in Fractured Media.* Paper presented at the SPE/DOE 10th Symposium on Improved Oil Recovery, Tulsa, OK, 21-24 April.

Dindoruk, B., & Firoozabadi, A. (1996b). *Crossflow in Fractured/Layered Media Incorporating Gravity, Viscous, and Phase Behaviour Effects: Part I - Formulation and Features in Layered Media.* Paper presented at the SPE/DOE 10th Symposium on Improved Oil Recovery, Tulsa, OK, 21-24 April.

Donohoe, C. W., & Buchanan, R. D. J. (1981). Economic Evaluation of Cycling Gas Condensate Reservoirs with Nitrogen. *JPT AIME, 263*(271).

Du, L., Walker, J. G., Pope, G. A., Sharma, M., & Wang, P. (2000). *Use of Solvents to Improve the Productivity of Gas Condensate Wells*. Paper presented at the SPE Annual Technical Conference and Exhibition, Dallas, Texas, 1-4 October.

Eckles, W. W. J., Prihoda, C., & Holden, W. W. (1981). Unique Enhanced Oil and Gas Recovery for Very High Pressure Wilcox Sands Uses Cryogenic Nitrogen and Methane Mixture. *JPT 971*.

El-Banbi, A. H., McCain, W. D., & Semmelbeck, M. E. (2000). *Investigation of Well Productivity in Gas Condensate Reservoirs.* Paper presented at the SPE/CERI Gas Technology Symposium, Calgary, Canada, 3-5 April.

Elliot, S., Hsu, H., O'Hearn, T., Sylvester, I., & Vercesi, R. (1998). The Giant Karachaganak Field: Unlocking its Potential. *Oilfield Review 10*(3), 16-25.

Engineer, R. (1985). *Cal Canal Field, California: Case History of a Tight and Abnormally Pressured Gas Condensate Reservoir.* Paper presented at the SPE California Regional Meeting, Bakersfield, CA, 27-29 March.

Evison, B., & Gilchrist, R. E. (1992). *New Developments in Nitrogen in the Oil Industry*. Paper presented at the SPE Mid-Continent Gas Symposium, Amarillo, Texas, 13-14 April.

Fan, L., Harris, B. W., Jamaluddin, A., Kamath, J., Mott, R., Pope, G. A., et al. (2005). Understanding Gas Condensate Reservoirs. *Oilfield Review 17*.

Fayers, F. J., & Lee, S. (1992). *Crossflow Mechanisms by Gas Drive in Heterogeneous Reservoirs.* Paper presented at the Annual Technical Conference and Exhibition, Washington, D.C., 4-7 October.

Ferer, M., Chuang, J., Bromhal, G. S., Cook, J., Ahmadi, G., & Smith, D. (2004). Crossover from Capillary Fingering to Viscous Fingering for Immiscible Unstable Flow. *Phys. Rev.* E70 (016303), 1-7.

Fevang, O. (1996). Modelling Gas Condensate Well Deliverability. *SPE REE*.

Fevang, O., & Whitson, C. H. (1995). *Modelling Gas Condensate Well Deliverability*. Paper presented at the SPE Annual Technical Conference and Exhibition, Dallas, Texas, 22-25 October.

Fevang, O., & Whitson, C. H. (2000). *Guidelines for Choosing Compositional and Black-Oil Models for Volatile Oil and Gas Condensate Reservoirs.* Paper presented at the Annual Technical Conference and Exhibition

Firoozabadi, A., Katz, D. L., Soroosh, H., & Sajjadian, V. A. (1988). Surface Tension of Reservoir Crude-Oil/Gas Systems Recognising the Asphalt in the Heavy Fraction. *SPE REE*, 265-272.

Fisherman, D. M., & Prior, E. M. (1983). *A Discussion of Alternative Recovery Mechanisms for Gas Condensate Reservoirs.* Paper presented at the Conference on North Sea Gas Condensate Reservoirs and their Development, London, UK.

Fishlock, T. P., & Probert, C. J. (1996). *Waterflooding of Gas Condensate Reservoirs.* Paper presented at the SPE/DOE Symposium on Improved Oil Recovery, Tulsa, Oklahoma, 21-24 April.

Fishlock, T. P., & Smith, R. A. (1993). Three-Phase Studies of Gas Condensate Flow Behaviour. *SPE Advanced Technology Services 1*.

Fulcher, R. A., Ertekin, T., & Stahl, C. (1985). Effect of Capillary Number and its Constituents on Two-Phase Relative Permeability Curves. *JPT*, 249-260.

Fussel, D. D. (1973). Single-Well Performance Predictions for Gas Condensate Reservoirs *JPT*, 860-870.

Gardner, J. W., & Ypma, J. G. (1984). An Investigation of Phase Behaviour/Macroscopic-Bypassing Interaction in CO_2 Flooding. *SPE Journal*, 508-520.

Garmeh, G., Johns, R., & Lake, L. (2007). *Pore-Scale Simulation of Dispersion in Porous Media*. Paper presented at the SPE 110228.

Giraud, A., Thomere, R., Gard, J., & Charles, M. (1971). *A Laboratory Investigation Confirms the Relative Permeability of True Miscible Drives, and Outlines New Concepts for Maximizing Oil Recovery by Gas Injection*. Paper presented at the SPE Annual Fall Meeting, New Orleans, LA, 3-6 October.

Goddin, C. S., Craig, F. F., Wilkes, J. O., & Tek, M. R. (1996). A Numerical Study of Waterflood Performance in a Stratified System with Crossflow. *JPT, 18*, 765-771.

Gravier, J. F., Lemouzy, P., Barroux, C., & Abed, A. (1986). Determination of Gas Condensate Relative Permeability on Whole Cores under Reservoir Conditions. *SPE Formation Evaluation, 1*, 9-15.

Green, D. W., & Willhite, G. P. (1998). *Enhanced Oil Recovery.* Richardson, Texas: Society of Petroleum Engineers.

Gringarten, A. C., & Al-Lamki, A. (2000). *Well Test Analysis in Gas Condensate Reservoirs.* Paper presented at the SPE Annual Technical Conference and Exhibition, Dallas, Texas, 1-4 October.

Habermann, B. (1960). The Efficiency of Miscible Displacement as a Function of Mobility Ratio. *SPE Journal, 219*, 264-272.

Hagoort, J. (1998). *Fundamental of Gas Reservoir Engineering.* New York City: Elsevier Science Publishers.

Harbert, L. W. (1983). *Low Interfacial Tension Relative Permeability.* Paper presented at the SPE Annual Technical Conference and Exhibition, San Francisco, CA.

Hartland, S. (2004). *Surface and Interfacial Tension: Measurement, Theory, and Applications.* New York City: Marcel Dekker Inc.

Hartman, K., & Cullick, A. (1993). Oil Recovery by Gas Displacement at Low Interfacial Tension. *Petroleum Science and Engineering, 10*, 197-210.

Henderson, G., Danesh, A., Tehrani, D., Al-Shaidi, S., & Peden, J. (1998). Measurement and Correlation of Gas Condensate Relative Permeability by the Steady-State Method. *SPE REE*.

Henderson, G. D., Danesh, A., & Peden, J. M. (1991). *Waterflooding of Gas Condensate Fluids in Cores above and below the Dewpoint.* Paper presented at the SPE Annual Technical Conference and Exhibition, Dallas, Texas, 6-9 October.

Henderson, G. D., Danesh, A., Tehrani, D. H., Al-Shaidi, S., & Peden, J. M. (1995). *Measurement and Correlation of Gas Condensate Relative Permeability by the Steady-State Method*. Paper presented at the Annual Technical Conference and Exhibition, Dallas, Texas, 22-25 October.

Henderson, G. D., Danesh, A., Tehrani, D. H., & Peden, J. M. (1993). *An Investigation into the Processes Governing Flow and Recovery in Different Flow Regimes in Gas Condensate Reservoirs.* Paper presented at the 68th Annual Technical Conference and Exhibition, Houston, Texas, 3-6 October.

Hinchman, S. B., & Barree, R. D. (1985). *Productivity Loss in Gas Condensate Reservoirs.* Paper presented at the SPE Annual Technical Conference and Exhibition, Las Vegas, Nevada, 22-26, September.

Hinderaker, L., Utseth, R., Hustad, O., Kvanvik, B., & Paulson, K. (1996). *A Comprehensive Norwegian R&D Program on IOR.* Paper presented at the SPE European Petroleum Conference, Milan, Italy, 22-24 October.

Hoier, l., Cheng, N., & Whitson, C. H. (2004). *Miscible Gas Injection in Undersatrated Gas Oil Systems.* Paper presented at the Annual Technical Conference and Exhibition, Houston, Texas, 26-29 September.

Holm, L. W. (1986). Miscibility and Miscible Displacement *Petroleum Technology*, 38 (8), 817-818.

Holm, L. W. (1987). *Miscible Displacement* Richardson, Texas: Society of Petroleum Engineers.

Honarpour, M., Koederitz, L. F., & Harvey, A. H. (1986). *Relative Permeability of Petroleum Reservoirs* (1 ed.). Boca Raton, Florida: CRC Press.

Hough, E., & Stegemeier, G. L. (1961). Correlation of Surface and Interfacial Tension of Light Hydrocarbons in the Critical Region. *SPE Journal, 29,* 259-263.

Hu, H., Whitson, C., & Qi, Y. (1990). *A Study of Recovery Mechanisms in a Nitrogen Diffusion Experiment.* Paper presented at the Annual Technical Conference and Exhibition, New Orleans, LA, 23-26 September.

Huang, W. W., Bellamy, R. B., & Ohnimus, S. W. (1986). *A Study of Nitrogen Injection for Increased Recovery from A Rich Retrograde Gas Volatile Oil Reservoir.* Paper presented at the SPE International Meeting on Petroleum Engineering, Beijing, 17-20 March.

Hugill, J. A., & Welsenes, A. V. (1986). Surface Tension: A Simple Correlation for Natural Gas and Condensate Systems. *Fluid Phase Equilibria, 29,* 383-390.

Jamaluddin, A. K., Thomas, S. Y., D'Crux, D., & Nighswander, J. (2001). *Experimental and Theoretical Assessment of Using Propane to Remediate Liquid Buildup on Condensate Reservoirs.* Paper presented at the Annual Technical Conference and Exhibition, New Orleans, LA, 30 Sep-3Oct.

Jessen, K., Stenby, E., & Orr, F. (2004). Interplay of Phase Behaviour and Numerical Dispersion in Finite-Difference Compositional Simulation. *SPE Journal*.

Ji, C., Ferer, M., Ahmadi, G., Bromhal, G., & Smith, D. (2002). *Experimental and Numerical Study of Gas-Liquid Displacements in Flow Cells, with Application to Carbon Dioxide Sequestration in Brine Fields.* Paper presented at the ASME FEDSM.

Johns, R., Sah, P., & Solano, R. (2002). Effect of Dispersion on Local Displacement Efficiency for Multicomponent Enriched-Gas Floods above the MME. *SPE REE, 5*(1).

Kalaydjian, F., Bourbiaux, B. J., & Lombard, J. (1996). *Predicting Gas Condensate Reservoir Performance: How Flow Parameters are Altered when Approaching Production Well's.* Paper presented at the SPE Annual Technical Conference and Exhibition, Denver, Colorado, 6-9 October.

Kalaydjian, F. J. (1992a). *Performance and Analysis of Three Phase Capillary Pressure Curves for Drainage and Imbibition in Porous Media.* Paper presented at the SPE Technical Conference and Exhibition, Washington, D. C., 4-7 October.

Kalaydjian, F. J. (1992b). *Dynamic Capillary Pressure Curve for Water/Oil Displacement in Porous Media: Theory vs. Experiment.* Paper presented at the SPE Technical Conference and Exhibition, Washington, D. C., 4-7 October.

Kamath, J. (2007). Deliverability of Gas Condensate Reservoirs - Field Experiences and Prediction Techniques. *Distinguished Author Series, Petroleum Technology*, 94-99.

Kossack, C. A., & Opdal, S. T. (1986). *Recovery of Condensate from a Heterogeneous Reservoir by Injection of a Slug of Methane Followed by Nitrogen*. Paper presented at the Annual Technical Conference and Exhibition, Houston, Texas.

Kumar, R. (2000). *Productivity Improvement of Gas Condensate Wells by Fracturing.* PhD Dissertation. The University of Texas at Austin, Texas

Kumar, V., Pope, G. A., Sharma, M., Ayyalasomayajula, P. S., & Kamath, J. (2006a). *Chemical Stimulation of Gas Condensate Reservoirs.* Paper presented at the SPE Annual Technical Conference and Exhibition, San Antonio, Texas, 24-27 September.

Kumar, V., Pope, G. A., Sharma, M., Ayyalasomayajula, P. S., & Kamath, J. (2006b). *Improving the Gas and Condensate Relative Permeability Using Chemical Treatments.* Paper presented at the SPE Gas Technology Symposium, Calgary, Canada, 15-17 May.

Lal, R. R. (2003). *Well Testing in Gas Condensate Reservoirs.* MSc Dissertation. Stanford University, California.

Lee, S., & Chien, M. (1984). *A New Multicomponent Surface Tension Correlations Based on Scaling Theory.* Paper presented at the SPE/DOE Enhanced Oil Recovery Symposium, Tulsa, OK.

Lemonnier, P., & Bourbiaux, B. (2010). Simulation of Naturally Fractured Reservoirs: State of the Art. *Oil and Gas Science and Technology 65*(2), 239-262.

Lewis, E. (2008). *Sweep Efficiency in Miscible Enhanced Oil Recovery Processes.* PhD Dissertation, University of Houston, Texas.

Li, K., & Firoozabadi, A. (2000). Experimental Study of Wettability Alteration to Preferential Gas Wetting in Porous Media and its Effects. *SPE REE*, 139-149.

Lolon, E. P., McVay, D. A., & Schubarth, S. K. (2003). *Effect of Fracture Conductivity on Effective Fracture Length.* Paper presented at the Annual Technical Conference and Exhibition, Denver, Colorado, 5-8 October.

Luo, K., Shi, L., Zeng, X., Chen, G., Dai, Z., & Liu, N. (2000). *Experimental Investigation in Revaporisation of Retrograde Condensate by Lean Gas Injection*. Paper presented at the SPE Asia Pacific Oil and Gas Conference, Jakarta, Indonesia, 17-19 April.

Maclead, D. B. (1923). On a Relation Between Surface Tension and Density. *Trans. Faraday Soci., 19*, 38-43.

Mani, V., & Mohanty, K. (1996). Effect of the Spreading Coefficient on Three-Phase Flow in Porous Media. *Colloid and Interface Science, 187*, 45-56.

Manrique, E. J., Muci, V. E., & Gurfinkel, M. E. (2007). EOR Field Experiences in Carbonate Reservoirs in the United States. *SPE REE, 10*(6), 667-686.

Marokane, D., Logmo-Ngog, A. B., & Sarkar, R. (2002). *Applicability of Timely Gas Injection in Gas Condensate Fields to Improve Well Productivity*. Paper presented at the SPE/ DOE 13th Improved Oil Recovery Symposium, Tulsa, OK, 13-17 April.

Martin, F. D., & Taber, J. J. (1992). Carbon Dioxide Flooding. *JPT*, 396-400.

Mathiassen, O. M. (2003). *CO_2 as Injection Gas for Enhanced Oil Recovery and Estimation of the Potential on the Norwegian Continental Shelf.* Trondheim, Stavanger: Norwegian University of Science and Technology

Melean, Y., Bureau, N., & Broseta, D. (2003). Interfacial Effects in Gas Condensate Recovery and Gas Injection Processes. *SPE REE*.

Melrose, J. C., & Brandner, C. F. (1974). Role of Capillary Forces in Determining Microscopic Displacement Efficiency for Oil Recovery by Waterflooding. *J. Can. Pet. Technol., 13*(4), 54-62.

Moffat, B. J., & Williams, J. M. (1998). *Identifying and Meeting the Key Needs for Reservoir Fluid - A Multi-Disciplinary Approach.* Paper presented at the SPE Annual Technical Conference and Exhibition, New Orleans, 27-30 September.

Mohanty, K. K., & Adibhatla, B. (2004). *Effect of Surfactants on Wettability of Near-Wellbore Regions of Gas Reservoirs.* Paper presented at the Wettability Conference, Houston, Texas.

Mohanty, K. K., Gupta, A., & Deruiter, R. A. (1994). Pore-Level Mechanisms of Residual Oil Formation during Miscible Displacement *Colloid and Interface Science. 163*, 199-216.

Moore, T. F., & Slobod, R. L. (1951). The Effect of Viscosity and Capillary on the Displacement of Oil by Water. *Producers Monthly 20*, 20-30.

Morel, D. (1991). *Basic Concepts in Enhanced Oil Recovery Processes*. England Elsevier Science Publishers

Morel, D. D., Latil, M., & Thiebot, B. (1990). *Diffusion Effects in Gas-Flooded Light Oil Fractured Reservoirs.* Paper presented at the Annual Technical Conference and Exhibition, New Orleans, LA, 23-26 September.

Moritis, G. (2004). EOR Continues to Unlock Oil Resources. *Oil & GAS 104*(14).

Mott, R. (2002). *Engineering Calculations of Gas Condensate Well Productivity*. Paper presented at the Annual Technical Conference and Exhibition, San Antonio, Texas, 29 Sep -2 Oct.

Mott, R., Cable, A., & Spearing, M. (2000). *Measurements and Simulation of Inertial and High Capillary Number Flow Phenomena in Gas Condensate Relative Permeability*. Paper presented at the SPE Annual Technical Conference and Exhibition

Mungan, N. (1966). Interfacial Effects in Immiscible Liquid-Liquid Displacement in Porous Media. *SPE Journal*, 247-253.

Munkerud, P. K. (1989). *Measurement of Relative Permeability and Flow Properties of a Gas Condensate System during Pressure Depletion and Pressure Maintenance*. Paper presented at the SPE Gas Technology Symposium, Dallas, Texas, 7-9 June.

Murtha, J. A. (1993). *Incorporating Historical Data in Monte Carlo Simulation.* Paper presented at the SPE Computer Conference and Exhibition, New Orleans, LA, 11-14 July.

Myers, D. (1999). *Surfaces, Interfaces, and Colloids: Principles and Applications* New York City: John Wiley Sons Inc.

Nagarajan, N. R., Honarpour, M., Sampath, K., & McMichael, D. (2004). *Comparison of Gas Condensate Relative Permeability Using Live Fluid vs. Model Fluids*. Paper presented at the SCA.

O'Connor, S. J. (2000). Hydrocarbon-Water Interfacial Tension Values at Reservoir Conditions: Inconsistencies in the Technical Literature and the Impact on Maximum Oil and Gas Column Height Calculations. *The American Association of Petroleum Geologists 84*(10), 1537-1541.

Oldenburg, C., Pruess, K., & Benson, S. (2001). Process Modelling of CO_2 Injection into Natural Gas Reservoirs for Carbon Sequestration and Enhanced Gas Recovery. *Energy and Fuels 15*, 293-298.

Ollivier, B., & Magot, M. (2005). *Petroleum Microbiology*. Herndon, Virginia: ASM Press.

Orr, F. M. J. (1984). The Use of Carbon Dioxide in Enhanced Oil Recovery. *Science 224*, 563-569.

Orr, F. M. J., Heller, J. P., & Taber, J. J. (1982). *Enhanced Oil Recovery - Facts and Challenges.* Paper presented at the 73rd Annual Meeting of the American Oil Chemists' Society, Toronto, Canada, 2-6 May.

Pande, K. K., & Orr, F. (1989). *Interaction of Phase Behaviour, Reservoir Heterogeneity and Crossflow in CO_2 Floods*. Paper presented at the SPE Annual Technical Conference and Exhibition, San Antonio, Texas, 8-11 October.

Perkins, T. K., Johnston, D. C., & Hoffman, R. N. (1965). Mechanics of Viscous Fingering in Miscible Systems *SPE Journal, 5*(301).

Perkins, T. K., & Johnston, O. (1963). A Review of Diffusion and Dispersion in Porous Media. *SPE Journal*.

Perrine, R. L. (1961). The Development of Stability Theory for Miscible Liquid-Liquid Displacement. *SPE Journal*, 17-25.

Pollard, T. A., & Bradley, H. B. (1962). *Gas Condensate Reservoirs.* New York McGraw-Hill.

Roussennac, B. (2001). *Gas Condensate Well Test Analysis.* MSc Dissertation. Stanford University, California.

Rowlinson, J. S., & Widom, B. (1982). *Molecular Theory of Capillarity*. New York Oxford University Press.

Saevareid, A., Whitson, C. H., & Fevang, O. (1999). *An Experimental Approach to Measuring and Modelling Gas Condensate Relative Permeabilites*. Paper presented at the SCA Conference, Goldon, CO, 2-4 August.

Sanger, P. J., & Hagoort, J. (1998). Recovery of Gas Condensate by Nitrogen Injection Compared with Methane Injection. *SPE Journal, 3*(1), 26-33.

Saraf, D. N., & McCaffery, F. G. (1985). Relative Permeabilities. In E. C. Donaldson, G. V. Chilingarian & T. F. Yen (Eds.), *Enhanced Oil Recovery: Fundamentals and Analyses.* New YorkCity; Elsevier Science Publishing Company

Schechter, D. S., & Guo, B. (1996). *Mathematical Modelling of Gravity Drainage after Gas Injection into Fractured Reservoirs.* Paper presented at the SPE/DOE 10th Symposium on Improved Oil Recovery, Tulsa, OK, 21-24 April.

Selley, R. C. (1998). *Elements of Petroleum Geology* Toronto, Canada: Academic Press.

Selroos, J., Walker, D., Stom, A., Gylling, B., & Follin, S. (2002). Comparison of Alternative Modelling Approaches for Groundwater Flow in Fractured Rock. *Hydrology, 257*, 174-188.

Settari, A., Bachman, R. C., Hovem, K., & Paulson, S. G. (1996). *Productivity of Fractured Gas Condensate Wells: A Case Study of Smorbukk Field*. Paper presented at the SPE Gas Technology Conference, Calgary, Canada, 28 Apr – 1 May.

Shi, C. (2009). *Flow Behaviour of Gas Condensate Wells.* MSc Dissertation, Stanford University, California.

Smits, R. M., Post, N. V. D., & Shaidi, S. M. A. (2001). *Accurate Prediction of Well Requirements in Gas Condensate Fields* Paper presented at the SPE Middle East Oil Show, Bahrain, 17-20 March.

Sognesand, S. (1991). *Long-Term Testing of Vertically Fractured Gas Condensate Wells.* Paper presented at the SPE Production Operations Symposium, Oklahoma City, OK, 7-9 April.

Sohrabi, M., Danesh, A., & Jamiolahmady, M. (2007). Visualisation of Residual Oil Recovery by Near-Miscible Gas and SWAG Injection Using High-Pressure Micromodels. *Transport in Porous Media*.

Sorbie, K., Zhang, H., & Tsibuklis, N. (1994). Linear Viscous Fingering: New Experimental Results, Direct Simulation and the Evaluation of Averaged Models. *Chemical Engineering Science 50*(4), 601-616.

Stalkup, F. (1983). *Miscible Displacement.* Dallas, Texas: Society of Petroleum Engineers of AIME.

Stalkup, F. (1983). Status of Miscible Displacement. *Petroleum Technology,* 815-826.

Stanley, H. E. (1971). *Introduction to Phase Transitions and Critical Phenomena.* New York City; Oxford University Press.

Stearn, D. (1991). *Near Miscible Displacements*. Paper presented at the Annual Technical Conference and Exhibition, Dallas, Texas, 6-9 October.

Stegemeier, G. L. (1959). *Interfacial Tension of Synthetic Condensate Systems.* PhD Dissertation. The University of Texas, Austin.

Sugden, S. (1924). A Relation between Surface Tension, Density and Chemical Composition *J. Chem. Soc., 168,* 1177-1189.

Taber, J. J. (1969). Dynamic and Static Forces Required to Remove a Discontinuous Oil Phase from Porous Media Containing Both Oil and Water. *SPE Journal, 9*(3), 3-10.

Tamhane, D., Wang, L., & Wong, P. M. (1999). *The Role of Geology in Stochastic Reservoir Modelling: The Future Trends.* Paper presented at the SPE Asia Pacific Oil and Gas Conference and Exhibition, Jakarta, Indonesia, 20-22 April.

Tang, G. Q., & Firoozabadi, A. (2000). *Relative Permeability Modification in Gas Liquid Systems through Wettability Alteration to Intermediate Gas-Wetting*. Paper presented at the Annual Technical Conference and Exhibition, Dallas, Texas, 1-4 October.

Tang, G. Q., & Firoozabadi, A. (2002). Relative Permeability Modification in Gas Liquid Systems through Wettability Alteration to Intermediate Gas-Wetting. *SPE REE*.

Thiele, M., Batycky, R., Blunt, M., & Orr, F. (1996). *Simulating Flow in Heterogeneous Systems Using Streamtubes and Streamlines* Paper presented at the SPE/DOE Improved Oil Recovery Symposium, Tulsa, OK, 17-20 April.

Thomas, F. B., Erian, A., Zhou, X., Bennion, D. B., Bennion, D. W., & Okazawa, T. (1995). *Does Miscibility Matter in Gas Injection?* Paper presented at the 46th Annual Technical Meeting, Banff, 14-17 May.

Thomas, F. B., Holowach, N., Zhou, X., Bennion, D. B., & Bennion, D. W. (1994). *Miscible or Near-Miscible Gas Injection, Which is Better?* Paper presented at the 9th Symposium on Improved Oil Recovery, Tulsa, OK, 17-20 April.

Thomas, F. B., Zhou, X. L., Bennion, D. B., & Bennion, D. W. (2009). *Towards Optimising Gas Condensate Reservoirs*: Petroleum Society of CIM and CANMET.

Todd, M., & Longstaff, W. (1972). The Development, Testing and Application of a Numerical Simulator for Predicting Miscible Flood Performance. *Trans. AIME, 253*, 874-882.

Ursin, J. (2004). Fluid Flow in Gas Condensate Reservoirs: The Interplay of Forces and Their Relative Strengths. *Petroleum Science and Engineering 41*, 253-267.

Vizika, O., & Lombard, J. M. (1996). Wettability and Spreading: Two Key Parameters in Oil Recovery with Three-Phase Gravity Drainage. *SPE REE, 11*(1), 54-60.

Wagner, O. R., & Leach, R. O. (1966). Effects of Interfacial Tension on Displacement Efficiency *Petroleum Technology, 6*(12), 335-344.

Walker, J. G. (2000). *Laboratory Evaluation of Alcohols and Surfactants to Increase Production from Gas Condensate Reservoirs.* PhD Dissertation. University of Texas at Austin.

Wall, C. G. (1982). *Characteristics of Gas Condensate Reservoirs and Traditional Production Methods*. London, England: Oyez Scientific & Technical Services Ltd.

Walsh, B., & Orr, F. (1990). Prediction of Miscible Flood Performance: The Effect of Dispersion on Composition Paths in Ternary Systems. *InSitu 14, 1*, 19-47.

Warren, J. E., & Root, P. J. (1963). The Behaviour of Naturally Fractured Reservoirs. *SPE Journal*, 245-255.

Weinaug, C., & Katz, D. (1943). Surface Tension of Methane-Propane Mixtures *Ind. Eng. Chem., 35*, 239-246.

Whitson, C., & Brule, M. (2000). *Phase Behaviour.* Monograph Series, SPE, Richardson, Texas (Vol. 20).

Whitson, C. H., Fevang, O., & Saevareid, A. (1999). *Gas Condensate Relative Permeability for Well Calculations.* Paper presented at the SPE Annual Technical Conference and Exhibition, Houston, 3-6 October.

Wu, R. S., Batycky, J. P., & Harker, B. C. (1969). *A New Approach to Modelling Miscible Displacement Tests*. Paper presented at the 64 Annual Technical Conference and Exhibition, San Antonio, Texas, 8-11 October.

Yokoymam, Y., & Lake, L. W. (1981). *The Effects of Capillary Pressure on Immiscible Displacements in Stratified Porous Media.* Paper presented at the Annual Fall Technical Conference and Exhibition, San Antonio, Texas, 5-7 October.

Zhenhao, D., & Rui, S. (2003). An Improved Model Calculating CO_2 Solubility in pure water and Aqueous NaCl Solutions from 273 to 533 K and from 0 to 2000 bar. *Chemical Geology. 193*, 257-271.

Zhou, D., Fayers, F. J., & Orr, F. (1993). *Scaling of Multiphase Flow in Simple Heterogeneous Porous Media.* Paper presented at the SPE/DOE Winter Meeting, New Orleans, LA, 28 Nov – 3 Dec.

APPENDIX

TABLE 1. CONDENSATE COMPOSITION

Component	Mol%	Weight%
Methane	0.00	0.00
Ethane	0.00	0.00
Propane	0.02	0.00
i-Butane	0.03	0.01
n-Butane	0.11	0.04
neo-Pentane	0.00	0.00
i-Pentane	0.23	0.10
n-Pentane	0.28	0.11
Hexanes	1.17	0.57
M-C-Pentane	0.54	0.26
Benzene	0.47	0.21
Cyclohexane	0.80	0.38
Heptanes	2.38	1.35
M-C-Hexane	2.85	1.59
Toluene	3.22	1.68
Octanes	4.96	3.22
E-Benzene	0.54	0.33
M/P-Xylene	2.34	1.42
O-Xylene	1.24	0.75
Nonanes	7.20	5.25
T-M-Benzene	0.94	0.72
Decanes	9.61	7.31
Undecanes	8.54	7.14
Dodecanes	8.04	7.36
Tridecanes	7.88	7.85
Tetradecanes	7.11	7.68
Pentadecanes	5.37	6.29
Hexadecanes	5.80	7.33
Heptadecanes	3.21	4.32
Octadecanes	3.23	4.61
Nonadecanes	2.37	3.55
Eicosanes	1.59	2.48
Heneicosanes	1.44	2.38
Docosanes	1.14	1.98
Tricosanes	0.86	1.56
Tetracosanes	0.79	1.49
Pentacosanes	0.63	1.24
Hexacosanes	0.53	1.09
Heptacosanes	0.44	0.93
Octacosanes	0.38	0.83
Nonacosanes	0.31	0.72
Triacontanes	0.25	0.59
Hentriacontanes	0.22	0.53
Dotriacontanes	0.18	0.46
Tritriacotanes	0.15	0.40
Tetratriacontanes	0.12	0.34
Pentatriacontanes	0.10	0.29
Hexatriacontanes plus	0.39	1.26

Measured Properties	
Whole Sample Density	0.8161 g/cc @ 60 ^{o}F
Whole Sample Mol. Wt.	175.8 g/mol

Plus Fraction Calculated Properties	Density g/cc @ 60 ^{o}F
Heptanes Plus	0.8179
Undecanes Plus	0.8374
Eicosanes Plus	0.8849
Triacontanes Plus	0.9156
Hexatriacontanes Plus	0.9301

Subtotals	Mole %
Heptanes	4.19
Octanes	11.03
Nonanes	11.32
Decanes	10.55

Notes
Calculated properties derived from Katz & Firoozabadi data
This condensate sample is from standard stock tank